Numerical Modelling of Turbulent Premixed Combustion for Gas Turbine Conditions with Incorporation of Molecular Transport Effects

(Numerische Modellierung turbulenter Vormischverbrennung bei Gasturbinenbedingungen unter Einbeziehung molekularer Transporteffekte)

Dissertation

zur Erlangung des akademischen Grades

DOKTOR-INGENIEUR

vorgelegt von

Naresh Kumar Aluri, M.Sc.

aus Jogannapalem, Andhra Pradesh, Indien

eingereicht dem

Fachbereich Maschinenbau

der Universität Siegen

Referent: Univ.-Prof. Dr. F. Dinkelacker

Korreferent: Univ.-Prof. Dr.-Ing. A. Leipertz

13th June 2007

Acknowledgments

I wish to specially thank my supervisor **Prof. Dr. Friedrich Dinkelacker** for his guidance, advice and support given throughout the entire work.

I am grateful to **Prof. Dr. –Ing. Alfred Leipertz** for offering me the position at LTT, Erlangen and for the financial support provided during my research work carried out at Erlangen from 2003 to beginning of 2006.

My sincere appreciation goes to my mentor and friend **Dr.-Ing Siva P. R. Muppala** for enlightening discussions and encouragement.

I express my sincere appreciation to **Dr. Fernando Biagoli** and **Dr. Peter Flohr** for providing me an opportunity to carry out part of this doctorial work at ALSTOM, Switzerland. Also, I thank Fernando for his scientific discussions.

I take this opportunity to express my love toward my parents, wife, brother and kids for their affection and care.

I express my thankfulness to my colleagues of LTT, Erlangen: Dipl.–Ing. Sebastian Pfadler, M.Sc. Lars Zigan, Dip.–Ing. Micha G. Löffler, and **Dr.–Ing. Frank Beyrau** for their scientific discourse.

I thank **Dipl.– Ing. Florian Altendorfner** from LTT, Erlangen for his help and support provided in tackling the computer related problems.

The thesis was financially supported in the major parts within the Bavarian research project **FORTVER** (Forschungsverbund Turbulente Verbrennung), hosted from the **Arbeitsgemeinschaft Bayerischer Forschungsverbünde (abayfor)**. Some part was funded by **ALSTOM**, the last months financial support was given from the **University of Siegen**. I am very thankful for all these supports.

Table of Contents

Abstract

Design of combustion systems with increased efficiency and reduced fuel consumption under controlled pollutant emissions is mandatory due to the fast depleting trend of the fossil fuel reserves, and environmental concerns. Premixed turbulent high pressure combustion is a practically viable option to tackle these issues, especially in relation with gas turbine combustion. The central theme of this research work is the numerical investigation of the molecular transport effects and the dynamics of turbulent premixed high-pressure flames. These elements of premixed turbulent combustion are exhaustively studied on five different flame configurations of varied degree of complexity, ranging from a simple Bunsen-like burner to an industrial gas turbine combustor.

The focus of this thesis is diversified on three subjects.

Firstly, the behaviour of various turbulent premixed combustion models for the variation of pressure and fuel types with a broad set of simple Bunsen-like flames are numerically tested, where the flow and turbulence field has a relatively simple structure and is calculated with the Reynolds averaged Navier-Stokes (RANS) approach. It is found that several of the existing reaction models are insensitive to the effects of pressure and fuel type. Therefore, a new reaction model is developed, being based on an Algebraic Flame Surface Wrinkling relation (AFSW model), which can describe well the broad set of over 100 Bunsen flame data. The fuel influence is modelled for several hydrocarbon fuels with a Lewis number effect, which shows that molecular transport effects are of importance even for high turbulence conditions. The AFSW model shows remarkable workability also for the other flame configurations, including the gas turbine combustors for pressure variation up to 32 bar. In a set of calculations of a gasturbine burner, it is found that the flame dynamics in conjunction with the vortex breakdown point is sensitive to the Lewis number (i.e., for fuel type). As an alternative reaction model, also the Lindstedt-Váos model is extended in a similar way with a pressure-term and the Lewis number, being described in the appendix.

Secondly, the applicability of the AFSW reaction model is tested in conjunction with more elaborate turbulence models, based on the time dependent large-eddy simulation (LES). Here, the AFSW reaction model was incorporated as a subgrid scale (sgs) reaction closure and was tested for three sgs turbulence models. Validation is done successfully against experimentally measured flame brush thickness and mean flame position on those flame configurations, where the turbulent flow pattern is rather complex with recirculation and swirl. This approach allowed for the first time the calculation and explanation of experimentally observed dual-flame instability of a specific gas-turbine burner.

Thirdly, a preliminary study is started to incorporate the possibility of hydrogen blended methane-air flames, which is of importance as a possible future fuel component, e.g., in the frame of reduced CO_2 emissions. As the molecular weight and with that the diffusivity of hydrogen differs significantly from that of other fuels, this is a non-trivial challenge for any reaction model. In an analytical analysis and with limited computations in the RANS context, it is found that the AFSW model is insensitive to the preferential molecular diffusion effects, occurring here. As an outlook a submodel for the chemical time scale is proposed, based on a leading point concept of critically curved laminar flames. Further studies of this new approach are necessary for thorough validation.

Zusammenfassung

Aufgrund endlicher fossiler Brennstoffreserven erfordert die Auslegung zukünftiger Verbrennungssysteme erhöhte Wirkunggrade und reduzierten Brennstoffverbrauch. Gleichzeitig müssen die Abgasemissionen kontrolliert werden, da sie unsere Umwelt belasten. Einer der modernen verbrennungstechnischen Ansätze ist die Anwendung von turbulenten Vormischflammen unter hohem Druck, beispielsweise in Gasturbinen-Brennern. Die vorliegende Arbeit befasst sich mit der Entwicklung effizienter numerischer Berechnungsverfahren solcher turbulenter Vormischflammen unter erhöhtem Druck. Hierbei spielen molekulare Transportvorgänge und dynamische Flammenvorgänge eine wichtige Rolle. Fünf verschiedene Brennerkonfigurationen wurden dafür in dieser Arbeit untersucht, die durch unterschiedliche Komplexität charakterisiert sind. Sie reichen von einfachen Bunsenflammen bis zu industriellen Gasturbinen-Brennern.

Die Dissertation befasst sich mit drei wesentlichen Themen.

Erstens wurden verschiedene Reaktions-Modelle für die Berechnung turbulenter Vormischflammen getestet. Dies wurde anhand eines breiten Datensatzes von Bunsenflammen bei variiertem Druck und Brennstoff durchgeführt, bei denen das Strömungs- und Turbulenzfeld relativ einfach strukturiert sind, so dass dieses mit der Methodik der gemittelten Navier-Stokes-Gleichungen (Reynolds averaged Navier-Stokes Simulation - RANS) berechnet werden konnte. Aufgrund der mangelhaften Vorhersagegüte von vielen der existierenden Reaktionsmodellen bei erhöhtem Druck und bei variiertem Brennstoff wurde hier ein neues Modell entwickelt. Dieses enthält eine algebraische Berechnungssgleichung der Verwinkelung der Flammenoberfläche (Algebraic Flame Surface Wrinkling (AFSW) Modell). Es ist in der Lage, den gesamten breiten Satz an über 100 Bunsenflammendaten recht gut zu beschreiben. Der Einfluss des Brennstoffes wurde hierbei über eine Lewiszahl beschrieben. Dies zeigt, dass molekulare Transportvorgänge sogar bei hohen Turbulenzbedingungen einen unerwartet starken Einfluss auf die mittlere Reaktionsrate haben. Auch die Anwendung dieses AFSW-Modelles auf andere Brennerkonfigurationen zeigte eine beachtliche Anwendbarkeit, beispielsweise bei der Berechnung eines Gasturbinen-Brenners bis zu 32 bar Betriebsdruck. Bei einer Brennstoff- (Lewiszahl-) abhängigen

Berechnung eines Gasturbinen-Brenners wurde gefunden, dass die dynamische Flammenstabilisierung im Zusammenhang mit der strömungsmechanischen Wirbelaufbruch-Stabilisierung stark von dieser Lewiszahl (also dem Brennstoff) abhängen kann. Alternativ wurde das Reaktionsmodell von Lindstedt und Váos recht erfolgreich mit ähnlichen druck- und Lewiszahlabhängigen Termen erweitert (was im Anhang der Arbeit beschrieben ist).

Zweitens wurde das neu entwickelte Reaktionsmodell auch im Zusammenhang der in der Strömungsmechanik in den letzten Jahren eingeführten zeitabhängigen Large-Eddy-Simulationsmethode (LES) erprobt. Hier wurde das AFSW-Reaktionsmodell als Subgrid-scale-Modell (sgs) formuliert und im Zusammenhang mit drei sgs-Turbulenz-Modellen erprobt. Vergleiche der Flammenlänge und der Flammenzonenausbreitung zeigen die erfolgreiche Anwendbarkeit auch bei Brennern mit komplexen Strömungsformen mit Rezirkulation und Drall. Dieser Ansatz erlaubte erstmalig die Berechnung und Erklärung einer experimentell beobachteten Doppel-Flammen-Instabilität eines speziellen Gasturbinen-Brenners.

Drittens wurde als Ausblick auf zukünftige Arbeiten die Berechnung von Wasserstoff-angereicherten Methanflammen untersucht, was beispielsweise für zukünftige CO_2-arme Brennerkonzepte von Bedeutung ist. Da Wasserstoff aufgrund seiner geringen Masse eine erheblich höhere molekulare Diffusionskonstante als andere Brennstoffe besitzt, ist dies eine nichttriviale Herausforderung für jedes Reaktionsmodell. Eine analytische Abschätzung und erste Berechnungen mit der RANS-Methodik zeigen, dass das AFSW-Modell die bei diesem Brennstoff auftretenden Effekte durch bevorzugte molekulare Diffusionsvorgänge nicht ausreichend beschreibt. Als Ausblick wird eine Modellerweiterung mittels einer chemischen Zeitskala vorgeschlagen, die auf einem "Leading-point"-Konzept von "kritisch gekrümmten" laminaren Flammen beruht. Zur Validierung dieses neuen Ansatzes sind weitere Studien notwendig.

List of Figures

List of Tables

Nomenclature

a	:	Model parameter	-
A	:	Fractal area	m^2
A_T	:	Turbulent flame surface area	m^2
$\overline{A}$	:	Averaged flame surface area	m^2
b	:	Model parameter	-
c	:	Model parameter	-
c	:	Reaction progress variable	-
C_R	:	A preconstant (reaction rate parameter)	-
C_s	:	Smagorinsky´s constant	-
$\widetilde{c}$	:	Favre-averaged reaction progress variable	-
$\overline{c}$	:	Reynolds-averaged reaction progress variable	-
$C_{P,Le}$	:	A pre-constant for pressure and Lewis number effects	-
c_μ	:	Coefficient of $k-\varepsilon$ turbulence model	-
D	:	Species diffusivity	m^2/s
D	:	Fractal dimension or fluid domain	-
Da	:	Damköhler number, $\tau_t/\tau_c = (l_x/u')/(\delta/s_L^0)$	-
E_A	:	Activation energy	J/kg
G	:	LES filter function	-
Ka	:	Karlovitz number	-
I_0	:	Stretch factor	-
k	:	Specific turbulent kinetic energy	m^2/s^2
$\widetilde{k}$	:	Turbulent kinetic energy	m^2/s^2
k_{sgs}	:	Subgrid scale kinetic energy	m^2/s^2
l_x	:	Integral length scale of turbulence	mm
l^3	:	Volume of flame element	m^3
l_F	:	Thermal flame thickness	mm

l_G	:	Gibson length scale	mm
l_λ	:	Taylor length scale, $l_x \cdot \mathrm{Re}_t^{-0.5}$	mm
l_k	:	Kolmogorov length scale, $\left(\nu^3/\varepsilon\right)^{1/4}$	mm
L_y	:	Length scale of Bray-Moss-Libby model	mm
$Le = \alpha/D$	:	Lewis number (of the fuel-air mixture)	-
Ma	:	Markstein number	-
p	:	Operating pressure	bar
p_0	:	Standard pressure	bar
P	:	Probability	-
P_R	:	Probability of occurrence of reaction	-
R	:	Universal gas constant	J/mol-K
Re_t	:	Turbulent Reynolds number, $u'l_x/\nu$	-
Re_Δ	:	Subgrid scale Reynolds number, $u'_\Delta l_\Delta/\nu$	-
s	:	Activity parameter	-
s^*	:	Subgrid activity parameter	-
s_L	:	Laminar flame speed (of unperturbed planar flame)	m/s
s_T	:	Turbulent flame speed (measure of average flame angle)	m/s
$Sc = \nu/D$	:	Schmidt number	-
S_{ij}	:	Strain rate tensor	1/s
$\left\|\tilde{S}\right\|$	:	Strain rate magnitude	1/s
t	:	Time	s
T_A	:	Activation temperature	K
T_r	:	Temperature in reaction zone	K
T_u	:	Unburned premixed mixture temperature	K
T_b	:	Adiabatic flame temperature	K
U	:	Mean inlet flow velocity	m/s
u_i	:	Flow velocity component	m/s
u'_Δ	:	Subgrid scalce turbulent velocity	m/s

u'	:	R.M.S turbulent velocity	m/s
$\tilde{u}$	:	Favre-averaged component of the gas flow velocity u	m/s
u''	:	Fluctuating component of the gas flow velocity u	m/s
$\overline{u''c''}$	:	Turbulent flux	m/s
V_K	:	Kolmogorov velocity, $(\nu_0\varepsilon)^{1/4}$	m/s
w	:	Reaction rate	kg-m/s^2
$\overline{w}_c$	:	Mean chemical reaction rate	kg-m/s^2
x, x_i	:	Spatial coordinate	m
x	:	Exponent	m

Greek symbols

α	:	Thermal diffusivity	m^2/s
β	:	Normalized activation temperature, T_A/T_b	-
Δ	:	Grid size or cut-off filter length	mm
δ_L	:	Laminar flame thickness $\left(\delta_L = 8-10\cdot l_F\right)$	mm
δ_T	:	Turbulent flame brush thickness	mm
θ	:	Flame cone angle	°
ε	:	Viscous dissipation rate	m^2/s^3
ε_i	:	Inner cut-off scale	m
ε_o	:	Outer cut-off scale	m
$\tilde{\varepsilon}$	:	Dissipation rate	m^2/s^3
ϕ	:	Equivalence ratio or LES filtered variable	-
$\varphi = \tilde{\varphi} + \varphi''$	:	Favre decomposition of quantity φ	-
γ	:	Unburned to burned density ratio	-
η	:	Kolmogorov scale	mm
μ	:	Dynamic molecular viscosity	kg-m/s
μ_t	:	Turbulent viscosity	kg-m/s
ν	:	Molecular kinematic viscosity	m^2/s
ν_{eff}	:	Effective viscosity	m^2/s

ν_{num}	:	Numerical viscosity	m^2/s
ν_{sgs}	:	Subgrid scale viscosity	m^2/s
ν_u	:	(Unburned) Molecular kinematic viscosity	m^2/s
ν_t	:	Turbulent viscosity	m^2/s
ν^*	:	Normalized pressure-variant ν, $\nu(p)/\nu(p_0)$	-
ρ	:	Density of gas	kg/m^3
ρ_u	:	Unburned density of premixed mixture	kg/m^3
ρ_b	:	Burned density of premixed mixture	kg/m^3
σ_c	:	Turbulent Schmidt number	kg/m^3
ζ	:	Molecular diffusion	m^2/s
τ_c	:	Chemical time scale	s
τ_t	:	Turbulent time scale	s
τ	:	Heat release parameter, $\tau = \left(\rho_u / \rho_b - 1 \right)$	-
τ_{cr}	:	Critical chemical time scale for highly curved flames	s
Σ	:	Flame surface density	m^2/m^3

1. Introduction

From a general perspective, combustion (Williams 1985) is the rapid oxidation of hydrocarbon and carbonaceous substances accompanied by generation of heat and light in the form of flame. Combustion is not only one of the oldest technologies of mankind, but has been the most important energy source for human activities. Its contribution in the total energy production stays significant (~90%), forecasting at least until mid of this century (Fig. 1.1). Despite of the depleting trend of the fossil fuel reserves, the demand for the power is estimated to increase due to the strong energy need in large fast developing countries like China, India or in South-East Asia. Combustion is related with the emission of environmentally harmful exhaust gases.

Quadrillion Btu
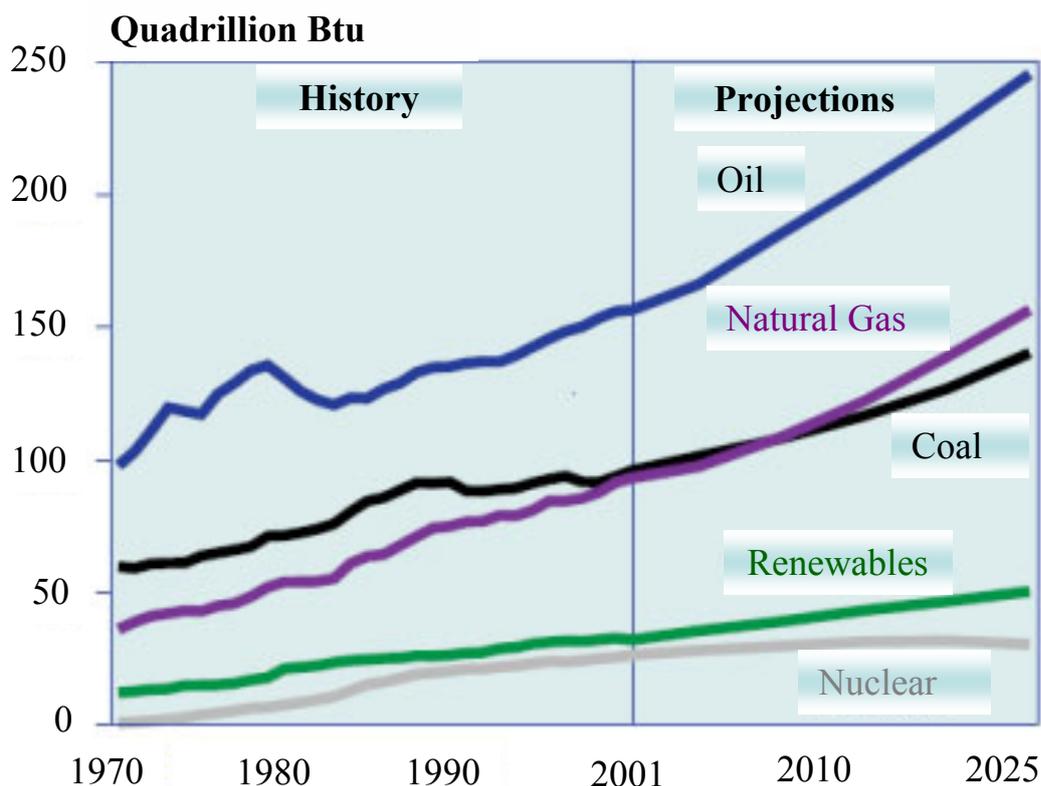
Figure 1.1: *Historical and projected world energy production from various energy sources, 1970-2025, Source: International Energy Outlook (2006)*

The primary combustion products of hydrocarbon fuels are water and carbon dioxide; the latter contributes to the greenhouse effect. Apart from CO_2, probably, the most hazardous compounds formed during combustion are NO_X (mixture of NO in greater

amounts and to a lesser quantity of NO_2). Some harmful effects of NO_X on the environment are acid fall-out and participation in the formation of photochemical smog and ozone. Currently, the annual man-made NO_X emissions in Europe are estimated at 7 Mt N (Mega tonnes of Nitrogen), of which 60% is produced from vehicular traffic, 30% from heat and power generation, and the rest contributed by other industries (Zevenhoven and Kilpinen 2004). NO_X is formed through different chemical mechanisms. Inspection of those mechanisms leads to the conclusion that the low-temperature combustion favours lower NO_X emissions. So far, the most popular method for achieving low temperatures is lean premixed combustion (Dinkelacker 2001) (Fig. 1.2). However, these premixed flames are prone to instabilities and produce higher CO emissions.
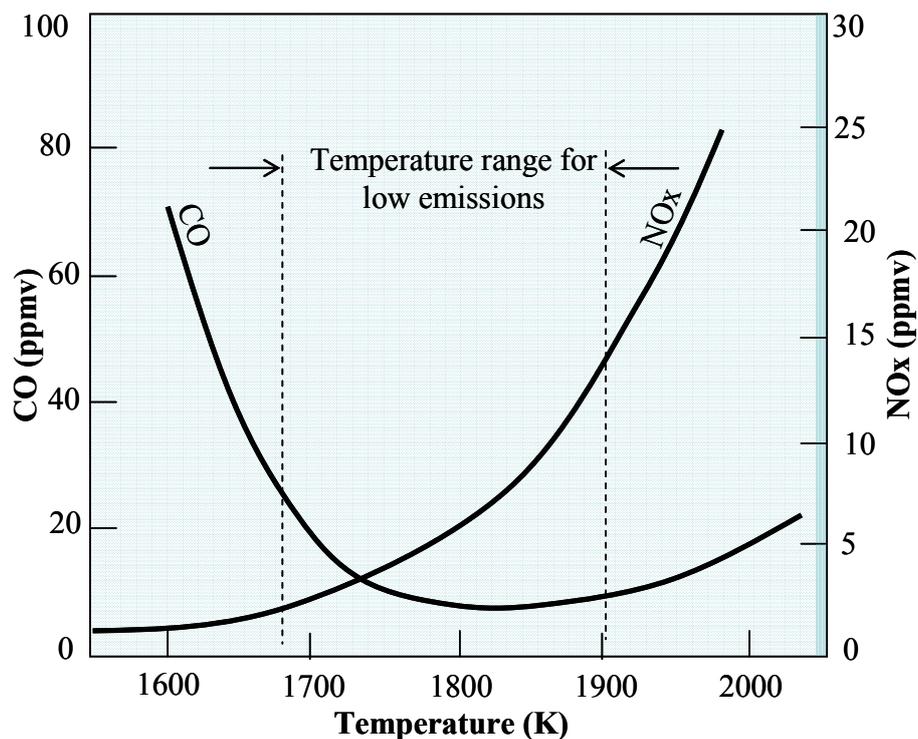
Figure 1.2: *Typical concentration levels of CO and NO_X noticed during lean premixed combustion as a function of combustion temperature (Cohen et al. 1996).*

With the growing expectations for increased efficiency and reduced fuel consumption under controlled pollutant emissions, design of combustion systems become more complex. Considering the complexity of the phenomena involved in premixed turbulent flames and the handling difficulties and the economical aspects in conducting experiments, numerical combustion (Veynante and Vervisch 2002) has the

potential to become a more and more preferred choice as supportive tool for burner development.

The motivation to this study has been these unresolved aspects of combustion which are considerate from their practical importance. The central theme of this research work is the numerical investigation of the molecular transport effects and the dynamics of the turbulent premixed flames. Within this subject, it is aimed to develop a reaction model for turbulent premixed combustion involving several parameters over a broad range of conditions such as fuel type, pressure, geometrical flame configurations, and turbulence levels. Investigations are incepted with the evaluation of various existing reaction models (Aluri et al. 2005a, Aluri et al. 2005b, Aluri et al. 2006, Muppala et al. 2005b) using the high-pressure experimental data of *Kobayashi et al.* from Japan (Kobayashi et al. 1996, Kobayashi et al. 1997, Kobayashi et al. 1998, Kobayashi 2001, Kobayashi et al. 2005) for three different fuels in the Reynolds-averaged Navier Stokes (RANS) approach. It is shown that most of these models are not influenced from the variation of fuel type and high-pressure in the reaction rate. Due to the lack of these important effects in these models, a new premixed combustion model, namely, the Algebraic Flame Surface Wrinkling (AFSW) model (Muppala et al. 2005a, Muppala et al. 2005b) has been developed, while two existing models are substantiated accordingly.

This new combustion model is successfully applied to configurations of varied degrees of complexity from a simple Bunsen flame to an industrial gas turbine combustor for variation of pressure and fuels in Reynolds Averaged Navier Stokes (RANS) approach. As a major step, the reaction closure is transformed to the context of Large Eddy Simulation (LES), which is the selective turbulence methodology employed for the current investigations. First, LES studies are carried out for the Bunsen flames measured by Kobayashi. This model is also extensively studied for the variation of pressure on a sudden expansion dump combustor, a more complex configuration which has been experimentally investigated at the Paul-Scherrer-Institute in Switzerland (Griebel et al. 2002, Griebel et al. 2005). Also, the same model is applied successfully to two variants of ALSTOM gas turbine burners (Fritz 2003, Biagioli 2005) using RANS, while LES are conducted on one of the variants to address an

experimentally observed sudden switch of the flame position (dual-flame mode), which has not been explained before.

In a final step, the sensitivity of the AFSW model for hydrogen doping effects is investigated and the ways to incorporate these effects are outlined as a future work.

The thesis is structured as follows: Chapters 2 to 4 deal with the basics and theoretical aspects of turbulence-combustion processes; Chapter 5, the quality assessment methods/tools for Large Eddy Simulation are addressed; in Chapter 6 constitutes experimental flame configurations employed and the operating conditions involved; results are presented in Chapters 7 to 10, while Chapter 11 gives the summary and conclusions from the whole study. Details follow.

In **chapter 2**, the basics of turbulence, and turbulence models employed for the present investigations, are outlined in the first two sections. In the last segment of this chapter, the elements of combustion processes are briefed.

In **chapter 3**, turbulent premixed combustion is described at length in the first section, while the progress variable approach and reaction modelling details are given in the last two sections.

In **chapter 4**, the molecular effects and dynamics of premixed flames are emphasized, with the inclusion of discussion topics: the importance Lewis number, preferential diffusion, high pressure and lastly about the dynamics of swirl flames.

In **Chapter 5**, various numerical assessment methods for the LES approach are outlined.

In **chapter 6**, the experimental details of all the employed five flame configurations are detailed. These are: the Kobayashi Bunsen burner (F-1 Configuration), PSI sudden expansion dump combustor (F-2), the F-3 & F-4 configurations are different ALSTOM gas turbine burner variants, and finally, the Orleans Bunsen flame which deals with the hydrogen-doping effects on lean premixed turbulent flames.

In **Chapter 7**, the predictions of various turbulent premixed combustion models for variation of fuel and pressure in RANS context on F-1 configuration are assessed. Also, the reaction closure (**A**lgebraic **F**lame **S**urface **W**rinkling Model) developed based on this experimental data is tested in LES on the same configuration.

In **Chapter 8**, the performance of the Algebraic Flame Surface Wrinkling (AFSW) model is investigated on more complex configurations using both RANS and LES

approaches. The preheated lean premixed turbulent flames investigated on a dump combustor (F-2 Configuration), in which a sudden expansion jet flow stabilizes the flame. Here, the pressure was varied between 1 and 14.4 bar. Owing to the complex flow configuration involving shear-generated turbulence exceeding the grid-generated turbulence by several folds, it has been interesting to validate the simulated non-reacting flow data with the corresponding available experimental data.

In **Chapter 9**, the applicability of the AFSW model on the ALSTOM gas turbine combustors for varied pressures and two different fuels and stoichiometric mixtures in both RANS and LES approaches is verified. Simulations are performed on two different configurations namely a conical swirl burner (F-3) and double-cone swirl burner (F-4). On the F-3 configuration, the reaction model performance for pressures as high as 32 bar in RANS context is tested. Also, the importance of Lewis number is demonstrated on this configuration. While on F-4 Configuration, both cold and reacting flow simulations are performed at atmospheric pressure using both turbulence approaches.

In **Chapter 10**, for hydrogen-doped fuel-air mixtures, the effects of preferential diffusion are discussed. Also, the sensitivity of the AFSW model to the enrichment effects is investigated. The ways to incorporate these effects are detailed for the future work.

In **Chapter 11**, the overall conclusions are drawn relating the whole of the current investigations.

2.   Description of Turbulent Reaction Flows

Combustion involves strong interaction between fluid mechanics, chemical reactions, and both heat and mass transfer. These phenomena are characteristically represented in conservation equations, given below. In the following, the modelling aspects of turbulent flows and turbulent combustion are elaborated. The models investigated in this work are particularly emphasized.

2.1   Turbulence

2.1.1   Characteristics of turbulence

It is rather easy to characterise the turbulent flows than giving a precise definition. Turbulent flow results when instabilities in a flow are not sufficiently damped by viscous action and all the variables of the flow exhibit random fluctuations (Turns 1996). Such a flow is comprised of many eddies with a multitude of time and length scales. In general, the size of the largest eddies is determined by the geometry of the flow configuration. These eddies extract the energy from the mean flow and fed to the small scales through cascading (Kolmogorov 1941). The smallest scales are dissipated due to viscous effects. The smallest of these eddies is given by the Kolmogorov (Kolmogorov 1941) length scale $\left(\eta_k\right)$ and these are determined by the amount of energy transferred along the energy cascade towards the small eddies and by the molecular kinematic viscosity of the fluid. The relevant turbulent scales for this study in descending order are the integral scale, Taylor and Kolmogorov micro scales, defined in the upcoming Sections.

General approaches to solve turbulent non-reacting and reacting flows are Direct Numerical Simulations (DNS), Large Eddy Simulation (LES), PDF-methods and RANS approach. The degree of complexity, lessening of accuracy and required computational resources slopes down from DNS to RANS.
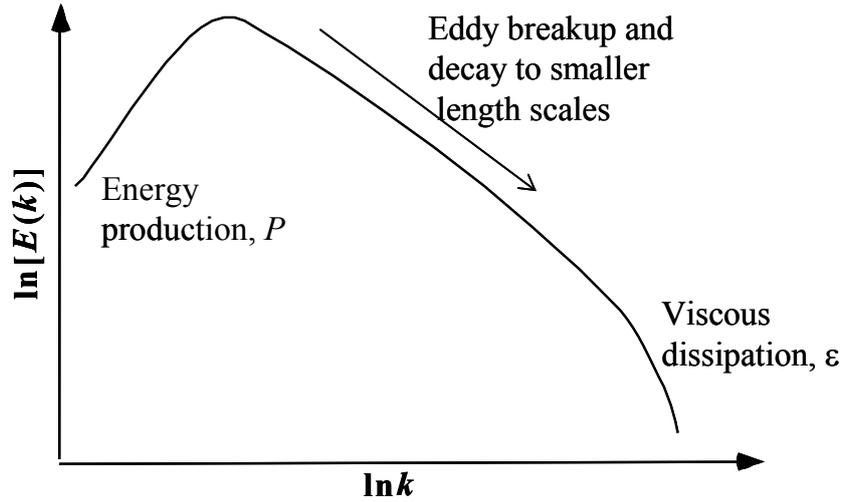
Figure 2.1: *Turbulent energy spectrum*

2.1.2 Turbulence modelling approaches

Reynolds averaged Navier-Stokes (RANS) Equations:

The classical approach to model a turbulent flow is based on Reynolds averaged Navier–Stokes (RANS) equations. In ensemble or Reynolds-averaging, the flow variables of a constant density flow are decomposed into mean and fluctuating components as

$$\bar{\phi} = \lim_{N \to \infty} \frac{1}{N} \sum_{1}^{N} \phi \; ; \quad \phi' = \phi - \bar{\phi} \tag{2.1}$$

But in variable density flows, Reynolds- averaging induces correlations of density and velocity fluctuations which require additional models. To avoid such complications, Favre- averaging (density weighted averaging) is applied for variable density flows

$$\tilde{\phi} = \frac{\overline{\rho\phi}}{\bar{\rho}} = \frac{\sum_{1}^{N} \rho\phi}{\sum_{1}^{N} \rho} \; ; \quad \phi'' = \phi - \tilde{\phi} \tag{2.2}$$

As this work is mainly devoted to combusting flows, the transport equations are given in Favre-averaged quantities. The governing equations with Favre averaged quantities in Cartesian coordinates (i, j = 1, 2, 3) are (Versteegh and Malalasekera 1995, Davidson 1998, Poinsot and Veynante 2001):

Continuity

$$\frac{\partial \overline{\rho}}{\partial t} + \frac{\partial \overline{\rho}\tilde{u}_i}{\partial x_i} = 0 \tag{2.3}$$

Momentum

$$\frac{\partial \overline{\rho}\tilde{u}_i}{\partial t} + \frac{\partial \overline{\rho}\tilde{u}_i\tilde{u}_j}{\partial x_j} = \frac{\partial \sigma_{ij}}{\partial x_j} - \frac{\partial p}{\partial x_i} - \frac{\partial \tau_{ij}}{\partial x_j} \tag{2.4}$$

where σ_{ij} is the molecular stress tensor and $\tau_{ij} = \widetilde{u_i'' u_j''}$ are the turbulent (or *Reynolds*) stresses.

Molecular stress tensor is given as

$$\sigma_{ij} = -\mu\left(\frac{\partial \tilde{u}_i}{\partial x_j} + \frac{\partial \tilde{u}_j}{\partial x_i}\right) + \delta_{ij}\frac{2}{3}\mu\frac{\partial \tilde{u}_k}{\partial x_k} \tag{2.5}$$

whereas, the turbulence model provides an approximation of the turbulent stress tensor, τ_{ij} . The details of the turbulence models are given in Section 2.2.

Chemical species (k=1 to N)

$$\frac{\partial \overline{\rho}\tilde{Y}_k}{\partial t} + \frac{\partial \overline{\rho}\tilde{u}_j\tilde{Y}_k}{\partial x_j} = -\frac{\partial \overline{\rho}\widetilde{u_j'' Y_k''}}{\partial x_j} - \frac{\partial \overline{\varsigma_j^k}}{\partial x_i} + \overline{\dot{\omega}}_k \tag{2.6}$$

Laminar diffusive fluxes $\overline{\varsigma_j^k}$ are usually small compared to turbulent fluxes and can be often neglected. It is common to close the turbulent fluxes $\widetilde{u_j'' Y_k''}$ with a gradient transport hypothesis as

$$\widetilde{u_j'' Y_k''} = -\frac{\mu_t}{Sc_t}\frac{\partial \tilde{Y}_k}{\partial x_j} \tag{2.7}$$

Where, μ_t is the turbulent viscosity and is estimated from the turbulence model and Sc_t is the turbulent Schmidt number. Despite of the evidence of counter gradient diffusion in experiments (Pfadler et al. 2005)and theoretically (Lipatnikov and Chomiak 2002) in premixed turbulent flames, the gradient approach is commonly used to close the turbulent fluxes, other approaches being the closure of second order moments (Lindstedt and Váos 1999). The last term on right hand side of Eq. (2.6) is the reaction source ($\bar{\omega}_k$). A major problem of modelling in premixed turbulent combustion is the closing of Eq. (2.6) with an appropriate model for the mean turbulent reaction rate $\bar{\omega}_k$, the current study focuses on this aspect.

A direct approach to close the reaction source term $\bar{\omega}_k$ is with Arrhenius formulation, but the non-linear characteristics of reaction rate coefficients and truncation errors in the expansion of the exponential term in the rate equation may introduce huge errors. Therefore, reaction rate closures are generally developed from physical analysis, for instance, on the basis of comparing chemical and turbulent time scales.

Direct Numerical Simulation (DNS):

To obtain a complete description of turbulence, it is required to resolve all the scales of turbulence, from the integral to the finest Kolmogorov length scale, as well as the time scales. In DNS, all these scales are resolved and hence no models are required. DNS (Poinsot et al. 1996, Cant 1998, Poinsot and Veynante 2001, Veynante and Vervisch 2002) is a 'numerical experiment' because of its ability to provide complete flow field information without any modelling.

The inherent drawback of DNS is its requirement of huge amount of computational resources. Additionally, high order discretization schemes are necessary to reduce the numerical error in the solution of the governing equations. Attention is also needed on providing turbulence boundary conditions. Despite of the rapid increase in the computational resources and techniques in the recent years, DNS still can be applied to low Reynolds number flows and simple geometries. Application of DNS to complex and huge configurations is seldom possible, as it requires extraordinarily huge computational resources. Therefore, a more soften procedure, the large eddy simulation, has been developed which yields acceptable accuracy within the manageable computational power requirements, relative to the ideal DNS approach.

Large Eddy Simulation:

As noted above, the intermediate approach between DNS and RANS is the Large Eddy Simulation (LES) (Ferziger 1996, Davidson 1998, Poinsot and Veynante 2001), which has become quite popular in the recent years. In LES, all large scales structures greater than the grid resolution are explicitly computed while the effect of scales is modelled using a subgrid model. The filtering process is schematically shown is Fig. 2.2.
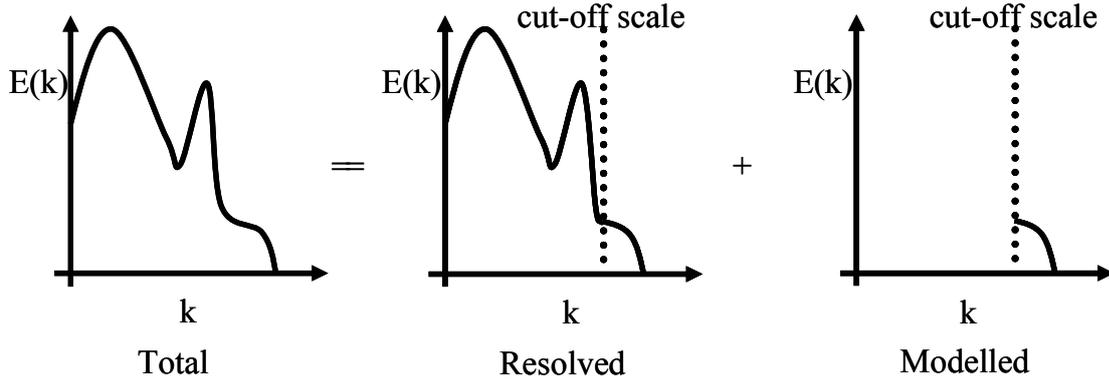
Figure 2.2: *Schematic of the filtering process in LES approach.*

In this approach, the time-dependent three-dimensional (filtered) continuity and Navier-Stokes equations describing the flow field are given in the spatially filtered form. As an illustration, a filtered variable is defined as

$$\tilde{\phi}(x) = \int_D \phi(x')G(x,x')dx' \qquad (2.8a)$$

where D is the fluid domain, G is the filter function determining the scale of resolved eddies. With the finite-volume discretization approach, the implicit filtering process is

$$\tilde{\phi}(x) = \frac{1}{V}\int_v \phi(x')dx' , \; x' \in v \qquad (2.8b)$$

where V is the cell volume. From these two above equations, the filter function is

$$G(x,x') = \begin{cases} 1/V & x' \in v \\ 0 & x' \, otherwise \end{cases} \qquad (2.9)$$

The filtering process effectively filters out eddies whose scales are smaller than the filter width or grid spacing used in the computations. The resulting equations thus

govern the dynamics of large eddies. These equations are integrated to the three-dimensional finite-volume solver, a general purpose CFD code FLUENT (Fluent 2005).

Filtering the instantaneous balance equations leads to equations formally similar to the RANS approach by replacing the averaged quantities with the filtered variables in Eq. (2.3) to (2.6). Similar to the RANS approach, the filtering process also introduces unclosed terms

$$\tau_{ij} = \overline{\rho} \left(\widetilde{u_j u_i} - \tilde{u}_j \tilde{u}_i \right) \tag{2.10}$$

which require modelling; the first term is the instantaneous product of two velocity components is not given from the set of equations.

2.2 Turbulence Models

2.2.1 Modelling Reynolds stresses

Boussinesq Hypothesis:

According to the Boussinesq theory, the turbulent terms can be modelled, analogous to molecular viscosity, Eq. 2.5, using turbulent viscosity, called eddy viscosity model. The Reynolds stress term $\tau_{ij} = \widetilde{u_i'' u_j''}$ is expressed in terms of eddy viscosity $v_t = \mu_t / \rho$ as

$$\widetilde{u_i'' u_j''} = -v_t \left(\frac{\partial u_i}{\partial x_j} + \frac{\partial u_j}{\partial x_i} \right) + \frac{2}{3} \left(k + \delta_{ij} v_t \frac{\partial u_k}{\partial x_k} \right) \tag{2.11}$$

where δ_{ij} is the tensorial Kronecker delta ($\delta_{ij} = 1$ for $i = j$ and $\delta_{ij} = 0$ for $i \neq j$). The kinematic eddy viscosity (v_t) requires modelling.

The standard $k - \varepsilon$ turbulence model:

The kinematic eddy viscosity (v_t) is related to the Favre-average turbulent kinetic energy ($\tilde{k} = \frac{1}{2} \sum_{k=1}^{2} \widetilde{u_k'' u_k''}$) and its dissipation $\tilde{\varepsilon}$ as

$$v_t = c_\mu \frac{\tilde{k}^2}{\tilde{\varepsilon}} \tag{2.12}$$

The standard $k-\varepsilon$ model (Jones and Whitelaw 1982) is a semi-empirical model based on model transport equations for the turbulence kinetic energy (k) and its dissipation rate (ε). The model transport equation for k is derived from the exact equation, while for ε it is obtained using physical reasoning and bears little resemblance to its mathematically exact counterpart.

The transport equation of the two quantities, turbulence kinetic energy, k, and rate of dissipation, ε, are:

$$\frac{\partial \bar{\rho} k}{\partial t} + \frac{\partial \bar{\rho} k u_j}{\partial x_j} = \frac{\partial}{\partial x_j}\left[\left(\frac{\bar{\rho} v_t}{\sigma_k}\right)\frac{\partial k}{\partial x_j}\right] + G_k + G_b - \bar{\rho}\varepsilon \qquad (2.13)$$

and

$$\frac{\partial \bar{\rho}\varepsilon}{\partial t} + \frac{\partial \bar{\rho}\varepsilon u_j}{\partial x_j} = \frac{\partial}{\partial x_j}\left[\left(\frac{\bar{\rho} v_t}{\sigma_\varepsilon}\right)\frac{\partial \varepsilon}{\partial x_j}\right] + C_{1\varepsilon}\frac{\varepsilon}{k}\left(G_k + C_{3\varepsilon}G_b\right) - C_{2\varepsilon}\bar{\rho}\frac{\varepsilon^2}{k} \qquad (2.14)$$

In these equations, G_k represents the generation of turbulence kinetic energy due to mean velocity gradients, calculated as $G_k = -\rho\overline{u_i' u_j'}\left(\partial u_j / \partial x_i\right)$. G_b is the generation of turbulence kinetic energy due to buoyancy, calculated as $G_b = \beta g_i\left(\mu_t / \mathrm{Pr}_t\right)\left(\partial T / \partial x_i\right)$, where $\mathrm{Pr}_t = 0.85$, g_i is the component of the gravitational vector in the ith direction, and $\beta = -(1/\rho)(\partial \rho / \partial T)_p$ is the coefficient of thermal expansion. In this approach, the turbulence is characterized by local values, being determined from modelled transport equations. Reynolds stresses are calculated by analogy with laminar flow, using a gradient transport assumption, with an eddy viscosity that is a function of $\tilde{k}$ and $\tilde{\varepsilon}$. And, $C_{3\varepsilon} = tanh|v/u|$, where v is the component of the flow velocity parallel to the gravitational vector, and u is the component of the flow velocity perpendicular to the gravitational vector. These assumptions are most appropriate in circumstances where near equilibrium has been achieved between production and dissipation. The model involves five empirical coefficients that are usually treated as universal constants. These constants $C_{1\varepsilon} = 1.44$, $C_{2\varepsilon} = 1.92$, and $C_\mu = 0.09$, turbulent kinetic energy Prandtl number $\sigma_k = 1.0$ and turbulent dissipation rate Prandtl number $\sigma_\varepsilon = 1.3$. These

default values were determined from experiments with air and water for fundamental turbulent shear flows including homogeneous shear flows and decaying isotropic grid turbulence. A number of numerical studies indicate its broad range of applicability for various degrees of complexity.

2.2.2 Modelling subgrid scale stresses

As a straightforward evaluation of the subgrid-scale stresses τ_{ij} of Eq. (2.10), introduced by filter process in LES approach is not possible, these quantities require modelling. In this study, three sgs turbulence closures are employed for closing Eq. 2.10, being developed based on the Boussinesq hypothesis. They are the Smagorinsky model with both classical and dynamic approaches and the 1-Equation model for the subgrid scale turbulence kinetic energy $\left(k_{sgs}\right)$.

The Smagorinsky sgs turbulence closure:

Smagorinsky (Smagorinsky 1963) was the first to propose the closure for the sgs stresses, assuming Boussinesq hypothesis. With

$$\tau_{ij} - \frac{1}{3}\tau_{kk}\delta_{ij} = -2\mu_t \tilde{S}_{ij} \tag{2.15}$$

where μ_t is the subgrid-scale turbulent viscosity, and $\overline{S_{ij}}$ the strain rate tensor, which is defined in terms of the components of the resolved shear stresses and given as

$$\tilde{S}_{ij} \equiv \frac{1}{2}\left(\frac{\partial \tilde{u}_i}{\partial x_j} + \frac{\partial \tilde{u}_j}{\partial x_i}\right) \tag{2.16}$$

Following the Smagorinsky model, the eddy viscosity is expressed as

$$\mu_t = \rho \, L_s^2 \left|\tilde{S}\right| \tag{2.17}$$

with

$$L_s = C_s \, V^{1/3} \tag{2.18}$$

$$\left|\tilde{S}\right| \equiv \sqrt{2\tilde{S}_{ij}\tilde{S}_{ij}} \tag{2.19}$$

where, L_s, the mixing length for subgrid scale, V is the volume of the computational cell, and $\left|\tilde{S}\right|$ is the strain rate magnitude of the resolved large scale flow. This relation serves as an inter-link between unresolved subgrid and resolved large-scale structures in the transfer of energy. The Smagorinsky constant $C_s = 0.1$ is used in this present study.

Following Lilly (Lilly 1992), and Germano (Germano et al. 1996), the Smagorinsky constant can be computed dynamically based on the information provided by the resolved scales of motion. The obtained constant varies in time and space over a fairly wide range. In the current solver, it is clipped between 0 and 0.23 to avoid numerical instability.

The two versions of the Smagorinsky model are algebraic models in which the subgrid scale stresses are closed using the resolved velocity scales. The underlying assumption of these models is the local equilibrium between the energy transfer through the filter scale and the dissipation of kinetic energy at the subgrid level.

The dynamic kinetic energy subgrid scale model:

An alternative to the eddy viscosity closure is a localized dynamic approach for the subgrid kinetic energy (Kim and Menon 1997). This model is based on the transport equation for the subgrid kinetic energy.

The subgrid stresses can be better modelled by accounting for the transport of the sgs turbulence kinetic energy.

$$\frac{\partial}{\partial t}(\overline{\rho}k_{sgs}) + \frac{\partial}{\partial x_j}(\overline{\rho}\tilde{u}_j k_{sgs}) = P_{sgs} - D_{sgs} + \frac{\partial}{\partial x_j}\left(\frac{\overline{\rho}\nu_t}{Pr_t}\frac{\partial k_{sgs}}{\partial x_j}\right) \qquad (2.20)$$

where $k_{sgs} = \left(\overline{u_k^2} - \overline{u}_k^2\right)/2$ is kinetic energy, Pr_t is the turbulent Prandtl number. The terms on the RHS of Eq. 2.22 represent, respectively, the production, the dissipation, and the transport of the subgrid kinetic energy.

The production term is modelled as

$$P_{sgs} = -\tau_{ij}^{sgs}\frac{\partial \tilde{u}_i}{\partial x_j} \qquad (2.21)$$

and the subgrid shear stresses τ_{ij}^{sgs} are evaluated as

$$\tau_{ij}^{sgs} = -2\bar{\rho}\nu_t\left(\tilde{S}_{ij} - \frac{1}{3}\tilde{S}_{kk}\delta_{ij}\right) + \frac{2}{3}\bar{\rho}k_{sgs}\delta_{ij} \qquad (2.22)$$

ν_t is the eddy viscosity and modelled as

$$\nu_t = C_k\sqrt{k_{sgs}}\bar{\Delta} \qquad (2.23)$$

The dissipation term is modelled as

$$D_{sgs} = C_\varepsilon\bar{\rho}\left(k_{sgs}\right)^{3/2}\Big/\bar{\Delta} \qquad (2.24)$$

The constants C_k and C_ε are determined dynamically (Kim and Menon 1997).

These set of equations are solved for the solution of isothermal flows. For the reacting case, extra species equations should be solved which are coupled to the previous set of equations describing the flow field through density.

2.3 Principles of Combustion

2.3.1 Basic flame classification

Combustion processes are usually categorized as premixed and non-premixed (or diffusion) flames depending on the location of mixing of the reactants. In non-premixed combustion (diffusion flames), the fuel and the oxidizer are initially separated, mixing and oxidation occurs simultaneously at the interface of the fuel and oxidizer streams. In distinction to this, the fuel and the oxidizer in premixed combustion are mixed prior to the reaction.

Another classification of combustion is based on the flow characteristics as laminar and turbulent combustion. In both laminar and turbulent flames, the same physical processes are active, and many turbulent flame theories are based on an underlying laminar flame structure.

2.3.2 Characteristics of laminar flames

Laminar premixed flames:

In premixed flames, a thin reaction zone separates the fresh and the burned gases. The general characteristics of the laminar premixed flame are sketched in Fig. 2.3. A premixed flame has the ability to propagate towards the unburned mixture. Due to the temperature gradient and the corresponding thermal fluxes, fresh gases are preheated and then start to burn. The local imbalance between diffusion of heat and chemical consumption leads to propagation of the flame front. The propagation speed s_{L0} of a laminar depends on various parameters such as equivalence ratio, fresh gas temperature, and pressure.
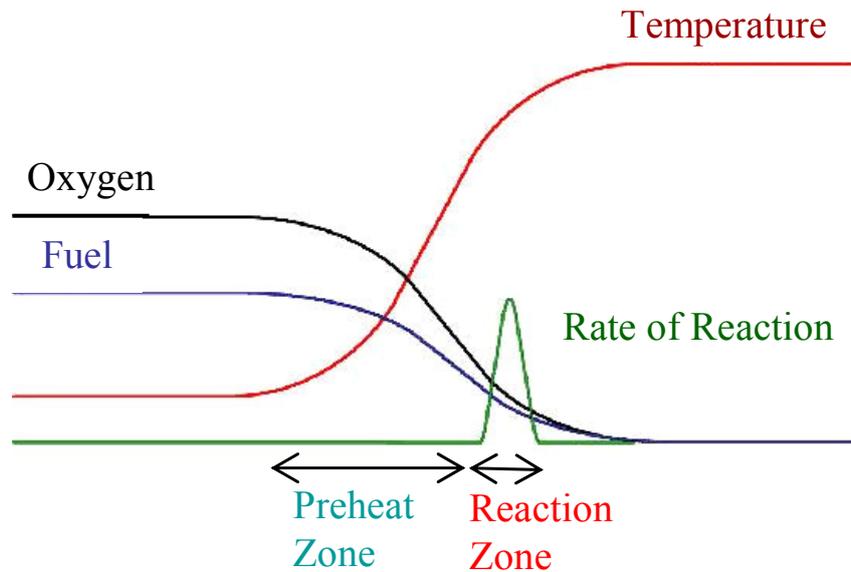
Figure 2.3: *Characteristics of laminar premixed flames.*

A premixed flame can be described with a progress variable *c* (Bray et al. 1985), being conditioned as *c* = 0 in fresh gases and *c* = 1 in completely burnt gases, see (Cant et al. 1990b) where the below relation's validity was discussed at length.

$$c = \frac{T - T_u}{T_b - T_u} = \frac{y_F - y_F^u}{y_F^b - y_F^u} \qquad (2.25)$$

where T, T_u and T_b are the local, the unburned gas and the burned gas temperatures respectively. y_F, y_F^u and y_F^b denotes the local, the unburned and burned fuel mass fractions.

Laminar diffusion flames:

In diffusion flames, the reaction zone lies in the interface of fuel and oxidiser streams. The burning process is controlled by molecular diffusion of the reactants towards the reaction zone. The temperature, fuel and oxidiser distribution in the flame are depicted in Fig. 2.4.
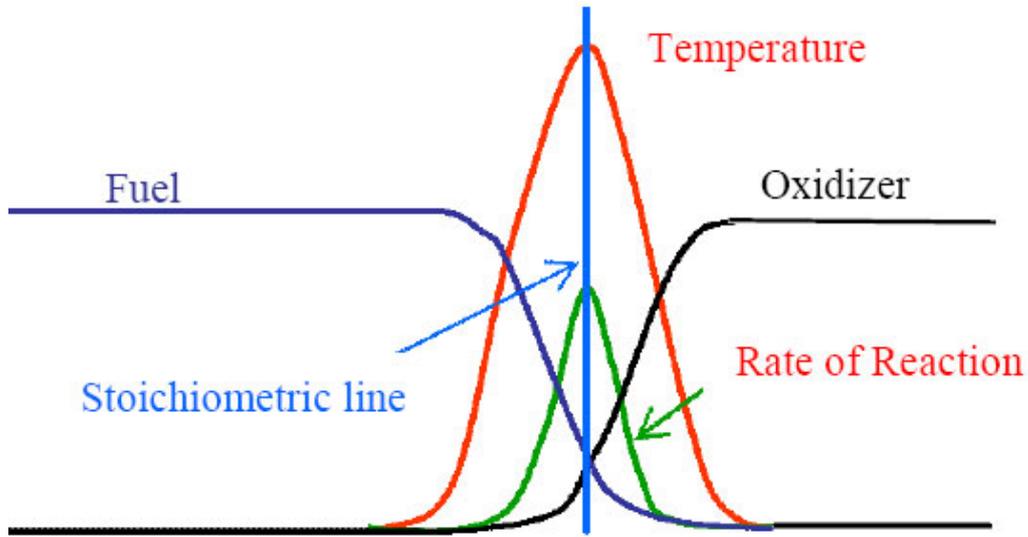
Figure 2.4: *Distribution of species and temperature in laminar diffusion flames.*

Mixing processes control a diffusion flame and its precise flame thickness is not definable. Combining the transport equation for fuel and oxidiser, a conserved scalar, $\varphi(y_F, y_O) = y_F - y_O/s$, is defined which is not influenced by chemical reaction. $s = (v_0 W_O / v_F W_F)$ is the mass stoichiometric coefficient. The mixture fraction Z is then defined by normalising φ, using values in the fuel and oxidiser streams. $y_{F,0}$ is the fuel mass fraction in the fuel feeding stream, $y_{O,0}$ is the oxidizer mass fraction in the oxidizer stream, ϕ is the equivalence ratio.

$$Z = \frac{\phi \dfrac{y_F}{y_{F,0}} - \dfrac{y_O}{y_{O,0}} + 1}{\phi + 1} \tag{2.26}$$

$$\phi = \frac{s y_{F,0}}{y_{O,0}} \tag{2.27}$$

2.3.3 Characteristic scales

Turbulent combustion is encountered in most practical combustion systems such as gas turbine burners, internal combustion engines, aircraft engines and so on and so forth. As turbulence enhances the mixing and thereby combustion reactions, the size of the combustor is greatly reduced compared to the laminar situation. As mentioned in § 2.1.2, direct modelling of the source terms of the species is not possible, so these should be modelled using physical analysis, comparing chemical and turbulent time scales.

In general, instead of solving all the species equations, turbulent premixed and non-premixed flames are often analysed with the progress variable c, and the mixture fraction Z equations, respectively. The enclosed terms arising either due to averaging or filtering process of these scalars should be modelled and in general is done with the above said physical analysis.

Turbulent combustion involves various lengths, velocity and time scales describing turbulence and chemical reactions. The physical analysis is mainly based on comparison between these scales. The important dimensionless numbers characterising these scales used are defined here:

Turbulent Reynolds number:

It is used to characterise turbulent flows comparing the turbulent transport to the viscous forces and is given as

$$Re_T = \frac{u' l_x}{\nu} \tag{2.28}$$

where u' is the turbulent velocity, l_x is the turbulence integral length scale and ν the kinematic viscosity of the flow.

Damköhler number:

It is the ratio of the turbulent $\left(\tau_t = l_x / u'\right)$ to chemical time $\left(\tau_c = \delta_l / s_{L0}\right)$ scales; where δ_l is the laminar flame thickness and s_{L0} is the laminar flame speed.

$$Da = \frac{\tau_t}{\tau_c} = \frac{l_x}{\delta_l} \frac{s_{L0}}{u'} \tag{2.29}$$

If, $Da \gg 1$, chemical time is short compared to turbulent time, this corresponds to a thin reaction which is distorted and convected by the flow field. The internal structure of the flame is not strongly affected by turbulence and may be described as a laminar flame element called a 'flamelet'. The turbulent structure wrinkle and strain the flame surface.

If $Da \ll 1$, chemical reaction is slow; turbulence mixes the reactants and products before reaction, so named as perfectly stirred reactor limit. In this limit the mean reaction rate can be expressed from Arrhenius laws using mean mass fractions and temperature.

Karlovitz number:

This corresponds to the smallest (Kolmogorov) eddies and is the ratio of chemical time scale to the Kolmogorov time and given as

$$Ka = \frac{1}{Da(\eta_k)} = \frac{\tau_c}{\tau_t} = \frac{u'(\eta_k)/\eta_k}{s_{L0}/\delta_L} = \frac{\sqrt{\varepsilon/v}}{s_{L0}/\delta_L} \qquad (2.30)$$

These three numbers are semi-empirically correlated as

$$\text{Re}_T = Da^2 Ka^2 \qquad (2.31)$$

These non-dimensional numbers are extensively used in modelling and characterisation of turbulent flames.

3. Turbulent Premixed Flames

The nature of premixed turbulent flames (Williams 1985, Peters and Vervisch 2001) depends on the length and time scales in the flame front and in the turbulent flow field. In order to understand and model the premixed flames, the knowledge of their behaviour and interaction with scales of different magnitudes is important.

3.1 Regime Diagram of Premixed Turbulent Combustion

Basing on the dominance of the physical and chemical time scales, different combustion regimes are identified. These are usually represented in the regime diagram proposed by Borghi (Borghi 1985) and recently extended by Peters (Peters and Vervisch 2001). Different regimes are depicted in Fig. 3.1.
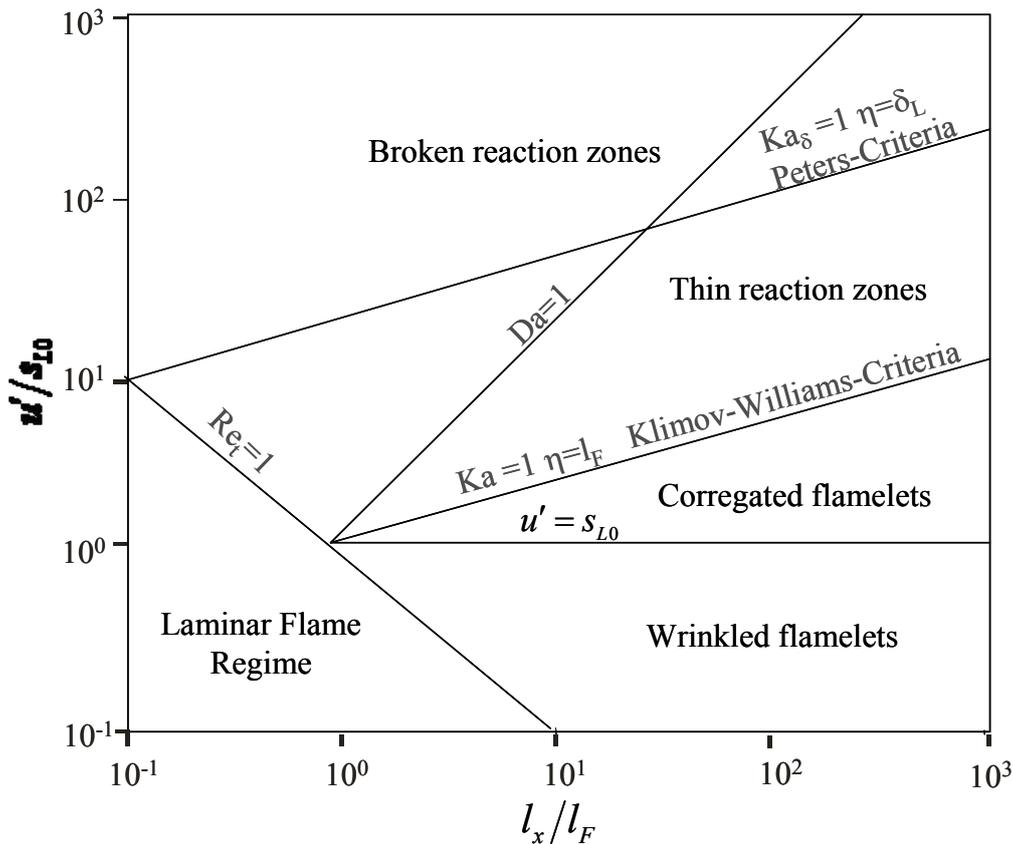
Figure 3.1: *Classical premixed combustion regime diagram; regimes are identified in terms of length $\left(l_x/l_F\right)$ and velocity $\left(u'/s_{L0}\right)$ ratio in a log-log plot.*

The area below $Re_t = 1$ line corresponds to the laminar flame regime. Below the $u' = s_{L0}$ line is the wrinkled flamelet regime where the velocity of the largest eddy is

less than the laminar flame speed. The regime bounded by $Ka = 1$ and $u' = s_{L0}$ lines is called the corrugated flamelet regime and the flame thickness l_F is thinner than the Kolmogorov length scale η (see § 2.1 for definition). The turbulence eddies can only wrinkle but cannot penetrate into the flame front.

The region between $Ka_\delta = 1$ (or equivalently, $Ka = 100$) and $Ka = 1$ corresponds to thin reaction zone; in this region η is equal to the inner layer thickness. According to Peters (Peters 1986), in this region the Kolmogorov eddies can enter into the preheat zone but cannot penetrate into the reaction zone. Thus, it is called thickened-wrinkled regime. The region above the line $Ka_\delta = 1$, lies the broken reaction zone, in which both the preheat zone and inner layer are disturbed by the turbulence eddies, where the thin flame assumption is no longer valid.

This diagram is extended to LES by (Pitsch and Lageneste 2002, Düsing 2004a) and formulated in terms of quantities and plotted for (Δ/l_F) to Ka at the filter level, see Fig. 3.2.
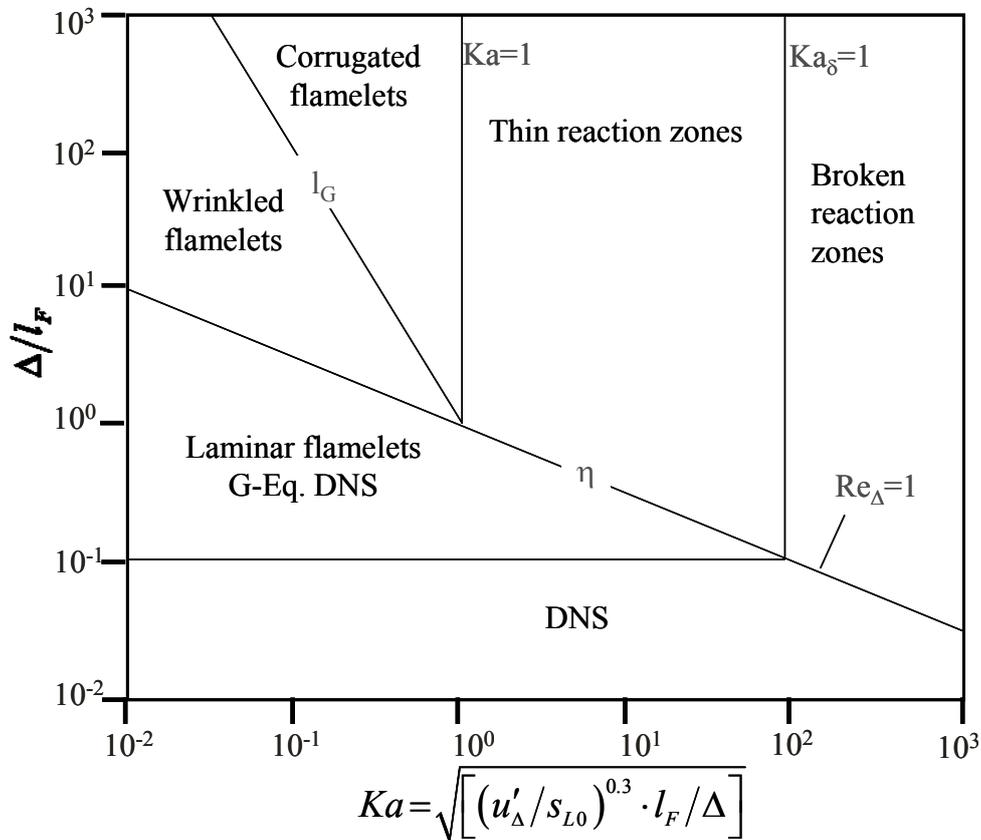
Figure 3.2: *LES regime diagram. The non-dimensional filter width is plotted as a function of the Karlovitz number.*

22

3.2 Reaction Progress Variable Approach

Numerical calculation of turbulent premixed flames is in general a non-trivial task due to the strong interaction between fluid flow, laminar, and turbulent transport and reaction processes. Typically, for non-reacting flows the coupled partial differential equations for the balance of the average of mass, momentum and turbulence parameters are solved, while for the calculation of flames, additional equations for species and energy are included. A common approach for turbulent premixed flames, as noted above, is the use of a mean reaction progress variable $\bar{c}$, describing the probability to find burned gas. The average reaction zone position is described by the increase of this property from 0 in the unburned mixture to 1 in the products. Taking adiabatic flame conditions (neglecting radiation) and fast reaction, as can be assumed to a first order approximation at least in non-sooting premixed flames, the average temperature and density follow as a function of the reaction progress variable c (e.g., (Bray et al. 1985)).

For combustion calculations the use of density-weighted (Favre-averaged) properties $\tilde{\varphi} = \overline{\rho \varphi} / \bar{\rho}$ is convenient, (with the decomposition $\varphi = \tilde{\varphi} + \varphi''$), having the advantage that the set of equations for mass and momentum of incompressible flows can be applied for the calculation of reacting flows (Jones and Whitelaw 1982). For comparative analysis with experiments, the calculated density-weighted results need to be transformed to the Reynolds-averaged quantities in a post-processing step (possible only for c not for velocity etc).

The balance equation for the Favre-averaged reaction progress variable c (see § 2.3.2 for definition) is given by

Progress variable

$$\frac{\partial \bar{\rho}\tilde{c}}{\partial t} + \frac{\partial \bar{\rho}\tilde{u}_j\tilde{c}}{\partial x_j} = \frac{\partial}{\partial x_j}\left(\bar{\rho}\bar{D}\frac{\partial \tilde{c}}{\partial x_j} - \overline{\rho u_j'' c''}\right) + \bar{w}_c \qquad (3.1)$$

where t is the time, x_j and u_j are the coordinates and the flow components, $\bar{\rho}$ is the gas density and $\bar{w}_c$ is the mean reaction source term. This equation requires the

modelling of the turbulent transport term (second term on the right hand side), and the mean reaction source term. For the turbulent transport the common turbulent gradient diffusion approach with turbulent kinematic viscosity ν_t and Schmidt number $Sc = 0.7$ is used

$$\widetilde{u_j'' c''} = -\frac{\nu_t}{Sc_t} \frac{\partial \tilde{c}}{\partial x_j} \tag{3.2}$$

In both RANS and LES contexts, the scalar fluxes are closed using the gradient approach. The primary focus of the current work is to develop and test the source term $\overline{\dot{w}_c}$ of the progress variable both in RANS and LES. There exists variety of models to close $\overline{\dot{w}_c}$ deduced from different approaches.

3.3   Reaction Modelling Approaches

In general, the chemical and hydrodynamic structure of a stretched laminar premixed flame can be preserved in a turbulent flow field over a range of conditions collectively known as the flamelet regime, and the premixed combustion in most of the practical devices falls within the domain of this regime. The major assumption in the laminar flamelet concept as applied to the turbulent premixed flames is that the flame front behaves as a constant-property passive scalar surface, and an increase in the wrinkled flame surface area with increasing turbulence intensity is the dominant mechanism for the observed flame velocity enhancement. For high Damköhler number Da, a premixed flame consists of reactants and products separated by thin laminar flamelets. Since the instantaneous behaviour of these thin layers is same as those of laminar flames, turbulent flame speed s_T can be approximated by the product of the flamelet surface area and laminar flame speed s_{L0} corrected for the effect of stretch and flame curvature by I_0, and the reaction rate is expressed as

$$\overline{\dot{w}_c} = \rho_u \, s_{L0} \, I_0 \, \Sigma \tag{3.3}$$

where, ρ_u is the reactant unburned density, s_{L0} the unstretched laminar flame speed, I_0 is the mean stretch factor. In this study, I_0 is normally set to 1.0. Modelling Σ, the flame surface density is the essential part of turbulent premixed flamelet models.

One major advantage of this approach is in decoupling chemistry from the flame-turbulence interaction described by Σ (flame surface-to-volume ratio), ρ_u is the unburned gas density and the factor I_0 includes the effects of flame stretch (Bray et al. 1985).

Several reaction models exist in the literature, which have been derived, based on physical argumentation for e.g., (Peters 2000), or through phenomenological approaches (see below for relevant citations). Here, only the ones relevant to this study are partially addressed, while the associated model development issues are discussed in detail.

3.3.1 Algebraic Flame Surface Wrinkling (AFSW) model

Following the algebraic approach, the flame surface density may be modelled with an algebraic relation for the flame-surface-wrinkling factor $A_T / \overline{A}$, the ratio of turbulent flame surface per unit volume A_T to its projection on its average surface per unit volume $\overline{A}$

$$\Sigma(x) = \frac{A_T}{\overline{A}} \cdot \frac{1}{L} \cdot P(x) \tag{3.4}$$

Here, L stands for the flame brush thickness, in which the average reaction zone is placed, and $P(x)$ describes the probability to find the flame front at location x. As an approximation, the last two terms can be described by the gradient of the reaction progress variable $|\nabla \tilde{c}|$. The ratio $A_T / \overline{A}$ may be related to the ratio of turbulent to laminar flame speed (s_T / s_{L0}), following *Damköhler* (Damköhler 1940). This implies a relation to the turbulent flame speed closure (TFC) approach of *Zimont* and *Lipatnikov* (Zimont and Lipatnikov 1995), where the turbulent flame speed is calculated with an algebraic approach (see for instance (Dinkelacker and Hölzler 2000, Muppala and Dinkelacker 2004)). The closure is directly applied to the flame-wrinkling ratio $A_T / \overline{A}$, leading to

$$\overline{w}_c = \rho_u \, s_{L0} \, \frac{A_T}{\overline{A}} \cdot \left| \nabla \tilde{c} \right| \tag{3.5}$$

The flame-wrinkling ratio (also equal to ratio of turbulent to laminar flame speed, according to the Damköhler's hypothesis (Damköhler 1940)) is modelled (Muppala et al. 2005b, Aluri et al.) with an algebraic flame surface parameterized relation given as

$$\frac{A_T}{\overline{A}} \sim \frac{s_T}{s_{L0}} = 1 + \frac{0.46}{e^{(Le-1)}} \cdot \mathrm{Re}_t^{\,0.25} \cdot \left(\frac{u'}{s_{L0}} \right)^{0.3} \cdot \left(\frac{p}{p_0} \right)^{0.2} \tag{3.6}$$

where p/p_0 is the ratio of the operating pressure to the atmospheric pressure, *Le* is the Lewis number. The importance of the Lewis number and other molecular effects are detailed in chapter 4. The concluded $exp(Le-1)$ relation was indeed extracted based on the substantiation (see Appendix: A1) of a relatively well known reaction model by Lindstedt and Vaos, the details of which are given below.

3.3.2   The reaction rate model by Lindstedt and Váos

This reaction closure hereafter is noted using the first initials of the original contributors as LV model. Of many possibilities in modelling this complex term Σ (for e.g., (Bray 1980, Gouldin 1987, Kerstein 1988, Duclos et al. 1993, Weller et al. 1994, Zhao et al. 1994, Peters 2000)), including the progress variable gradient approaches (Zimont and Lipatnikov 1995, Muppala et al. 2005b), the fractal concept from which the LV reaction model derived is discussed in the following. It was developed on the assumption that the flame surface geometry is fractal (Gouldin 1987), following a self-similarity power law between an inner and an outer cut-off scale. The fractal theory was applied in order to evaluate the increase in flamelet surface area by turbulent eddies. According to this theory the mean flame surface density $<\Sigma>$ is

$$<\Sigma> \equiv A/l^3 \; \frac{1}{l} \left(\frac{\varepsilon}{l} \right)^{2-D} \tag{3.7}$$

with $2 < D < 3$. For its compatibility with the diffusive/dissipative characteristics of passive or reactive scalars, a finite limit for the surface area is established, with an inner cut-off ε_i introduced such that $l_x \geq \varepsilon \geq \varepsilon_i$. Gouldin (Gouldin and Dandekar 1984) has argued to identify the inner cut-off scale as the Kolmogorov length scale (i.e., $\varepsilon_i = l_k$). Similarly, to accommodate for the geometrical constraints, the largest self-similar scales of wrinkling is related to the l_x, with outer cut-off $\varepsilon_o \cong l_x$, so that $l \geq \varepsilon_o \geq \varepsilon \geq \varepsilon_i$. To ensure isotropicity and for l to be at least equal to the expected largest scale of wrinkles, it leads to $l = \varepsilon_o = l_x$. Thus,

$$< \Sigma > \propto \frac{1}{l_x} \left(\frac{l_k}{l_x} \right)^{2-D} P_R \qquad (3.8)$$

where P_R is the probability of reaction occurring within the volume under consideration. For the probability of reaction, following (Gouldin et al. 1989), Lindstedt and Váos used the empirical relation satisfying the extremum flame boundary conditions $c = 0$ and $c = 1$ across the flame front for the flamelet regime of combustion:

$$P_R = \tilde{c}(1 - \tilde{c}) \qquad (3.9)$$

Lindstedt & Sakthitharan (Lindstedt and Sakthitharan 1991) proposed D equal to 7/3 = 2.33. Substituting this value Eq. (6), with the introduction of Kolmogorov velocity V_K and assuming $l_x \propto \tilde{k}^{3/2}/\tilde{\varepsilon}$, the Lindstedt–Váos (LV) reaction model is (Lindstedt and Váos 1999)

$$\bar{w}_c = C_R \rho_u \frac{s_{L0}}{V_K} \frac{\tilde{\varepsilon}}{\tilde{k}} \tilde{c}(1 - \tilde{c}) \qquad (3.10)$$

where C_R is the model constant.

The critical assumption implicit in the derivation of above expression is that vortices of all sizes between the integral and the inner cut-off Kolmogorov length scales (Gouldin 1987) contribute to the wrinkling of the flame surface. *Gülder et al.* (Gülder et al. 2000) found from other experiments the fractal dimension D to be 2.2, rather

than 2.33 used in the LV model (see also (Gülder and Smallwood 1995, Charlette et al. 2002)). Other expressions found in literature relate the inner cut-off to the Gibson scale (Peters 1986), or the laminar flame thickness δ_L (Murayama and Takemo 1988). The quantity s_{L0}/V_K is stated to represent the relation between reacting (laminar flame propagating with s_{L0}) and passive scalars (turbulent mixing). Lindstedt and Váos set the reaction rate parameter C_R =2.6 to reach quantitative agreement with counter flow experiments (Lindstedt and Váos 1999). The exact value seemed to depend on the flame geometry (Váos 1998). Additionally, it should be noted, that Lindstedt and Váos modelled the turbulent flux term with a second moment closure, while in the following study a simpler eddy viscosity approach is used. Váos investigated the cross-influence between turbulent flux model and reaction model (Váos 1998). For an increased C_R value, the simple eddy viscosity approach gave reasonable results (C_R=3.25 for the eddy viscosity approach compared to C_R=1.5 for the second moment closure for the discussed experimental data (Abdel-Gayed et al. 1984)). Therefore, the eddy viscosity closure for turbulent flux in the combustion progress variable transport equation is an acceptably practised approach, at least as long as the prediction of flame brush thickness is not the central focus.

The reaction model by Lindstedt and Vaos has been numerically investigated (Lindstedt and Váos 1999) for its range of extendibility using an extensive datasets from Kobayashi, consisting of three fuels, three equivalence ratios, over a wide range of turbulence conditions.

4. Molecular Transport Effects and Dynamics of Premixed Flames

In turbulent flames, the flame speed depends on both kinetics and the local turbulence. The turbulent flame speed s_T is influenced by the following factors in varied amount depending on the situation:

- Fuel composition (equivalence ratio)
- Turbulence
- Fuel type (Lewis Number of the fuel air mixture)
- Preferential diffusion effect
- Operating pressure

This chapter deals with the latter three effects, being related to molecular transport effects (thermal diffusion, species diffusion of the individual components).

4.1 Importance of Lewis Number in Premixed Combustion

The Lewis number is defined commonly as the ratio of thermal diffusivity α to species diffusivity D of that reactant, which is in the minority. For lean fuel/air mixtures this is normally the diffusivity of the fuel. $Le = \alpha / D_{minor}$. For lean methane flames the thermal diffusivity is nearly similar to the molecular diffusivity of the fuel, leading to a near-unity Lewis number. For larger hydrocarbon fuels the molecular diffusivity is reduced, leading to Lewis numbers above one, while for instance for lean hydrogen/air flames the Lewis number is significantly below one.

An important effect of the Lewis number Le, consists in the duration of flame quenching by strain. The long duration of the quenching implies that the (expanding / unsteady) flame characterized by large Le values can survive under relatively intense oscillating strain, as compared with a steady one. For e.g., a flame can survive under oscillating strains even if the amplitude of these oscillations are two times higher than the critical steady strain rate. DNS (Trouvé and Poinsot 1994) shows that the Le effects are of more importance for the flame surface area, rather than for the consumption velocity; such effects have not been elaborated yet.

Its effect is directly connected to the molecular heat and mass transport into and away from the reaction occurring flame zone. The flame velocity decrease occurs for $Le > 1$, because thermal diffusivity exceeds molecular diffusivity. Therefore, the rate of heat losses from the reaction zone exceeds the rate at which the reactant is transported into the reaction zone. Hence the enthalpy and consequently the temperature decreases in the reaction zone while both increase in the preheat zone. Since flame velocity depends exponentially on temperature, this causes the decrease in flame velocity. The increase of enthalpy and temperature in the preheat zone results in an accelerated ignition of the reactant at the interface between preheat zone and reaction zone. This is a velocity increasing effect that counteracts the first, but to a lesser degree with increase in Le value.

Phenomenon of local flamelet quenching by turbulent eddies must substantially depend on the Lewis number, according to the theory. It is worth-noting that even the premixed turbulent combustion analysis by Peters (Peters 2000) does not include of molecular transport property Lewis number into scaling laws in combustion. For higher Lewis number fuel-air mixtures ($Le > 1$), maximum growth rate and the wave number at the maximum growth rate are much smaller that for near-unity Le fuel-air mixtures. This is due to the effects of large Le, which enhances the diffusive thermal effects to restrain the flame instability. Smaller maximum growth rate and smaller wave number at the maximum growth rate cause the smaller increase in total flame area, resulting in smaller increase in turbulence flame propagation, having, for example, application in lean burning automotive engines.

The exponential dependency $1/exp(Le-1)$ is consistent with the Leading Point Model by Lipatnikov and Chomiak (Lipatnikov and Chomiak 2005). Salient features of this model, that goes in par with the proposals made in (Lipatnikov and Chomiak 2005), are:

a) Premixed turbulent flame propagation is considered to be controlled by the flamelets that advance farthest into the unburned mixture (the so-called leading points).

b) The leading flamelets are assumed to have an inner structure same as a critically perturbed laminar flame. A critically curved laminar flame is invoked to model the inner structure the leading flamelets.

c) Accordingly, s_T is controlled by the characteristics of the critically curved laminar flame.

d) Recent theory shows that the burning rate in the unperturbed planar laminar flame by a factor of $exp(1-Le)$ (Lipatnikov and Chomiak 2005).

e) These above formulations lead to the deduction that s_T is proportional to $exp(1-Le)$.

See § 7.4.1 for an important application of Le effect on the anomalous flame behaviour under some conditions, in a complex combustor configuration.

4.2 Preferential Diffusion Effects

The effect of the preferential diffusion (PD) is observed for the cases when diffusivity difference of the fuel from the oxidizer is distinct and the concentration of a larger diffusivity species of the fuel or oxidizer is deficient. Characteristically, preferential diffusion is evaluated using for example the local burning velocity and the local equivalence ratio. These two quantities are evaluated at the so-called leading point of the flame with positive curvature on the downstream of the flame, i.e., facing towards the unburned premixed mixture. These two quantities are expected to qualify the leading flamelet of highest flame propagation (Lipatnikov and Chomiak 1998, Muppala and Papalexandris 2006). Its significance is imminent in, for example, lean and rich light and heavy fuel-mixtures. Also, its importance is evident at high turbulence and for low laminar flame speeds. It is worth noting that the influence of the PD effect diminishes with higher unstretched laminar flame speed, because, higher its value, greater is the Damköhler number, which means that the flame falls into the laminar flamelet regime.

Here, the role of PD and/or Le in premixed combustion is demonstrated with a schematic of a curved flame in Fig. 4.1a. Due to the higher influx[1] (see Fig. 4.1a) of premixed unburned gas mass flow along the dominant convex part directing towards the inflow unburned gas as compared to that at the convex part directing towards the burned gas, it can be inferred that the change in the local equivalence ratio at this dominant part can possibly cause an effect as if equivalence ratio in the whole combustion field had changed, see Fig 4.1b. In addition, the changes in the equivalence ratio can bring forth the change in the (mean) local burning velocity of turbulent flame. It was also experimentally demonstrated in (Nakahara 2006) that the preferential diffusion is the most probable cause leading to the change of local equivalence ration at this dominant part as follows. In the turbulent combustion field of multi-reactant system with diffusivity of the fuel not equal to the diffusivity of oxidant (see Fig. 4.1b), the higher diffusive reactant can reach this dominant part of flame more rapidly than the lower diffusive one, caused by the preferential diffusion. Therefore, the flame wrinkles caused by turbulence induce local equivalence ration variations. The dominant parts convex toward the unburned gas are relatively enriched with the higher diffusive reactant, leading to change in the local equivalence ratio. This change inevitably leads to the change in the local burning velocity which is the same as the laminar flame speed in the case of no turbulence. Therefore, apparently, the mean equivalence ratio and the local burning velocity in the whole turbulent combustion field are changed from the original equivalence ratio and the laminar flame speed, respectively, caused by the preferential diffusion. Because, in the case of $Le<1$ mixtures, the turbulent burning velocity and local burning velocity are much affected by PD or Le, and are more changed than $Le>1$ mixtures. As a matter, of course, as $Le<1$, molecular diffusivity is more dominant in turbulent flames than

---

[1] Fig. 4.1a is an illustration of unburned gas flow consumed by a turbulent flamelet. It is reasonable to suppose that unburned premixed gas would flow along the streamlines toward the flame and these lines are positioned perpendicular to the flame sheet. From a geometrical consideration of the region of volume AA'B'B, the ratio of mass flow passing into the convex part BC toward the unburned gas to that into the convex part AC toward the burned gas can be approximated as 3:1. Thus, the convex part of the flamelet toward the unburned gas can possibly play an important role, governing the characteristics of whole combustion field, and so affect s_T predominantly (Nakahara 2006).

thermal diffusivity. This indicates that the molecular transport such as preferential diffusion is dominant in determining the local burning velocity.
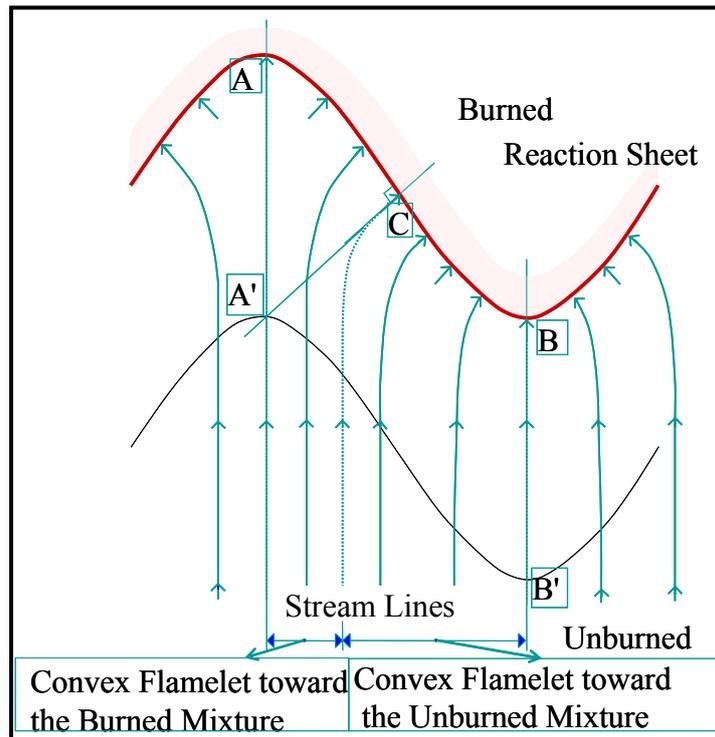
Figure 4.1a: *Schematic illustration of stream lines toward the flame*
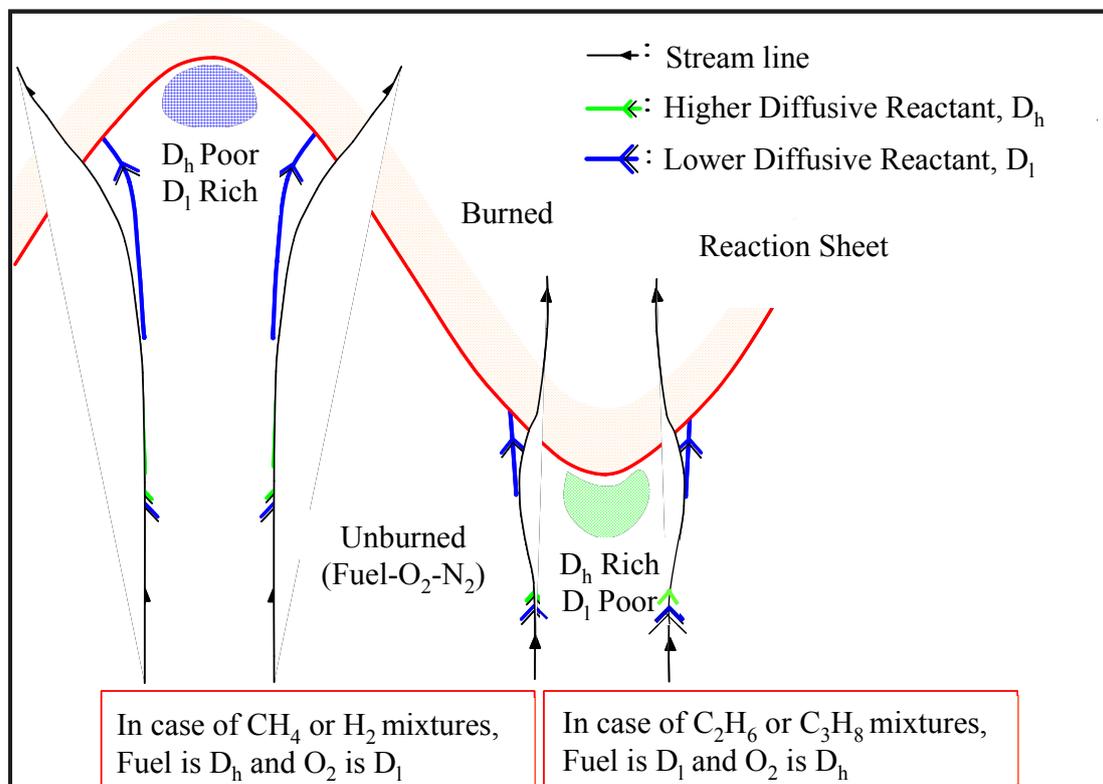
Figure 4.1b: *Schematic representation of preferential diffusion effects in curved flames*

4.3 High Pressure Effects

Despite its strong industrial relevance, investigation of premixed turbulent high-pressure combustion has been in research with a relatively low profile. Increase of pressure is known to influence both turbulence as well as laminar premixed flame characteristics. Experimentally observed flames are more wrinkled at increased pressure, where especially smaller turbulence scales (Taylor scale, Kolmogorov scale) decrease, while the turbulent integral scale remains nearly unaffected by pressure. This can be understood from the classical turbulence theory, based on decrease of kinematic viscosity $\nu = \mu / \rho$ with pressure. Thus, increased pressure induces higher turbulent Reynolds number, $Re_t = u' l_x / \nu$ (if the mean velocity is held constant, typically the turbulence intensity u' is also only weakly affected by pressure). The small scales of turbulence depend inversely on the turbulent Reynolds number (Taylor scale $l_\lambda \propto l_x / Re_t^{0.5}$; Kolmogorov scale $\eta_k \propto l_x / Re_t^{0.75}$; l_x the integral length scale). Correspondingly, measured energy spectra on turbulence show the shift to higher frequency regions. On the other hand, also the structure of laminar flames depends on pressure. It is known from detailed laminar flame calculations that the laminar flame speed decreases with increase of pressure. It is approximated for methane as $s_{L0} \propto p^{-0.5}$, and for ethylene and propane as $s_{L0} \propto p^{-0.25}$. The laminar flame thickness also decreases with increasing pressure, depending on the details of the local transport and reaction processes, where asymptotic theories predict a dependency like $\delta_L \propto \alpha / s_{L0} \propto \nu / s_{L0}$. The kinematic viscosity can thus be featured as a fundamental parameter relating to the influence of pressure on flame characteristics. It is of particular interest to note that the mean reaction rate of premixed turbulent flames increases with pressure, despite decrease in s_{L0}. This is the result of aforementioned pressure effects on turbulence-induced flame wrinkling and laminar flame, and is discussed in more detail in the frame of this study.

4.4 Dynamics of Swirl Flames

Usually, a flame is made to stabilise at a specific location in a combustor. The simplest way of stabilisation is behind a sudden expansion like a backward-facing step. The flow is strongly decelerated and forms an outer recirculation zone (ORZ). The recirculation zone stabilises the flame through mixing of burned gases with the incoming fresh mixture. On inducing swirl for such a flow makes the flame much compact. The swirling flow forms a central recirculation zone (CRZ) which acts as a flame holder in the centre of the flow. The flow characteristics of a swirling flow are sketched in Fig. 4.2.
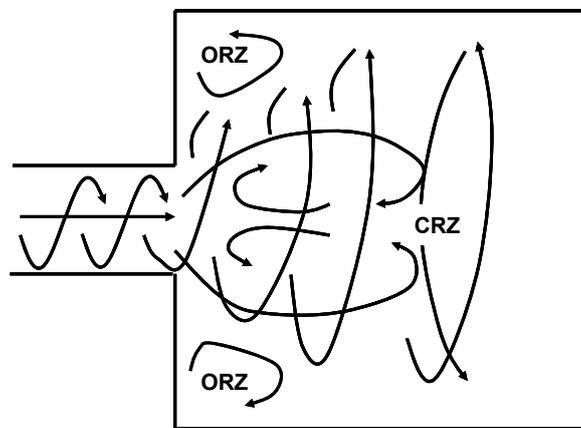
Figure 4.2: *Schematic of a swirl flow depicting the central recirculation zone (CRZ) and outer recirculation zone (ORZ)*

A swirling flow (Syred 2006) always exhibits lower pressure levels in its centre than far from the axis, discharging such a flow into a sudden expansion chamber reduces the circumferential velocity (through conservation of momentum) and therefore a negative axial pressure gradient is created. If this axial pressure gradient is strong enough, it will cause flow recirculation and the CRZ is formed. This process is called "Vortex Breakdown" (VB). It either breaks down completely into turbulence or forms a different vortical structure. Therefore, the CRZ is a source of intense turbulence and/or coherent structures such as the "Precessing Vortex Core" (PVC) (Syred 2006).

Due to the excellent flame holding, mixing, burnout and emission characteristics, swirling flames are exclusively used in gas turbine combustors. The reliability of swirl burners is determined by its capability to prevent flashback into the mixing zone.

Flame flashback is an intrinsic behaviour of premixed systems as the flame may stabilize where fuel and oxidizer mix, upstream of the combustion chamber. Different modes of flashback are detailed in the upcoming sections.

Despite of the well developed theories on flashback (Ashurst 1996, Chomiak and Zhou 1996, Sattelmayer 2000), the type of flashback occurring in lean-premixed GT combustors is not clearly defined. Understanding flame propagation and stabilization in the mixing zone of these configurations is essential either to avoid flashback or to set the flashback limits of a particular burner. Flashback can occur in the following situations:

1. Flashback by auto ignition
2. Flame propagation in boundary layers
3. Turbulent flame propagation in the core flow
4. Combustion instabilities leading to flashback
5. Flashback induced by vortex breakdown
6. Baroclinic push

1. Flashback by autoignition

Auto ignition does not involve flame propagation and occurs when the gas residence time exceeds the fuel ignition delay time, leading to the ignition of the mixture in the mixing zone. Auto ignition delays depend mainly on local temperature, pressure and equivalence ratio (Williams 1985)}.

2. Flame propagation in boundary layers

In boundary layers, the velocity is sufficiently low to allow upstream propagation of the flame. However, this propagation is limited by wall quenching. Lewis and von Elbe (Lewis and von Elbe 1961) have proposed a criterion for the laminar flame, which relies on a comparison between the wall velocity gradient and the ratio of the laminar flame speed s_L over quenching distance d_q:

$$g = \left.\frac{\partial u}{\partial r}\right|_{wall} \leq \frac{s_L}{d_q} \tag{4.1}$$

This criterion states that flashback occurs when the flow velocity at a distance d_q from the wall is lower than the flame speed (at distances smaller than d_q, the flame cannot survive). Flashback in boundary layers seems to be predominant in non-swirling low turbulent flows.

3. Turbulent flame propagation in the core flow

This propagation is possible when the turbulent flame velocity s_T becomes higher than the local flow velocity. Such a situation may occur in swirling flames, where turbulence is intense and the flame surface available is significantly larger than the flame surface of a laminar flame leading to a possible flashback on the burner axis (Guin 1998).

4. Combustion instabilities leading to flashback

Combustion instabilities are due to a coupling between heat release, pressure fluctuations and flow hydrodynamics. The velocity fluctuations induced by instability can be as large as the mean flow velocity and lead to a transient flashback during the oscillation cycle. Since swirled burners are sensitive to combustion instabilities, these scenarios may trigger flashback in these combustors (Keller et al. 1982).

5. Flashback induced by vortex breakdown

Vortex breakdown is one of the various mechanisms controlling the behaviour of swirling flows. It can be defined as an abrupt change in the jet topology and can take several forms. From the phenomenological point of view, the breakdown of a vortex occurs when its azimuthal velocity is larger than its axial velocity. This complex and highly 3D phenomenon depends on the flow circulation (or the swirl number) and the Reynolds number. In combustion chambers, vortex breakdown is accompanied by a large recirculation zone with high reverse flow velocities, of the order of the outgoing exit velocity. In a swirled stabilized flame, these reverse velocities can promote upstream flame propagation and flashback. This type of flashback has been experimentally observed and identified in a swirled burner by *Fritz et al.* (Fritz et al. 2001).

6. Baroclinic push

Coupling of the density gradient across the flame (occurring due to difference in unburned and burned gas velocities) and the radial mean pressure gradient in the unburnt swirling gas ahead of the flame, results in generation of azimuthal vorticity (Ashurst 1996, Chomiak and Zhou 1996) counter acting against the axial jet in the mixing tube. Despite of the turbulent flame speed being lower than the axial jet, as the azimuthal vorticity enhances the flame propagation by retarding the axial jet. In the third (F-3) configuration investigated in this study, it is shown that the later i.e., the Baroclinic push is active in the flame propagation mechanism.

5. LES Quality Assessment Methods

Only recently, quality assessment methods have been proposed (Geurts and Fröhlich 2002, Celik et al. 2005, Klein 2005b) to estimate the uncertainty of the obtained LES results. The LES results obtained in this study are assessed with several of the proposed indicators of LES quality which estimate the numerical and modelling accuracy. The assessment of uncertainty in LES is not so trivial, as both the numerical discretization error and the sub-grid scale contributions are proportional to grid size. As emphasised in (Celik et al. 2005, Klein 2005b) that, a good LES is one which tends to DNS as the grid resolution tends to the smallest scales, i.e. the Kolmogorov micro scales. Therefore, there is no such thing as grid independent LES in theory, because a grid independent LES is essentially DNS.

Numerical accuracy concerns about the grid resolution and the model accuracy says about the precision of the sgs model w.r.t a true DNS and/or to experimental data. In most applications the filtering process is convoluted with the numerical discretisation errors, so, it is hard to segregate these errors.

Roache (Roache 1998) give the following taxonomy for obtaining information for error estimates which has been used in the context of RANS but are in principal also applicable to LES:

1. Auxiliary algebraic evaluations on the same grid
2. Additional solutions of the governing equations on other grids
3. Additional solutions of the governing equations on the same grid
4. Auxiliary PDE solutions on the same grid.

In the first approach, it is possible to estimate the accuracy of the results obtained on a single grid with relevant theoretical assumptions, these are called single grid estimators (Geurts and Fröhlich 2002, Celik et al. 2005, Klein 2005b). The second approach corresponds to a two-grid estimator, which requires solutions obtained on two grid levels; the method proposed in (Celik et al. 2005) corresponds to this category. And, the third approach involves the model variation on the same grid; the method proposed by Klein (Klein 2005b) corresponds to second and third approaches. Finally, the fourth method is solving of an extra error equation, which is rather difficult with any CFD code.

In the current study, second and third approaches are used in estimating the quality of the LES results obtained on the sudden expansion dump combustor, both for non-reacting and reacting situations. While for the industrial double cone burner, only the "cold flow" results are assessed with the first approach.

5.1 Single Grid Estimators

Geurts and Fröhlich (Geurts and Fröhlich 2002) proposed to use the activity parameter s defined as

$$s = \frac{\left\langle \varepsilon_{ij} \right\rangle_{turb}}{\left\langle \varepsilon_{ij} \right\rangle_{lam} + \left\langle \varepsilon_{ij} \right\rangle_{turb}} \qquad (5.1)$$

where, ε is the dissipation rate.

Celik et al. (Celik et al. 2005) proposed a modified subgrid activity parameter (Eq. 5.2), measures relative to Kolmogorov scale index, relative viscosity index and relative resolved kinetic energy content. All these parameters use the effective quantities which includes the effect of numerical dissipation as well as the filter length, Δ. These are defined in Table 5.1.

Modified subgrid activity parameter:

$$s^* = \frac{\left\langle \nu_t \right\rangle + \left\langle \nu_{num} \right\rangle}{\left\langle \nu_t \right\rangle + \left\langle \nu_{num} \right\rangle + \nu} = \frac{\nu_{t,eff}}{\nu_{t,eff} + \nu} \qquad (5.2)$$

In all the estimators given in Table 5.1, the numerical contribution is unknown and must be either approximated or should be obtained with solution obtained on a second grid level. Owning to demand of high computational times, the LES of both cold and reacting flows for the double cone burner were performed on a single grid level only. The quality of the cold flow results is estimated with the viscosity index with the assumption that the numerical dissipation is 50% of the unresolved energy.

Table: 5.1 *Estimation of relative quantities*

Kolmogorov Scale Index	-Viscosity Index	Resolved kinetic energy content
$LES\_IQ_\eta = \dfrac{1}{1+\alpha_\eta\left(\dfrac{h}{\eta_{k,eff}}\right)^m}$	$LES\_IQ_v = \dfrac{1}{1+\alpha_v\left(\dfrac{\langle v_{eff}\rangle}{v}\right)^n}$	$\dfrac{k_{res}}{k_{tot}} = \dfrac{k_{res}}{k_{res}+k_{sgs}+\left|k_{num}\right|}$
$\alpha_\eta = 0.05; m = 0.5$ $\eta_{k,eff} = \left(v_{mol}^3 / \varepsilon_{eff}\right)^{0.25}$ $\varepsilon_{eff} = v_{eff}\left|S_{ij}\right|^2$	$\alpha_v = 0.05; n = 0.53$ $v_{eff} = v_{sgs} + v_{num} + v_{mol}$ $v_{num} = c_v h\sqrt{k_{num}}$ $c_v = 0.178$	$k_{num} = c_n\left(\dfrac{h}{\Delta}\right)^2 k_{sgs}$ $if \ \ h = \Delta \ \ \ \ k_{num} = k_{sgs}$ $h/\Delta \rightarrow 0 \ k_{num} \rightarrow 0$

5.2 Two Grid Estimators

An example of the two-grid estimator is the LES_IQ suggested by *Celik et al.* (Celik et al. 2005) which require solutions obtained on two grid levels. It is defined with respect to the amount of resolved energy and given as:

$$LES\_IQ_k = 1 - \frac{\left|k^{tot} - k^{res}\right|}{k^{tot}} \tag{5.3}$$

Total amount of kinetic energy is approximated as,

$$k^{tot} = k^{res} + k^{sgs} + k^{num} \cong k^{res} + a_k h^p \tag{5.4}$$

where, k^{tot}, k^{res}, k^{SGS} and k^{num} are respectively the total, resolved, subgrid and numerical kinetic energy, and $h = (\Delta x \Delta y \Delta z)^{1/3}$ is grid spacing. In the above expressions, p is assumed a constant value of 2, whereas a_k and k^{tot} are unknowns, and are estimated by Richardson extrapolation from two grid levels

$$a_k = \frac{1}{h_2^p}\left[\frac{k_2^{res} - k_1^{res}}{\alpha^p - 1}\right] \tag{5.5}$$

with $\alpha = h_1 / h_2 > 1$, the grid refinement parameter. In a recent work, *Çelik et al.*, (Celik et al. 2005) proposed that an amount of 75 to 80 percent for the resolved kinetic energy may be considered as well-resolved LES.

Application of Eq. (5.3) to transitional flows may result in unreasonable indices in the laminar flow regimes (Celik et al. 2006). Correction for laminar flow regions is necessary where LES-IQ has no real meaning. In the transition regions, it should be allowed to go to zero smoothly. This is done by introducing a laminar flow correction factor

$$f_{lam} = 0.5\left[1 + \tanh\left\{\beta\left[\operatorname{Re}_t^{0.5} - \sqrt{2}\operatorname{Re}_{t,crt}^{0.5}\right]\right\}\right] \qquad (5.6)$$

This function tends to zero for $Re_t \ll Re_{t,crt}$ and it has a value of 0.5 at $Re_t = 2 Re_{t,crt}$ and the value of β determines how sharp the transition is and is set equal to 0.5. In order to estimate Re_t, integral length scale l_x should be calculated from the LES solution having uncertain accuracy.

Also, the LES-IQ is restricted at the other end, which is at the high Reynolds number limit with another factor as 100% resolution or perfect LES or DNS is possible only if the grid resolution is achieved to the extent of Kolmogorov scales. The correction factor for this is

$$f_{\operatorname{Re}t} = \exp\left[-0.02\left[abs\left(\frac{h}{\eta} - \frac{h}{\eta_{\min}}\right)\right]^{0.5}\operatorname{Re}_t^{0.25}\right] \qquad (5.7)$$

where Re_t is the estimated effective turbulence Reynolds number and $h/\eta_{\min} = 5.0$.

This approach is used to analyse the results of the sudden expansion dump combustor in both cold and reacting flow situations.

5.3 Systematic Grid and Model Variation

This procedure proposed by Klein (Klein 2005b) is the combination of second and third approaches mentioned above. As mentioned earlier, in implicit filtering, the separation of modelling and numerical contributions is difficult as both interact with each other and varies strongly with grid refinement making the evaluation of grid refinement studies difficult. To separate the two elements, Klein (Klein 2005b) has proposed a technique

based on Richardson extrapolation with systematic variation of grid and the model term, for example the Smagorinsky constant C_S. In the context of LES with implicit filtering where the filter length is proportional to grid size h, the extrapolated solution u, a generic variable solved numerically, can be expressed in terms of discrete solution u_h, grid spacing h and the contribution of the model as

$$u = u_h + c_n h^n + c_m h^m \tag{5.8}$$

with n and m being the order of numerical and model contributions. Treating this equation as the solution obtained on a particular grid, by halving the model contribution ($c_m/2$, in the above equation) and halving the grid size ($h/2$), a set of three equations can be derived. There are five unknowns, namely u, n, m, c_n and c_m. Additional simplifications are mandatory to be able to solve for three of the five unknowns. One possible approach is to assume $m=n$ and the order of the numerical error $n=2.0$, i.e. the sgs modelling is assumed to introduce second-order dissipation (Klein 2005b). This leads to estimation and separation of discretization and model contributions.

$$2\left(u_2 - u_1\right) = c_m h^m \tag{5.9}$$

$$\frac{\left(u_3 - u_1\right)}{\left(1 - 2^n\right)} = \left(c_n + c_m\right) h^n \tag{5.10}$$

where u_1, u_2 and u_3 are any characteristic quantities obtained on fine grid, by halving the C_S constant on fine grid and by halving the grid size, respectively. This equation set can be generalised to any order and grid refinement ratio. This facilitates the estimation and separation of the energy dissipation through the numerical discretization and through the modelling. This method is applied only to the Smagorinsky model on the dump combustor.

6.   Experimental Details of the Simulated Geometries

In this chapter, the experimental details of the simulated configurations are elaborated and the details of the measurement techniques are briefly outlined. And, the respective flame data are depicted into the premixed regime diagram.

6.1   Bunsen Flame Data of *Kobayashi et al*

The two premixed turbulent reaction models used in this study are developed using physically simple experimental data of *Kobayashi et al.* up to 10 bar (Kobayashi et al. 1996, Kobayashi et al. 1997, Kobayashi et al. 1998). With the understanding of the importance of high pressure and fuel types, nearly a decade ago Kobayashi and co-workers have conducted series of experiments on a Bunsen-type burner for pressures up to 30 bar for CH_4, C_2H_4, and C_3H_8 air lean mixtures over a range of stoichiometric ratios and turbulence conditions. However, sufficient details on the inflow turbulence conditions are made available only up to 10 bar, due to the associated practical problems in obtaining accurate statistical data beyond this pressure level.

A 20 mm Bunsen burner was enclosed in a pressure vessel (diameter 498 mm, and height up to 1150 mm) with sufficient optical access (Fig. 6.1) (Kobayashi et al. 1997). A perforated plate acted as a turbulence generator, which was located at 40 mm upstream from the nozzle exit. An annular H_2 diffusion flame around the nozzle outlet served as torch to ignite the flame, and later was put off. This test rig is represented as F-1 configuration in this study.

In this configuration, turbulence was produced from grids with hexagonal pitch and hole diameters between 1 and 4 mm and blockage ratio of 0.5. Turbulence measurements were performed with constant-temperature hot-wire anemometry at the centre of the burner exit. The transverse integral length scale l_x was measured up to 10 bar, which was obtained from temporal autocorrelation measurements of velocity and assuming Taylor's hypothesis. The axial turbulent velocity (u') and l_x were measured at the axis just above the nozzle burner outlet. This data is used in feeding the inlet conditions for the solver in this study.
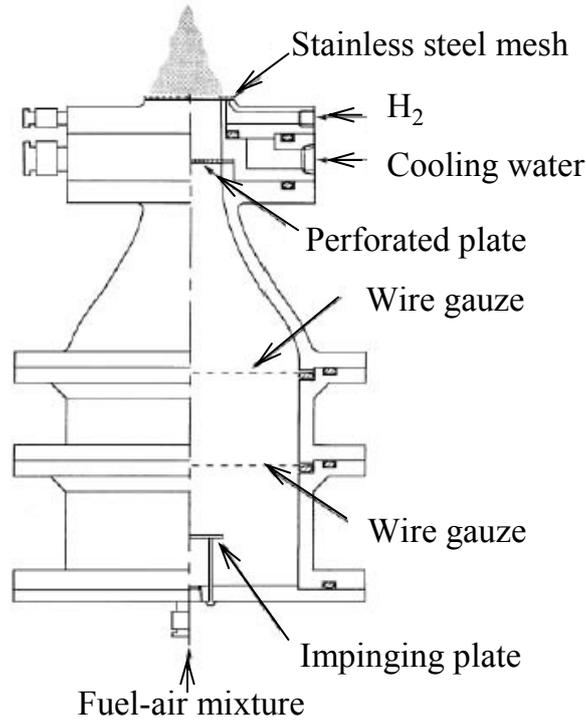
Figure 6.1: *Schematic of the Bunsen burner of Kobayashi et al (Kobayashi et al. 1997).*

In experiments, the averaged flame cone angles of the Bunsen flames were determined from the ensemble average of 50 images for every operating point. Every image was obtained with planar laser tomography, where Mie scattering of small particles were used to visualize the instantaneous flame contour (Argon-ion laser, CCD camera with electrical shutter speed of 100 μs) (Kobayashi et al. 1996, Kobayashi et al. 1997). This allowed the determination of the Reynolds averaged field of the mean reaction progress variable $\bar{c}$. The fitted contour line with $\bar{c} = 0.5$ was chosen to describe an average flame cone angle θ. In order to describe the resulting flame shapes independent of the mean bulk flow exit velocity U, results are presented in the form of a turbulent burning velocity s_T, defined as

$$s_T = U \sin(\theta/2) \tag{6.1}$$

Measured data were obtained for operating pressures up to as high as 30 bar, covering 108 different flames (Kobayashi 2001). Nozzle exit velocities (of the unburned premixed mixture) ranged between 0.86 and 8.86 m/s, with geometrical Reynolds numbers (based on nozzle exit diameter) from 1,640 to as high as 115,000; turbulence velocity and transverse integral length scale data range from 0.02 to 2.06 m/s and 0.70 to 1.90 mm, respectively. Three gaseous hydrocarbon fuels have been investigated, of

lean methane/air with the equivalence ratio of ϕ = 0.9 for 1, 5, 10, 20 and 30 bar,

ethylene/air with varied stoichiometry of ϕ = 0.5, 0.7 and 0.9 for 1, 5 and 10 bar, and

propane/air mixtures with ϕ = 0.9 for 1 and 5 bar. For the full data-set along with the

relevant quantities refer to Muppala (Muppala 2005).

In Fig. 6.2, the experimental data are shown in a premixed turbulent regime diagram. While some of the flames (especially at weak pressure), fall into the classical flamelet regime, the high-pressure flames are expected to take corrugated or thickened flame fronts, following older theories. However, both direct numerical simulations (Poinsot et al. 1990, Meneveau and Poinsot 1991) as well as evaluation of some of the detailed experiments (Dinkelacker et al. 1998, Dinkelacker 2001, 2003) and theoretical evaluations (Peters 1999, 2000, Dinkelacker 2003) show an increased spread of thin flame regime, especially, if the turbulent Reynolds number is not too high. And, as s_{L0} is a strong decreasing function of pressure, higher ratios of turbulence-chemistry interactive term u'/s_{L0} are reachable at elevated pressures, reaching partly up to

$u'/s_{L0} = 24$.
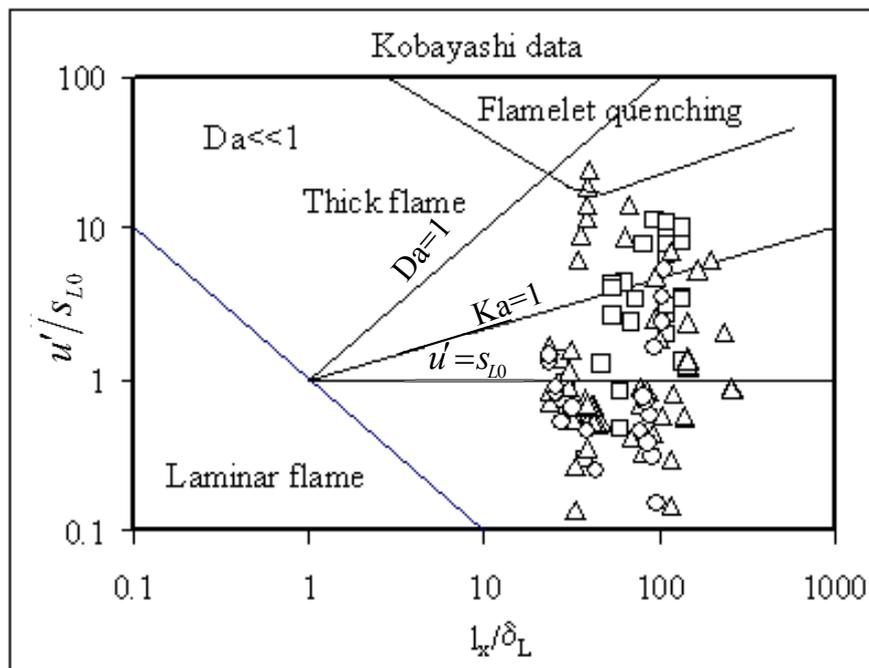
Figure 6.2: *Full set of experimental data of Kobayashi et al. (Kobayashi et al. 1996, Kobayashi et al. 1997, Kobayashi et al. 1998), along with the boundary of flamelet quenching, and thick flame in the modified phase diagram of turbulent premixed combustion. Methane (□), Ethylene (∆), and Propane (○).*

6.2 Sudden Expansion Dump Combustor

Measurements on this configuration were performed on a cylindrical sudden expansion dump combustor at *Paul Scherrer Institute* (PSI) (Griebel et al. 2003). Because of underlying advantages due to high-efficacy and low emission energy conversion of gaseous fuels, turbulent premixed combustion rapidly spread its wings into technical applications, finds its place especially in stationary gas turbines (GTs). Experimental studies by *Griebel et al.* (Griebel et al. 2003, Griebel et al. 2005) on lean premixed flames, gains significant relevance owning to (preheated) high-pressure and high turbulence levels, with operations close to stationary GT inlet conditions. This test rig designed for a maximum thermal power of 400 kW can have a maximum operating pressure of 30 bar, airflow rate of 750 Nm^3/h, air can be preheated up to 823 K with an electrical heater and can withstand exhaust gas temperatures up to 1850 K.
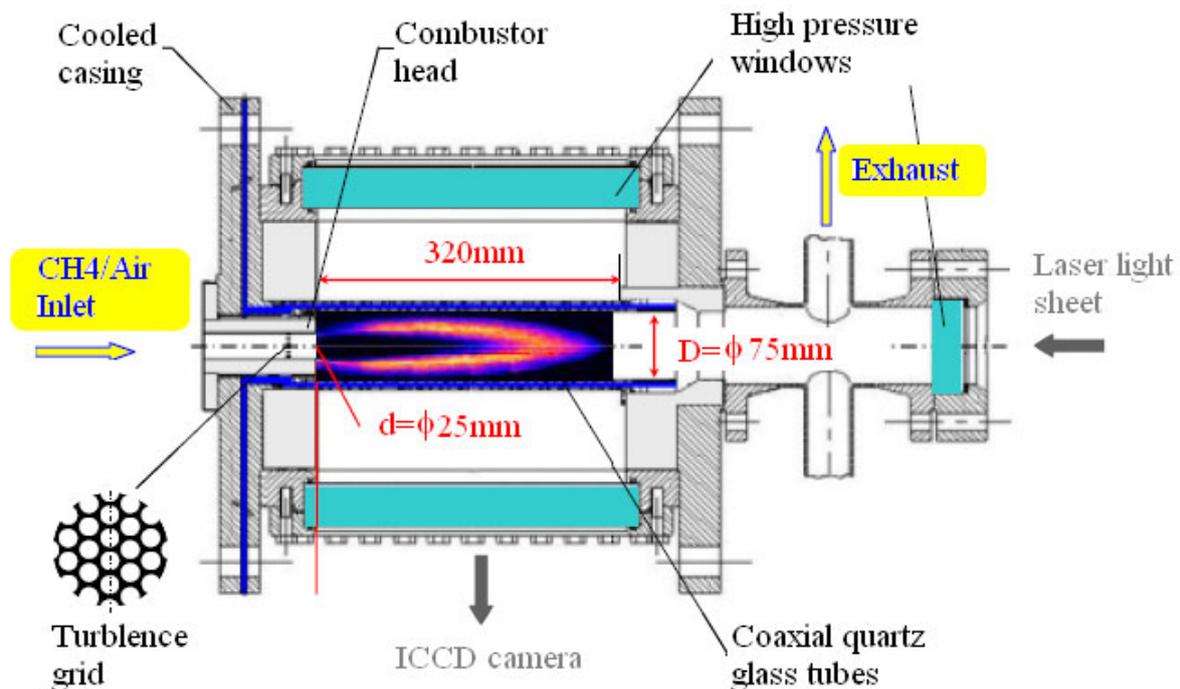
***Figure 6.3**: Experimental high-pressure combustion chamber of Griebel et al. (Griebel et al. 2003)*

The test rig marked with all the important accessories is shown in Fig. 6.3 and it is here after referred as F-2 flame configuration in this study. It consists of two coaxial quartz glass tubes (inner quartz glass tube diameter *D* = 75 mm) which are convectively air-cooled and the combustor inlet diameter *d* is 25 mm. The flame is stabilized aerodynamically via the outer recirculation of hot flue gases, induced by the

combustor geometry with sudden expansion. The three large high-pressure windows provide the optical access required for non-intrusive laser diagnostics (PIV, PLIF). Inlet turbulence was generated with a turbulence grid having hexagonal pitch with a hole diameter of 3 mm, placed at 30 mm upstream of the sudden expansion. In this configuration, only the cold flow velocity field was measured with the help of 2D Particle Image Velocimetry (PIV). The laser beam generated by a double pulse twin-YAG laser after passing through a set of lenses results in a laser sheet of 75 mm height. The glass tube was shielded with black screens to lower the amount of light reflections. The camera image was 72 mm high and 86 mm wide. The flow field was imaged at 4 to 5 different axial positions with an overlap of $7 - 30\%$. The images were analyzed with 32x32 pixel interrogation spot size and an overlap of 75%. These settings were found to be optimal for the desired high spatial resolution. Therefore, the flow field consists of 125 vectors in span wise and 157 vectors in stream wise direction with a resulting spatial resolution of 0.55 mm. The mean axial velocity and turbulent kinetic energy in the centre plane along the combustor axis after the sudden expansion are available for the numerical validation.

The reacting flow field was characterized using Planar Laser Induced Fluorescence (PLIF) of the OH radical as a marker of the instantaneous flame front. The flame front detection method is shown in Fig. 6.4 (Griebel et al. 2003). For the statistical analysis of the flame data, nearly 800 samples of the single shot flame front contours are summed up to create a 2D image representation of the spatial flame front distribution. This number of samples was found to be the optimum of a sufficiently high signal level and a tolerable data acquisition time. For this number of samples the statistical results (relative probability of the flame front position, x_{mp}, and flame front contour) are independent of the number of samples. The most probable flame front position at the centreline x_{mp} is defined by the axial position of the maximum of the centreline profile extracted from the 2D image (refer Fig. 6.4). The overall estimated error of the flame front position measurements (x_{mp}) was $\pm 7\%$.

The turbulent flame regime analysis (Fig. 6.5) shows that with increase of pressure, the flame conditions move into the thickened reaction zone ($Ka > 1$), with the reduction of the Kolmogorov scale (which is smaller than flame thickness at high pressures).

Nevertheless, the DNS studies by *Poinsot et al.* (Poinsot et al. 1996) indicate the flamelet regime extending well above the $Ka = 1$ line.
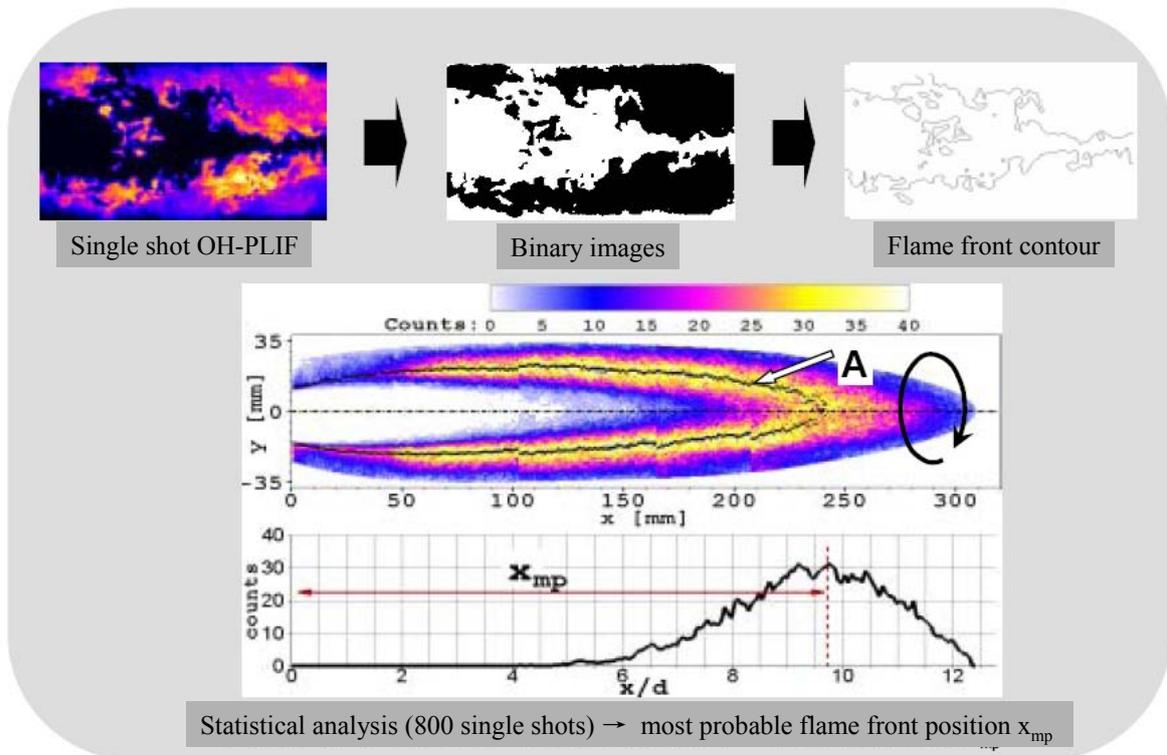
Figure 6.4: *Flame front detection method and most probable flame front position estimation (Griebel et al. 2003).*
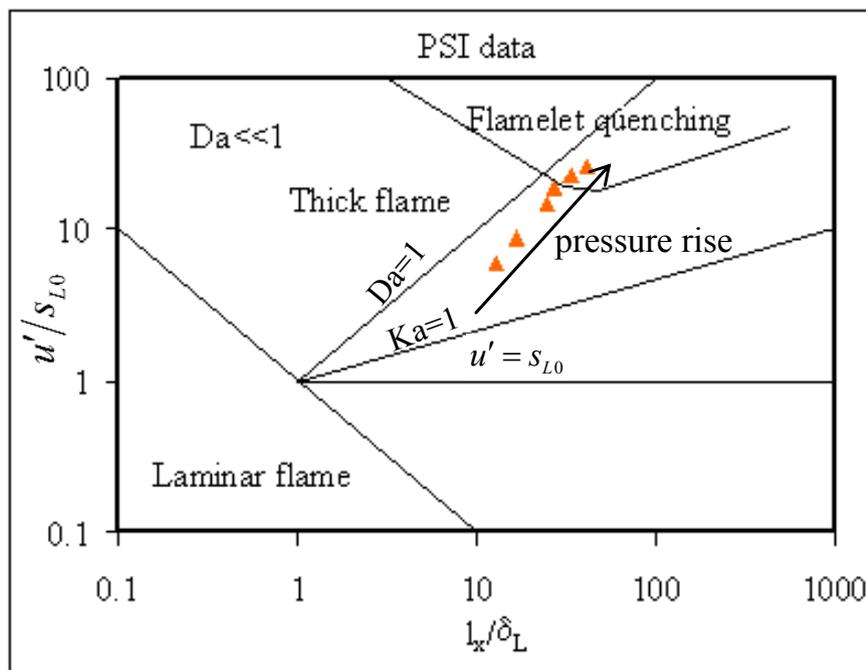
Figure 6.5: *High-pressure flames from PSI (Griebel et al. 2003) plotted into the Borghi diagram with turbulence quantities measured at the sudden expansion region.*

The general flow characteristics of this configuration are: grid generated turbulence is dominant in the core flow region and shear-generated turbulence in the post-region (downstream side) of the flame. The simulated cases are presented in the test-matrix at the end of this chapter in Table: 5.1 and 5.2. This data enables to test the generality of the model developed using the experimental data of Kobayashi and to test its veracity at high turbulence and pressure. Also, the extension of the model to LES is studied for the three pressure cases.

6.3 ALSTOM Gas Turbine Burners

As mentioned in the introduction, the ultimate aim of this thesis is to develop and test a turbulent premixed combustion model which may be usable for varied fuels at high pressures. This is tested with two different configurations of ALSTOM gas turbine burners without and with mixing tube. The purpose of the mixing tube is to ensure better mixing of fuel and air before the combustion zone to reduce the NO_X emission to ultra low levels. These two configurations are named as F-3 and F-4 here. The schematic of these are shown in Fig. 6.6.
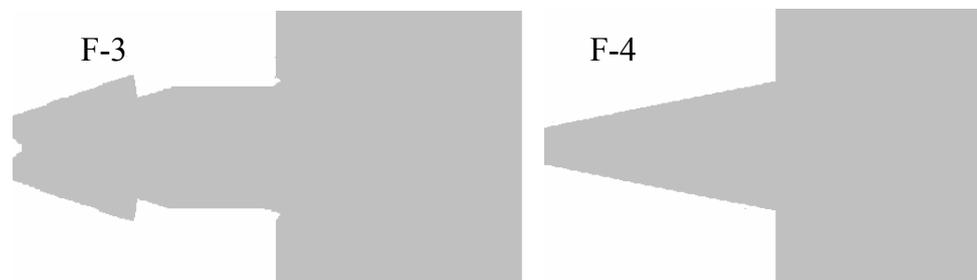
Figure 6.6: *ALSTOM gas turbine burners, F-3: A conical burner with mixing tube, F-4: A double cone burner.*

With the F-3 configuration both fuel and high-pressure influences and behaviour of the novel reaction closure at gas turbine conditions are studied in RANS context. While on the F-4 configuration both steady state RANS and LES of cold and reacting flow simulations are performed at atmospheric pressure.

For the F-3 configuration no detailed experimental data have been measure so for. Nevertheless, this configuration is useful for the numerical study, where the importance of the fuel influence in the reaction closure is demonstrated by artificially varying the Lewis number of the fuel air mixture for a liquid fuel (assuming the

properties of n-heptane) at an operating pressure of 14 bar. The flame stabilisation mechanism is explained with relevant theoretical justification.

The dynamics of the flow in F-3 configuration is studied in RANS and LES before performing the reacting flow simulations and validated against the cold flow PIV measurements (Biagioli 2006). In this configuration, simulations are carried out assuming perfect premixing for three adiabatic flame temperatures of 1650 K, 1700 K, and 1800 K to study the dual-flame mode of this burner. More details about this burner and its behaviour are furnished in the upcoming chapters.

6.4 Orleans Bunsen Flame Data

On this relatively new Bunsen-like burner configuration (Lachaux et al. 2005), experiments of lean turbulent premixed methane/hydrogen/air flames were conducted for systematic variation of pressures, equivalence ratio and hydrogen content. Detailed flame front data for methane-air flames are obtained separately with Mie scattering tomography and Rayleigh scattering. The experimental data is available for turbulent flame speed (s_T), reaction progress variable (c), its gradient ($|\nabla \overline{c}|$) and flame surface density (Σ) for equivalence ratio (0.6, 0.7 and 0.8) variation at 1 bar, and pressure (1, 5 and 10 bar) variation at an equivalence ratio of 0.6. Also, the axial plots of the progress variable are available for hydrogen doped methane-air flames. Hydrogen was doped in concentrations of 10 and 20% (volume) of the total fuel content at a fixed equivalence ratio with pressure variation of 1, 5 and 10 bar. All the measurement data are available for a constant inlet velocity of 2.1 m/s, turbulent intensity of 8% and integral length scale of 3 mm. Cold flow measurements obtained with Laser Doppler Anemometry (LDA) indicated that the turbulence intensities and the integral length scale are not sensitive to pressure. Due to the decreased kinematic viscosity with increasing pressure, the turbulent Reynolds number increases, and isotropic turbulence scaling relations indicate a larger decrease of the smallest turbulence scales.

6.4.1 Details of the experimental configuration

Stainless steel cylindrical water-cooled combustion chamber of 600 mm high with a diameter of 300 mm and it consists of four quartz glass windows of 100 mm for the optical diagnostics. The internal volume is approximately 80 litre. The centrally placed

burner can traverse the chamber's vertical (z-) axis by a stepping motor. The laser light traverses the combustion chamber through two opposite windows. The windows are electrically warmed to avoid water condensation, and a nitrogen flow dries the windows during measurements.
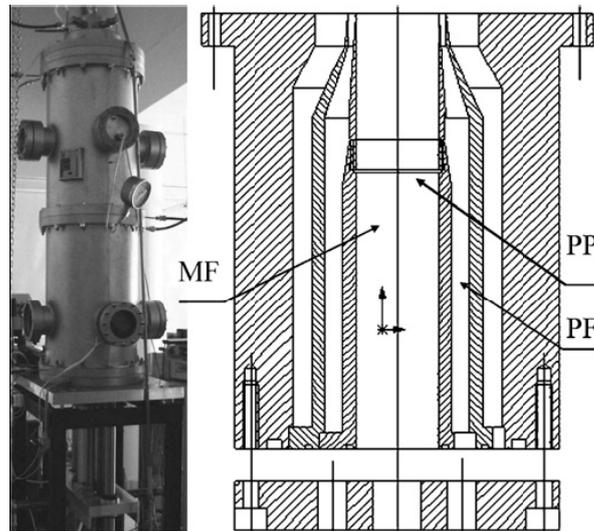
Figure 6.7: *Combustion chamber (left) and schematic view of the burner (right) PF, pilot flame annular channel; PP, perforated plate; and MF, main flame tube (Lachaux et al. 2005).*

The burner shown in Fig. 6.7 is an axisymmetric Bunsen burner, fed by premixed methane–air mixture(s). The internal burner diameter D is 25 mm, and length is 230 mm. A perforated plate, blockage ratio 0.51, with 2.5 mm diameter holes in a hexagonal array, is located 50 mm upstream of the burner exit and generates the cold flow turbulence. The flame characteristics are measured with both Mie scattering (Lachaux et al. 2005) and Rayleigh scattering (Halter et al. 2003, Olivani et al. 2003, Halter 2005), described in detail.

6.4.2 Mie scattering tomography

A 15 Hz pulsed Nd-YAG laser (Spectra Physics GCR 130) at 532.5 nm was used for Mie scattering flame tomography. The pulse energy was 270 mJ. The laser beam passing through a 1000 mm focal length spherical lens and a 25.4 mm focal length cylindrical lens produces a light sheet of 200 μm thick and approximately 90 mm high. The flow was seeded by olive oil droplets supplied by an atomizer. The mean droplet diameter was measured by Phase Doppler Anemometry at 4.3 μm. The LDA with a probe resolution of 80 μm was used to obtain the turbulence quantities.

At each pressure, 160–250 Mie scattering tomography images were collected and analysed. First, an edge finding algorithm is applied to each image and from the edges, binarized images are generated, summed, and averaged to produce <c> maps.

6.4.3 Rayleigh scattering

The same Nd-YAG laser was used for Rayleigh measurements. The laser beam passing through a 500 mm focal length spherical lens and a -50 mm focal length cylindrical lens produces a light sheet 50 μm thick and approximately 50 mm high. The Rayleigh scattered light was collected at 90° to the sheet by an intensified camera. The field of view of the camera is 14x14 mm^2. The overall resolution was 27.3 μm/pixel. The size of the area investigated was limited to increase the magnification. As the Rayleigh scattering signal is less intensive than the Mie scattering signal, the size of the laser sheet was reduced to increase the energy density of the laser light and with that the signal strength. The area investigated is the same for all flame cases. For each case, 500 flame images were obtained and analysed. Temperature profiles through instantaneous flame fronts were determined from Rayleigh scattering images. The local flame front thickness was obtained with the usage of the thermal flame thickness definition as $l_F = (T_p - T_r)/(dT/dz)_{max}$ with T_p and T_r representing the products and reactants temperature respectively. For each Rayleigh image, the flame contour at $c = 0.5$ ($c = (T - T_r)/(T_p - T_r)$) was identified. Inlet flow conditions and other relevant data for simulated cases are shown in the regime diagram in Fig. 6.8.
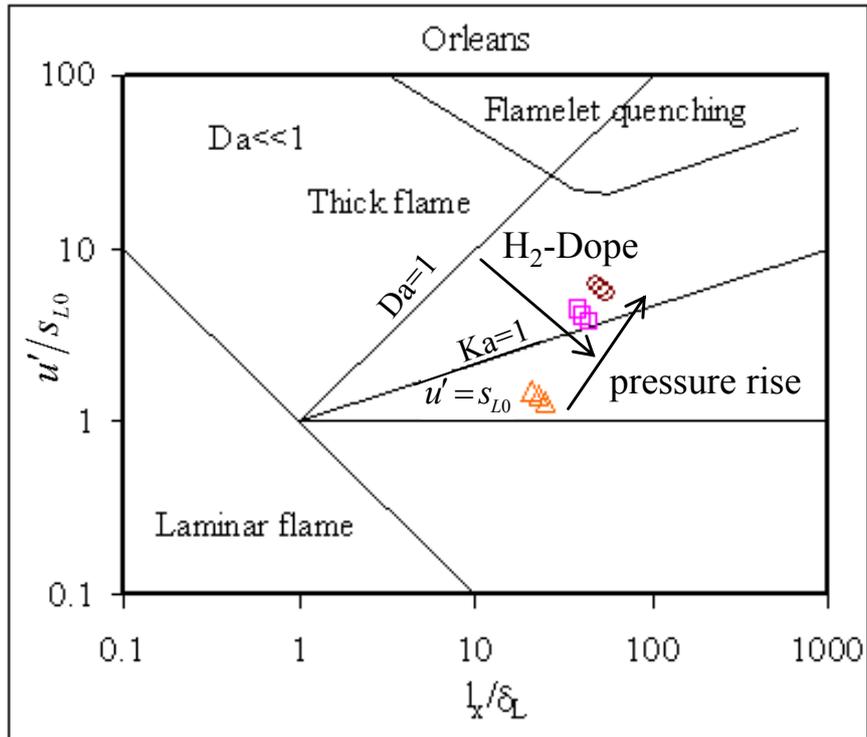
Figure 6.8: *Hydrogen doped methane flame data (Halter 2005) with pressure variation are plotted into the Borghi diagram with turbulence quantities measured at the combustor inlet.*

6.5 Simulation Matrix

The simulated cold and reacting cases are presented in Table 6.1 and 6.2, respectively. Cold flow simulations are performed for two different configurations F-2 and F-4, the details of which are given in Table 6.1. Both cases are simulated in the RANS and LES contexts, to ascertain the advantages and limitations of each one through relative comparison of flame data. In the LES cases, three turbulence sgs closures – the classic Smagorinsky, dynamic Smagorinsky, and one-equation kinetic energy transport equation – are used.

Table 6.2 gives a complex data distribution for five different burner configurations. On the second column are the calculated flames for the Bunsen burner of Kobayashi (F-1), sudden expansion dump configuration from *Griebel et al.* (F-2), the two ALSTOM configurations (F-3 and F-4), and the other Bunsen burner from *Halter et al.* (F-5), for varied Lewis numbers and pressures. The flame simulations are repeated for two reaction models. The AFSW model has been verified in both RANS and LES contexts, along with an additional study for effects of hydrogen doping and preferential diffusion.

Table 6.1: *Test matrix of the cold flow simulations, depicted are the 3D outline of the dump combustor (F-2) and ALSTOM double cone burner-combustor configuration (F-4)*

Name	Geometry	P (bar)	RANS	LES		
				SM	DS	K_{SGS}
F-2		1	✓	✓	✓	✓
		5, 10	✓	✓	✓	✓
F-4		1	✓	✓	✓	✓

Table 6.2: *Test matrix of the combusting flow simulations, shown are the 2D cross-sectional views along the axis of the respective geometries*

Name	Geometry	Le	P (bar)	RANS		LES
				AFSW	ELV	AFSW
F-1		1.0	1, 5, 10	✓	✓	✓
		1.2 , 1.3	1, 5, 10	✓	✓	–
F-2		1.0	1, 5, 10	✓	–	✓
F-3		1.0	1, 16, 32	✓	–	–
		1.0, 1.3, 1.8, 2.3	14	✓	–	–
F-4		1.0	1	✓	–	✓
F-5		≈1.0	1, 5, 9	✓	Effects of hydrogen doping and preferential diffusion are addressed with the AFSW model	
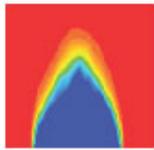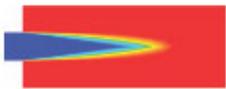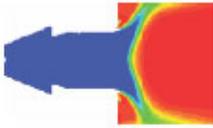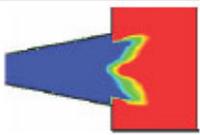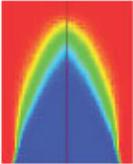
7.   Model Development and Implementation to LES

Premixed turbulent combustion has its technical application in gas turbine combustors, SI engines and other industrial burners. At least in the first two cases the working pressure is significantly above atmospheric condition. Additionally, different fuels are used, e.g., in gas-turbines natural gas (mainly methane) and in dual fuel systems also diesel consisting of broad range of hydrocarbons; in other applications ethylene, propane, butane; in IC engines, it is prevaporized octane-blends. Even hydrogen may become a very important fuel either to be added to other fuels (hydrogen doping) for flame stabilization purposes or for hydrogen combustion in the frame of CO_2-free power plants or even as primary fuel in IC engines.

Literature on numerical premixed flame modelling, however, indicates that most of the proposed combustion models are devised for atmospheric pressure only often neglecting the fuel dependency, for e.g., (Bray 1990) (Weller et al. 1990{Lindstedt, 1999 #1273); the earliest modelling studies that incorporated for the fuels effects can be seen in (Bradley 1992)

Since few years, the working emphasis in our group is therefore oriented to the development of premixed combustion models, where the pressure and the fuel-dependency are regarded (Muppala and Dinkelacker 2003, 2004, Muppala et al. 2005b) (Aluri et al. 2005a, Aluri et al. 2006). Based on a broad comparison of different models from the literature, essentially, two models are either developed or extended: the Algebraic Flame Surface Wrinkling (AFSW) model and the Extended Lindstedt-Váos model (ELV model) on a Bunsen burner. Appendix A1 details on the Extended Lindstedt-Váos model. This work is partly belonging to the current thesis, however, the model development issues are already described in the recent thesis of Muppala (Muppala 2005). Therefore, the first part of this chapter contains only a short review, including some new observations and modifications of the models (§ 7.1 to 7.3). The important new aspects in this thesis are the incorporation of Lewis number as an exponential term, verification of the model capabilities at gas turbine operating conditions and the applicability of the reaction model in the frame of the Large-Eddy-Simulation (LES) approach. These aspects are dealt on configurations of various degrees of complexity from a simple Bunsen flame to a complex gas turbine combustor.

The focus of this thesis, as noted in introductory part, is laid in three directions:

- First, the behaviour of various turbulent premixed combustion models is tested for the variation of pressure and fuel types (Lewis number variation) with the simple Bunsen (F-1 Configuration) burner in § 7.1. The workability of the AFSW model in gas turbine combustors is demonstrated on the conical swirl burner (F-3 Configuration) for pressure variation of 1 to 32 bar. Also, the importance of the Lewis number influence is demonstrated with the same configuration in Chapter 9.1. All these issues are handled in the RANS context.

- Second, the applicability of the AFSW model as subgrid scale reaction closure is tested in LES approach in conjunction with the three widely employed turbulence models (for F-1, F-2 and F-4 configurations). The simulated results for the F-1 configuration are presented in § 7.4. The results of F-2 and F-4 configurations are detailed, respectively, in **Chapter 8** and **9** in comparison with the model predictions in RANS approach.

- Third, the behaviour of the AFSW model for hydrogen blended methane-air flames is studied analytically and with limited computations (only with RANS approach). Some directives of numerical handling of hydrogen-blended flames are outlined in **Chapter 10**.

The experimental data of *Kobayashi et al* is a good source to check the predictive capabilities of the reaction models due its physically simple configuration and due to the systematic variation of pressure, equivalence ratio and fuel types.

7.1 Predictions of Various Reaction Models in the RANS Context

In this chapter, various premixed combustion models existing in the literature are tested for varied degrees of turbulence levels, pressure and fuel-type of different datasets, using the CFD solver FLUENT (Fluent 2005). Figure 7.1 shows the resulting flame cone angle as a measure of flame height (in non-dimensional flame speed s_T/s_L) of Kobayashi flames calculated using various existing reaction models (Bray 1990, Cant et al. 1990a), compared along with the experimental data (Kobayashi et al. 1996, Kobayashi et al. 1997, Kobayashi et al. 1998). Most of the proposed models show strong deviations from the experimental flames (scattered point far away from

the 45° line), and even the trend behaviour is not fitting. The TFC reaction closure by Zimont and Lipatnikov (progress variable gradient approach) (Zimont and Lipatnikov 1995) and the algebraic fractal closure by Lindstedt and Váos (Lindstedt and Váos 1999), were found to be in reasonable qualitative agreement with the experiment for turbulence variation (the latter yielding a relatively good trend behaviour), but both have failed to acknowledge the important pressure and fuel effects.

The numerical predictions of these models for the Kobayashi Bunsen flame data for the variation of pressure and fuel are shown in a correlation plot in Fig. 7.1. As none of these models are sensitive to the influence of pressure and fuel, a novel reaction closure namely Algebraic Flame Surface Wrinkling (AFSW) model is developed based on the above shown experimental data of *Kobayashi et al.* by incorporating the above said effects. These model development details are detailed in § 3.3. In a similar procedure as adopted in the new model development, the Lindstedt and Váos (LV) reaction model is extended for these two effects, explicitly.
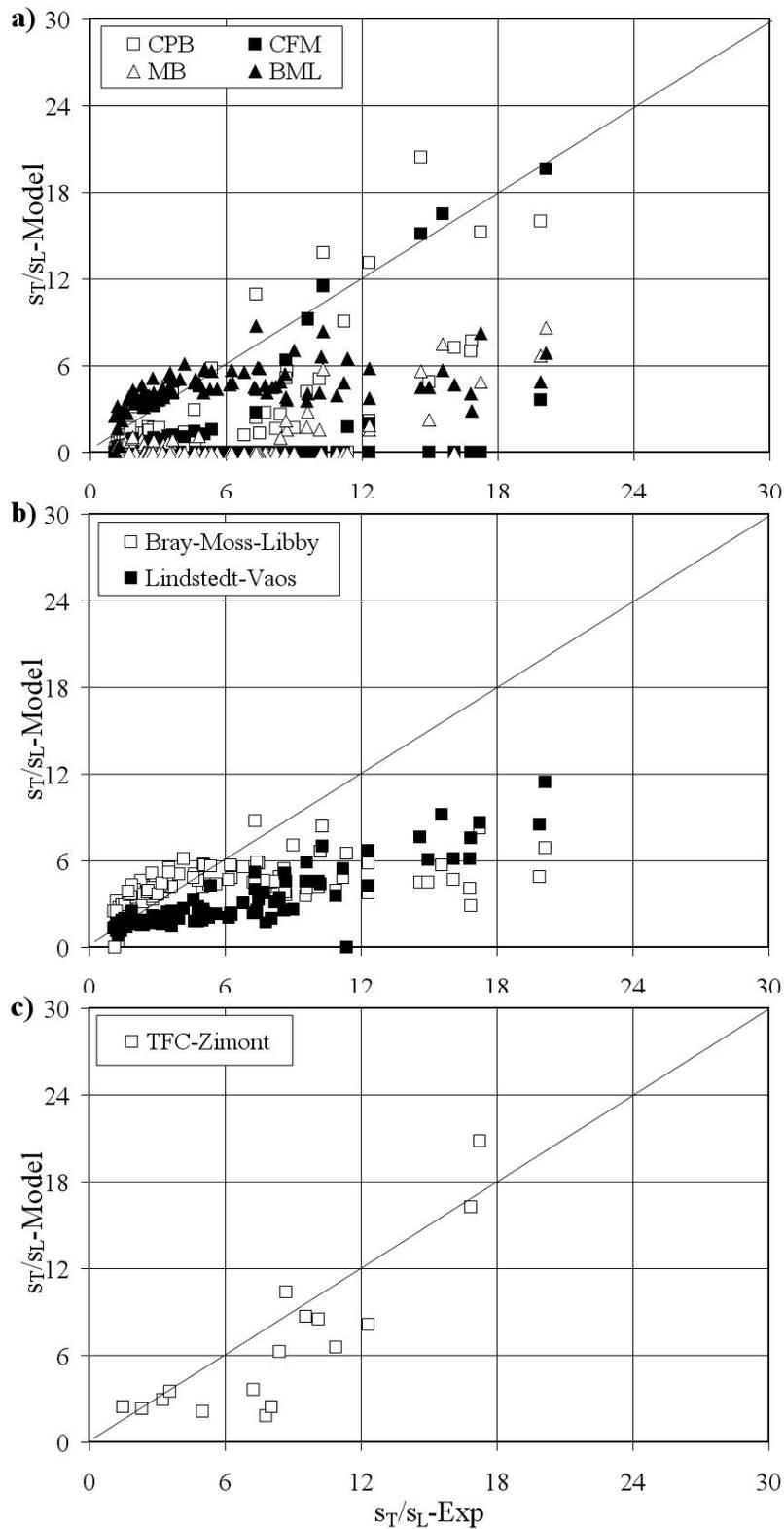
Figure 7.1: *Correlation plots in s_T/s_L of various models simulated in RANS (using standard $k - \varepsilon$ model approach). Plotted data are the experimental values on the abscissa, and on the ordinate are the numerical predictions. In a) and b), all hundred plus data for variation of pressure, equivalence ratio and fuel are plotted; whereas in c), only the 1bar cases are shown for the variation of equivalence ratio and fuel. In c) the points lying on the 45° line are the CH_4-air flames and the points away from this line are ethylene and propane data.*

7.2 Extended Lindstedt-Váos (ELV) Reaction Model

Specifically, the chosen Lindstedt and Váos (LV) reaction model has been substantiated to incorporate for the missing above-noted effects through semi-empirical approach with the help of Kobayashi data (Kobayashi et al. 1996, Kobayashi et al. 1997, Kobayashi et al. 1998, Kobayashi 2001). The details of the model development procedure and other related issues are given in **Appendix: A1**. Here, only the final form of the reaction source term with Lewis number and pressure terms is given. The Extended Lindstedt and Váos model has the following form (Aluri et al. 2006)

$$\overline{w}_c = C_R C_{P,Le} \rho_u \frac{s_{L0}}{V_K} \frac{\tilde{\varepsilon}}{\tilde{k}} \tilde{c}(1-\tilde{c})$$

$$C_R = 4.0 \; ; \; C_{P,Le} = \sqrt{\frac{v_0}{v}} \left(\frac{1}{e^{Le-1}} \right)$$

(7.1)

7.2.1 Predictions of the ELV model

Before presenting the performance of the reaction model in the correlation plot, the necessity of the relation $1/\exp(Le-1)$ in Eq. 7.1 is outlined. In an earlier modelling approach, an approximated $C_{P,Le} \propto 1/Le$ dependency was used (Aluri et al. 2005a). The difference between these two dependencies in terms of normalised turbulent flame speed (s_T/s_{L0}) as a function of normalised turbulent velocity (u'/s_{L0}) in comparison with the experiments are shown in Fig. 7.2. The difference is small for the flame angles (s_T/s_{L0}) for methane- and ethylene-air flames, but it is significant for the propane-air flames with Le of 1.62, as can be seen in Fig. 7.2. The $1/Le$ relation over predicts, especially at increased pressure or, equivalently, turbulence level.
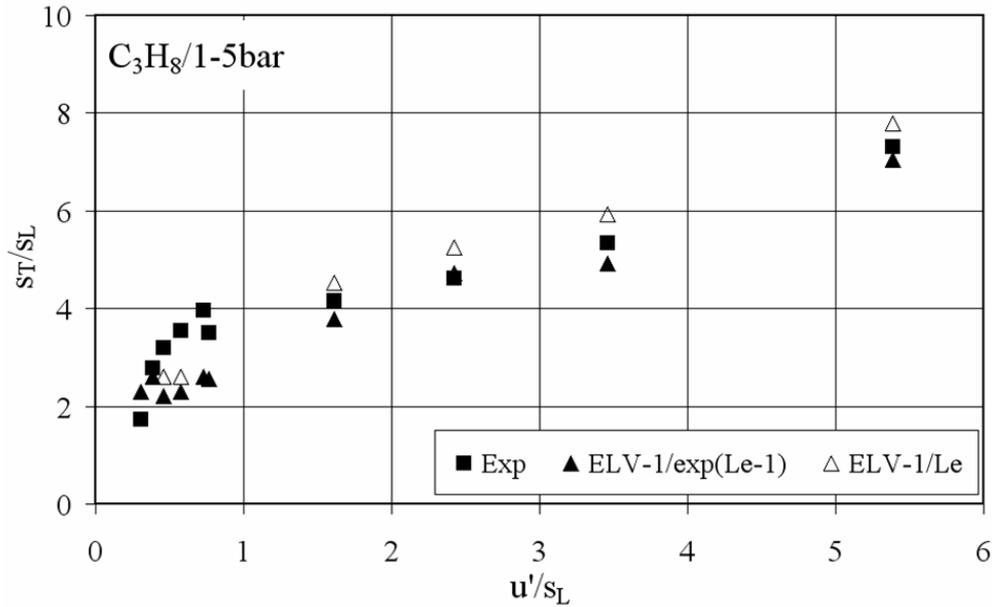
Figure 7.2: *Propane flame angles (φ = 0.9) at 5 bar using the ELV (calculated using the exponential Lewis number relation, Eq. 7.1) models. The open triangles show the turbulent flame speed evaluated using the* $1/Le$ *relation which over predicts at increased turbulence level.*

The empirically found exponential dependency is consistent within the leading point concept discussed by Lipatnikov and Chomiak ((Lipatnikov and Chomiak 2005), pages: 38-48), which also detailed in this work in § 4.1.
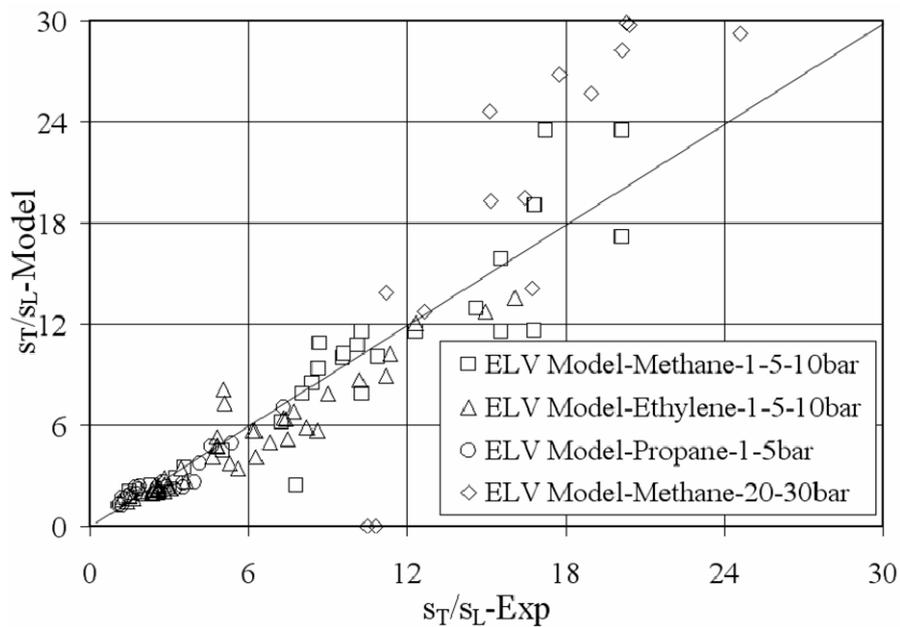
Figure 7.3: *Correlation plot of the numerical predictions from the Extended Lindstedt-Váos model in RANS context shown with the experimental data of Kobayashi et al. (Kobayashi et al. 1996, Kobayashi et al. 1997, Kobayashi et al. 1998, Kobayashi 2001)*

7.2.2 Delimits of the ELV model

Applying the ELV model to the Kobayashi experimental data it is found that simulated flame data differ from measurements at very weak turbulence level at elevated pressures. For few such flames falling in the range $u'/s_{L0} < 1$ at and beyond 5 bar, the calculated flames are partly suppressed to a flat flame at the very exit of the nozzle (similar to "numerical flashback" due to over predicted reaction rate). On the other hand, the propane flames at 5 bar have been found with under predicted flame angles. It should be noted that for the very low turbulence intensities the rather complex phenomenon of laminar flame instabilities as well as possible mis-modelling of eventually re-laminarized turbulence may be of additional importance. Lindstedt and Váos (Lindstedt and Váos 1999) proposed an empirical procedure, formally adopted from Sreenivasan (Sreenivasan 1984), for low turbulent flows. This method evaluates the reaction rate via an exclusive expression for the outer cut-off (integral length) scale $l_x = C_L u'^3/\varepsilon$, where $C_L(\mathrm{Re}_\lambda)$, in order to reconcile calculations and experiments. Allowance of this approach to the current data has not benefited, so far (not shown here) that the results were found inconsistent over the span of very weak turbulence data.

It is therefore necessary that special care be taken in simulating flames at very low turbulent, which seems to be the case with any other existing reaction model when used in conjunction with the standard $k - \varepsilon$ turbulence model.

7.3 Algebraic Flame Surface Wrinkling (ASFW) Model

Even in the AFSW model (Muppala et al. 2005b), the fuel dependency term ($1/Le$) is exchanged for $1/\exp(Le-1)$ due to the analysis given in § 7.2.1 and Appendix: A1, with this the flame-wrinkling ratio takes the form

$$\frac{A_T}{\overline{A}} = \frac{s_T}{s_{L0}} = 1 + \frac{A_0}{e^{(Le-1)}} \cdot \mathrm{Re}_T^{0.25} \cdot \left(\frac{u'}{s_{L0}}\right)^{0.3} \cdot \left(\frac{v_0}{v}\right)^{0.2} \qquad (7.2)$$

where the ratio of turbulent flame surface area normalized by the averaged flame surface area is equated to the ratio of turbulent flame speed unstretched laminar flame

speed $A_T / \overline{A} = s_T / s_{L0}$, according to the Damköhler hypothesis (Damköhler 1940), $A_0 = 0.46$ is the model constant, Le is the Lewis number of the fuel-air mixture, Re_t is the turbulent Reynolds number, u' / s_{L0} is the normalized turbulent intensity, and $v_o / v (= p / p_o)$ is the normal molecular kinematic viscosity.

The numerical prediction of the new model for the data on which it has been worked out is shown in Fig. 7.4, as a correlation plot in s_T / s_{L0} for experiment vs. simulation.
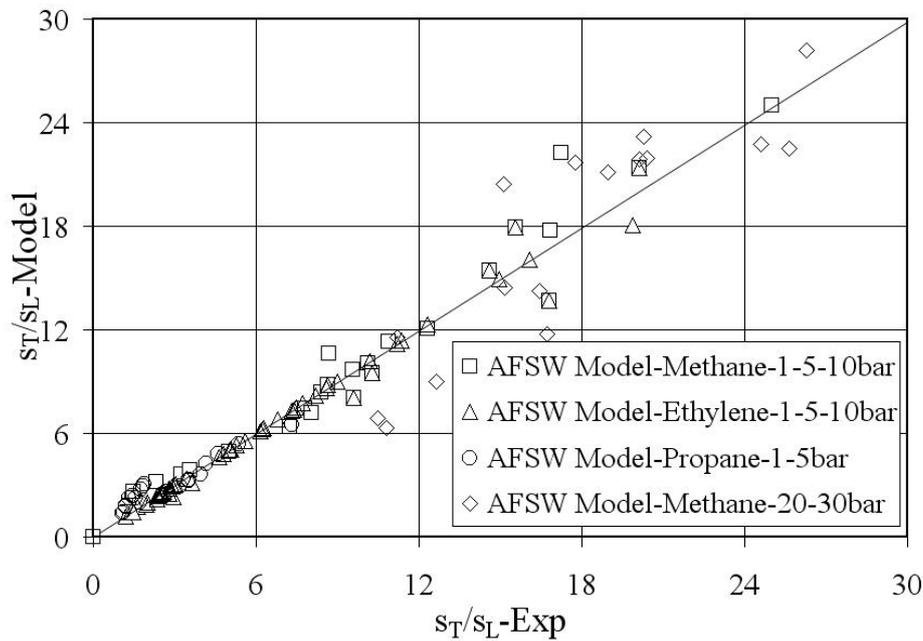
Figure 7.4: *Correlation plot: numerical predictions from the algebraic flame surface-wrinkling model in RANS context shown with the Kobayashi experimental data (Kobayashi et al. 1996, Kobayashi et al. 1997, Kobayashi et al. 1998, Kobayashi 2001)*

7.4 Implementation of the AFSW Model to LES

In the earlier § 7.3, the performance of the AFSW model using the Kobayashi experimental data based on RANS approach are presented. It is interesting to see the viability of the same reaction closure in the context of an advanced turbulence approach, LES. Here, three data points from the F-1 configuration at different pressure (1, 5 and 10) having near-identical flow and turbulence conditions for an equivalence ratio of 0.9 are chosen, more details are given in Table 7.1.

Table 7.1: *Flow, turbulence and chemical data of the three pressure cases (p - pressure, U_{in} - inlet velocity, u' - turbulent velocity, l_x - integral length scale and s_{L0} - laminar flame speed)*

p (bar)	1	5	10
U (m/S)	2.36	2.21	2.11
u' (m/s)	0.46	0.4	0.36
l_x (mm)	1.25	1.15	1.10
s_{L0} (m/s)	0.34	0.152	0.11

The characteristics of the three flames are represented in the LES premixed turbulent combustion phase diagram of Düssing (Düsing 2004), Fig. 7.5. The two parameters Δ and l_F are the computational grid size and laminar flame thickness, respectively, and the Karlovitz number (*Ka*) is estimated at the subgrid level.
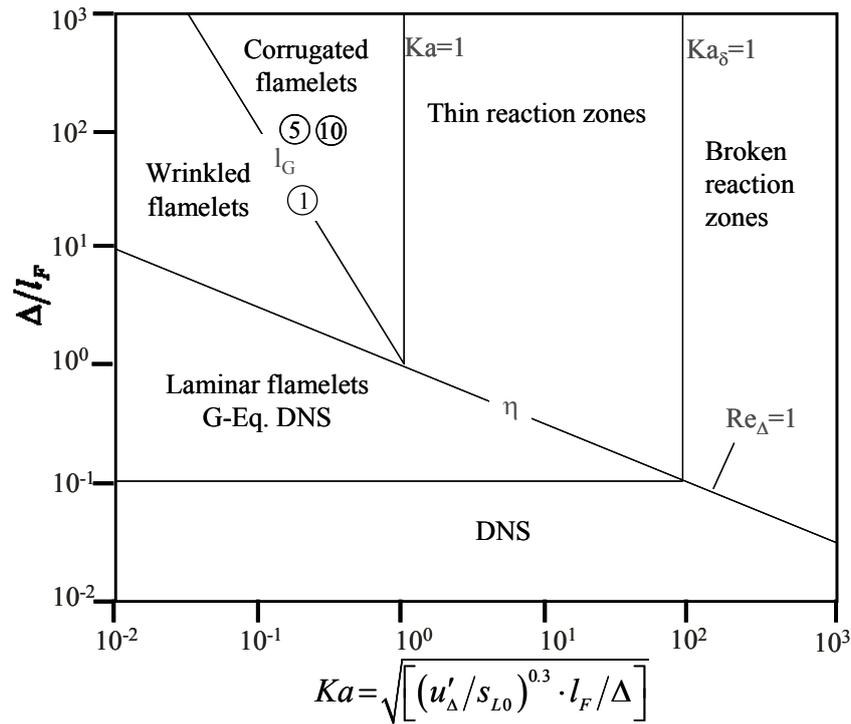
Figure 7.5: *The three flame data points marked as 1, 5, and 10 in the LES premixed turbulent combustion phase diagram of Düssing (Düsing 2004). Δ and l_F are computational grid size and laminar flame thickness, respectively, and the Karlovitz number (Ka) is estimated at the subgrid level. The encircled numbers marked in the diagram correspond to the respective pressure cases.*

Numerical investigation of this simple Bunsen flame is a good test case, as the flow is relatively simple and facilitates to directly test the behaviour of the reaction closure. The computational domain of 50x50x50 mm³ is allocated with an orthogonal mesh of approximately 1.3 million cells with a regular grid spacing of 0.5 mm. A 20 mm diameter burner nozzle inlet carrying premixed fuel-air mixture is centrally staged for symmetry.

The AFSW model given in Eq. 7.2 is directly transformed to the respective subgrid scale (sgs) quantities to close the reaction rate

$$\frac{A_T}{\overline{A}} = \frac{s_T}{s_{L0}} = 1 + \frac{0.46}{e^{(Le-1)}} \cdot \text{Re}_\Delta^{0.25} \cdot \left(\frac{u'_{sgs}}{s_{L0}}\right)^{0.3} \cdot \left(\frac{\nu_0}{\nu}\right)^{0.2} \qquad (7.3)$$

where, u'_{sgs} subgrid turbulence velocity is modelled with the Smagorinsky model $u'_{sgs} = C_S \Delta |\tilde{S}|$, where C_S is the Smagorinsky constant, $u'_{sgs} = \sqrt{2k_{sgs}/3}$ with the dynamic 1-equation k_{sgs} model and Δ is the computational mesh size; the subgrid Reynolds number $\text{Re}_\Delta = u'_{sgs} C_s \Delta / \nu$.

Combusting LES is performed with the three subgrid scale turbulence models (details presented in **Chapter 3**) in combination with the AFSW model for the atmospheric case and the two high-pressure cases are simulated in combination with the simple Smagorinsky model.

The LES of the atmospheric flame with the three turbulence models and AFSW model resulted in a higher flame cone angle, see Table 7.2, the over prediction decreased with the increase of the turbulence model complexity (Table 7.2 and Fig. 7.6). Note that, the RANS based value using this reaction closure was 60° (Table 7.2). A likely reason for LES over prediction is addressed below, considering the aspect of Gibson microscale $l_G = l_x \left(s_{L0}/u'\right)^3$, which is considered as a measure of the smallest flame wrinkles (Peters 1986), as the 1 bar case lies exactly on the l_G line in the regime diagram (Pitsch and Lageneste 2002, Düsing 2004b). For the 1 bar flame and turbulence inlet conditions, l_G equals 0.7 mm, greater than the grid size Δ (of 0.5 mm) used. As stated by Janicka and Sadiki (Janicka 2005), if l_G is greater than or equal to

Δ, the ratio subgrid turbulent flame area normalized by the projected area $A_T^\Delta / \overline{A}$ should be set equal to 1.0 (Janicka 2005). With this rectification, see Fig. 7.6, the resulting cone angle predicted by the three turbulence models in combination with the reaction model is in good agreement with the measured value.

Table 7.2: Flame angles obtained from the AFSW (default) model and rectified with the Gibson scale (l_G) for all the three sgs models in comparison with RANS and experiments (Exp-SM-Smagorinsky, DS-Dynamic Smagorinsky, 1-Equation model for kinetic energy, Exp-Experiments)

Exp	RANS	SM		DS		k_{sgs}	
		Default	with l_G	Default	with l_G	Default	with l_G
61.5°	60°	88°	65°	77°	66.4°	74°	66°
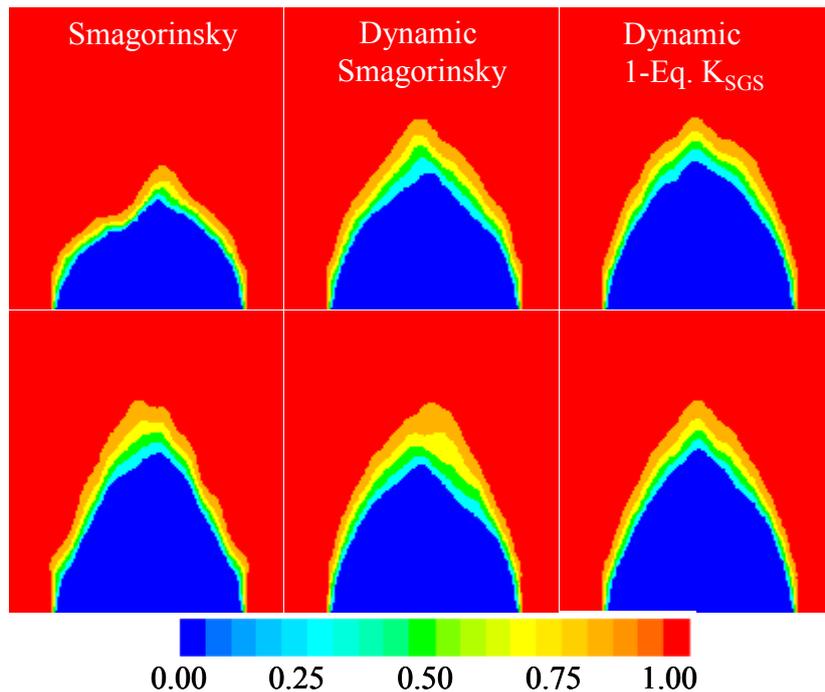
Figure 7.6: Flame shapes obtained from the AFSW (top row) model and rectified with Gibson scale (bottom row) for all the three models (from left to right: Smagorinsky, dynamic Smagorinsky and dynamic one-equation k_{sgs} models)

The other two pressure cases are simulated with the default model in combination with the Smagorinsky model. Some instantaneous flames predicted by the model are shown in Fig. 7.7. It is clearly visible that the flame wrinkling increased with the pressure.
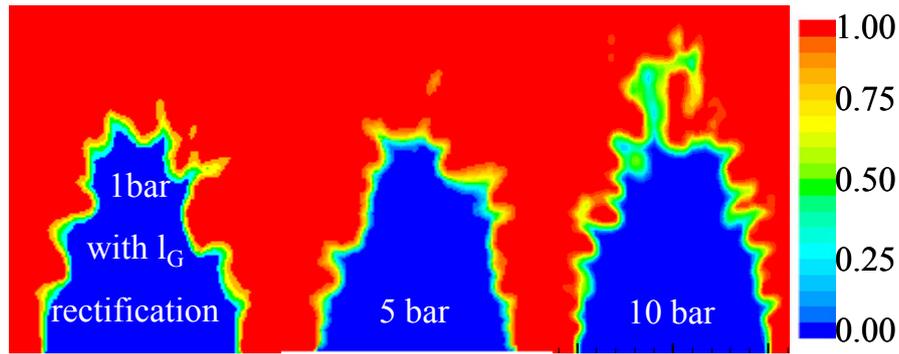
Figure 7.7: *Simulated instantaneous flame shapes of three pressures indicating the increase of flame wrinkling with pressure (1, 5 and 10 bar, from left to right).*
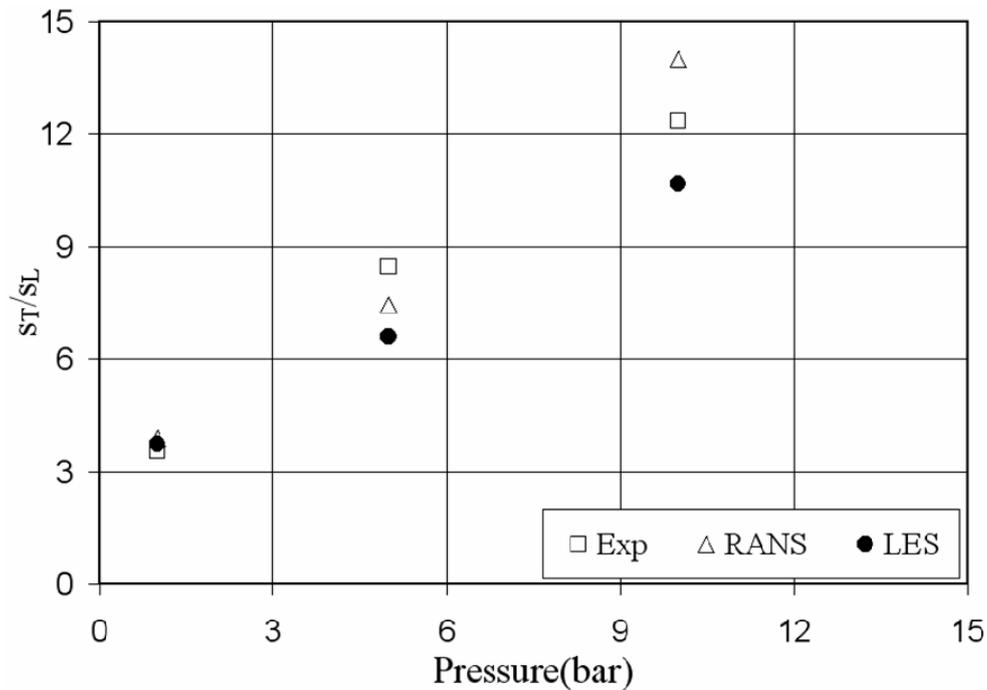
Figure 7.8*: The flame cone angle predicted by the novel reaction closure transformed to s_T/s_{L0} plotted with the increase of pressure in comparison with the RANS predictions and experimental findings.*

The flame angles estimated with the flame cone angle method from the time-averaged mean progress variable contours are then transformed to the usual normalised turbulent flame speed s_T/s_{L0}. The latter is plotted as a function of pressure in comparison with the results from the RANS approach and experiment, Fig. 7.8. The obtained results are in close proximity with the experimental data. This indicates the direct usage of the reaction closure developed in RANS context as a valuable sgs reaction model.

In the next chapter, the AFSW model will further be applied to investigate a relatively new experimental flame data (Griebel et al. 2003, Griebel et al. 2005). These high-pressure preheated lean premixed turbulent data were obtained inside a dump combustor of sudden expansion that stabilizes the flame. This complex flow involves shear-generated turbulence exceeding the grid-generated turbulence by several folds. Further details follow.

8. Model Predictions on a Dump Combustor with RANS and LES Approaches

In this and successive chapters, the performance of the Algebraic Flame Surface Wrinkling (AFSW) models is investigated for more complex flames. This is in so far difficult as sufficiently resolved experimental data of advanced and larger burners under high pressure are often not available for premixed flames. A relatively new experimental flame data measured by *Griebel et al.* (Griebel et al. 2003, Griebel et al. 2005) have been used for comparative studies. These preheated lean premixed turbulent flames were investigated inside a dump combustor, wherein a sudden expansion stabilizes the flame. The pressure was varied between 1 and 14 bar. In addition, non-reacting flow data have been measured, as this complex flow involves shear-generated turbulence exceeding the grid-generated turbulence by several folds. Thus, these measurements (details furnished in **Chapter 5**) are a good source to validate the performance of turbulence models in the non-reacting (cold) flow, and of reaction models in the combusting flow situations. The employed turbulence models and the numerical schemes along with the grid details are presented in Table 8.1.

8.1 Cold Flow RANS Simulations

In a first step, non-reacting simulations were performed using RANS ($k - \varepsilon$ model) approach on a three dimensional domain to study the influence of the turbulence grid located at 30 mm upstream of the sudden expansion (Fig. 6.3). The operating conditions and the geometric Reynolds number (Re) of the non-reacting and reacting cases are given in Table 8.2. The nomenclature of the cases is as follows: C_COLD represents the cold case, C_COMB represents the combusting case and the following number represents the operating pressure.

Table 8.1: *The employed turbulence models in RANS and LES, numerical schemes, and grid details (CDS-Central Difference Scheme, TKE-Turbulent Kinetic Energy, TDR-Turbulent Dissipation Rate).*

	for RANS	for LES
Turbulence models	Standard $k - \varepsilon$ model	Smagorinsky Dynamic Smagorinsky Dynamic K_{SGS}
Pressure	II-order	II-order
Momentum	II-order upwind	II-order CDS
Pressure-Velocity Coupling	SIMPLE	SIMPLE
TKE, TDR	II-order upwind	-
Progress Variable	II-order upwind	II-order CDS
Temporal Discretisation		II-order
k_{SGS}	-	II-order CDS
Grid spacing	≈ 1 mm (3D-RANS) ≈ 0.25mm (2D-RANS)	≈ 1 mm (fine) ≈ 2 mm (coarse)
Cell count	≈ 6 million (3D-RANS) $\approx 45,000$ (2D-RANS)	≈ 1.1 million (fine) ≈ 0.4 million (coarse)
Smagorinsky's model Constant (C_s)	-	0.1 (actual solution) 0.05 (for analysis)

The dimensions of the domain are depicted in Fig. 8.1; the whole computational field is meshed unstructured with nearly 6 million tetrahedral cells. The dimensions of the holes, pitch, and placement of the turbulence grid replicate the experimental setup shown in Fig. 6.3. Typical flow characteristics of the simulated geometry are numbered in Fig. 8.1, where '1' is the high velocity core flow region with grid-generated turbulence, '2' is the recirculation region formed due to sudden expansion, in between these two, is '3', the region of shear generated turbulence, which extends to the downstream region.

Table 8.2: *Operating conditions of the selected cases (units in m/s, K, and bar)*

Case	U_{in}	T_{in}	p	Re	RANS	LES	T_f/T_{in}
	m/s	K	bar	-	-	-	K
C_COLD1	45	300	1	81,000	YES	YES	300
C_COLD5	45	673	5	405,000	YES	NO	300
C_COLD10	45	673	10	810,000	YES	NO	300
C_COMB1	45	673	1	16,000	YES	YES	1750
C_COMB5	45	673	5	80,000	YES	YES	1790
C_COMB10	45	673	10	160,000	YES	YES	1795
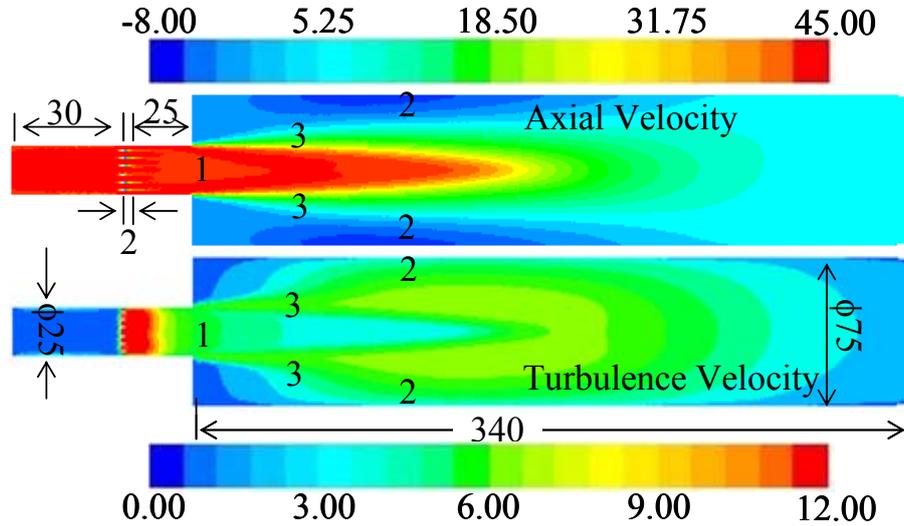
Figure 8.1: *Predicted axial (top) and turbulent (bottom) velocities by the $k - \varepsilon$ model, different regions of the flow are marked with numbers.*

The radial profiles from 5 mm downstream of the turbulence grid (x = -25 mm) up to the sudden expansion (x = 0 mm) indicate the penetration of the jets into the combustor (sudden expansion) to some extent, see Fig. 8.2.
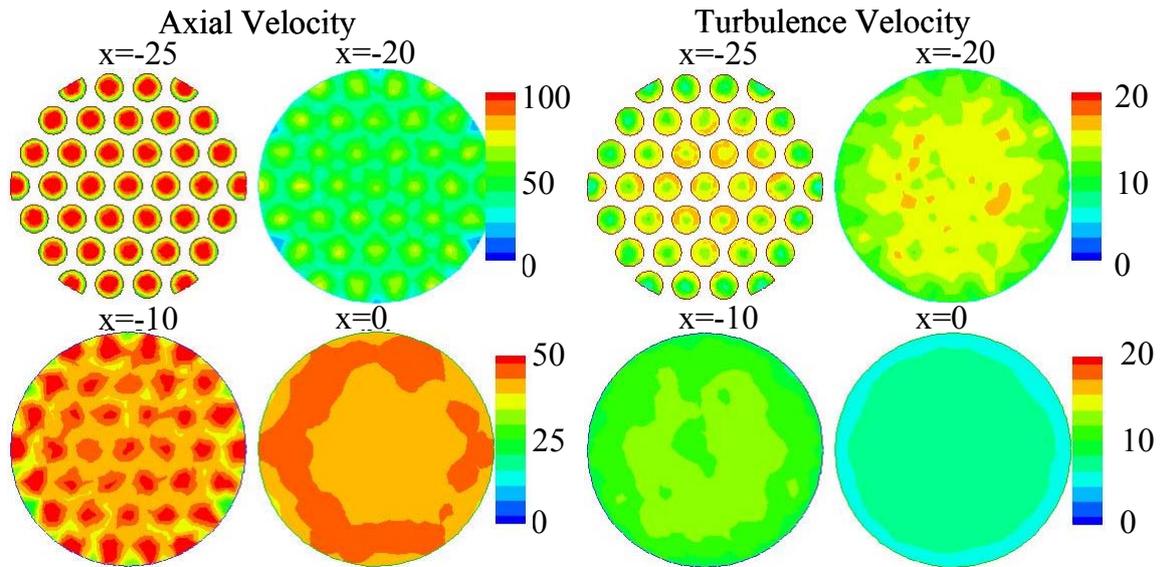
Figure 8.2: *Predicted axial and turbulent velocities by the $k - \varepsilon$ model, at different levels upstream of the sudden expansion (x = 0 mm corresponds to the sudden expansion location and -25 mm to the location of the turbulence grid).*

This can better be visualised with the axial turbulent kinetic energy (TKE) profiles shown in Fig. 8.3. In the plots, both the axial and radial distances are normalised with the inlet diameter (d = 25mm). Also, the jet break-up length is over predicted by as much as 2 times the inlet diameter. Though the TKE peak is predicted reasonably, its width in the axial direction is very narrow (Fig. 8.3). To reduce the computational burden, 2D axis-symmetric simulations were performed for the domain behind the turbulence grid by imposing constant inlet velocity and turbulence levels for varied pressures. The results are close to the 3D simulation except in the region of x/d < 2.5 where the TKE in the 3D case is higher due to the penetration of the mentioned individual jets produced by the turbulence grid. The main TKE peak is predicted very similar to that in the three dimensional case and jet break-up length is slightly extended downstream by 0.2 d. The three pressure non-reacting cases simulated with 2D RANS approach are very similar to each other (Fig. 8.3).
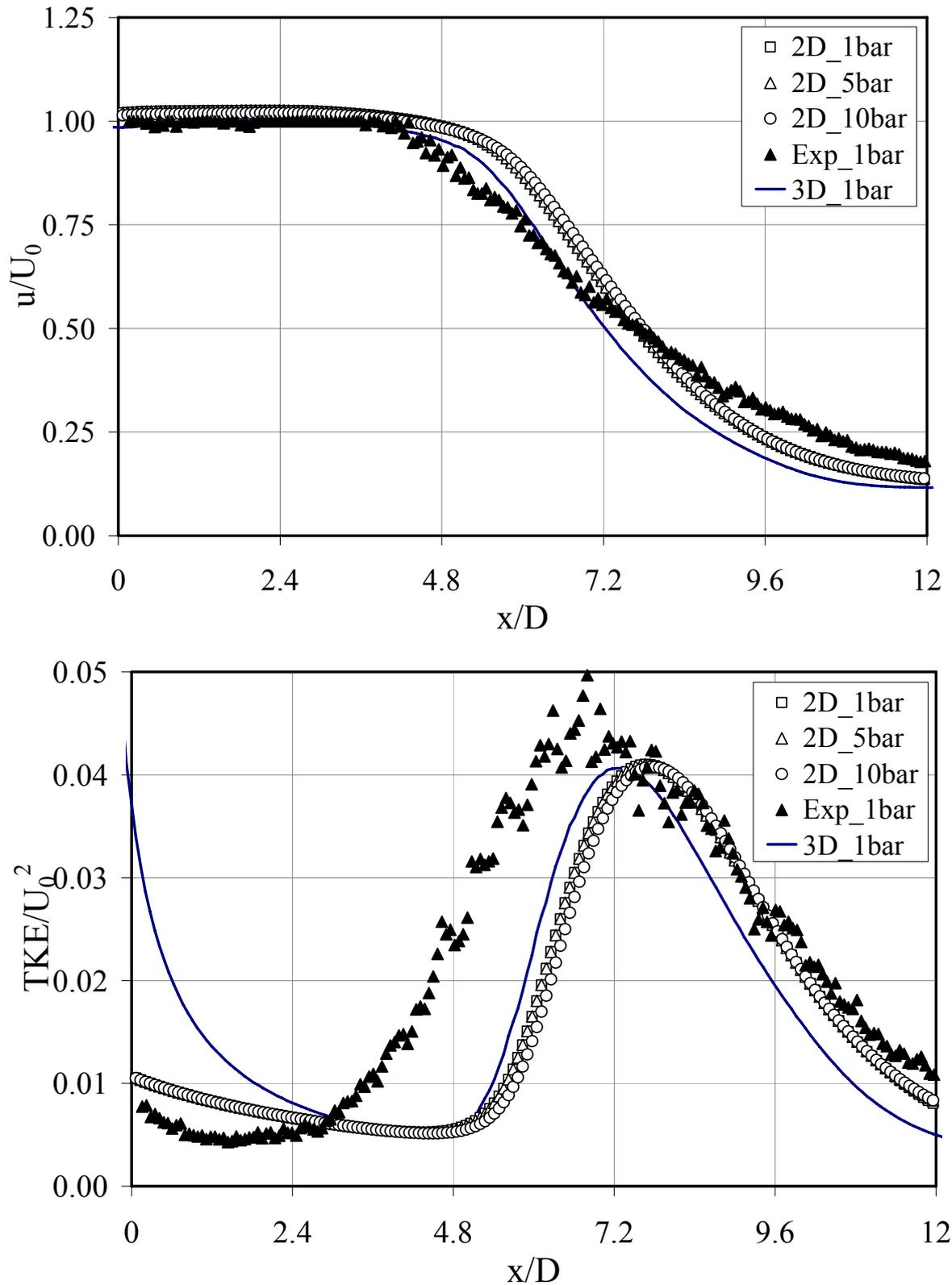
Figure 8.3: *Comparison of axial velocity (top) and TKE (bottom) of 2D and 3D cases with that of experiments along the axis of the combustor. Also, shown are high-pressure cases simulated on 2D domain.*

The radial profiles at three axial junctions of $x/d = 1$, 5 and 11 are presented in Fig. 8.4. The axial velocity predictions in both 2D and 3D simulation at the first two

junctions closely follow the experiments but the TKE mismatches considerably. At the last junction the 2D simulation follows the experimental data better than the 3D simulation. As a whole, independent of 2D or 3D the $k-\varepsilon$ model predicts the TKE distribution in a very narrow range. In, (Manickam 2006), various turbulence models with different inlet profiles were simulated on a 2D domain in RANS context. It was shown that none of these combinations replicate the experiments satisfactorily. Also, reported that the tuning of the $k-\varepsilon$ turbulence model constants $c_{\varepsilon 1}$ and c_{μ} following (Pope 2000), yielded very little success. Both the TKE peak and its onset were not accurately predictable simultaneously despite carrying out parametric adjustments. Therefore, in the current study as a next step, simulations are performed with LES approach to understand this complexity of flow behaviour in a better way; the results of which are presented in the upcoming sections, 8.3 and 8.4.
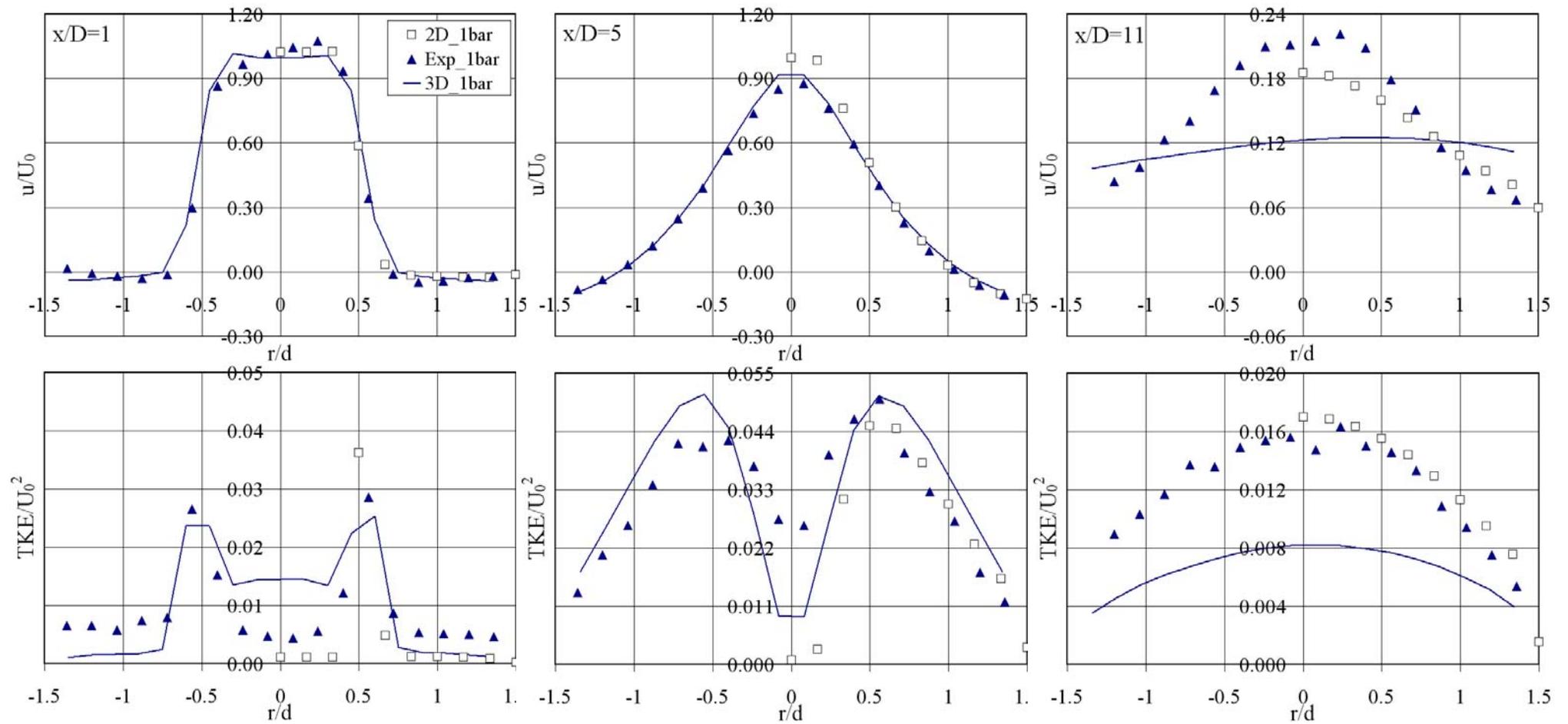
Figure 8.4: *Comparisons of axial velocity and TKE of 2D and 3D cases with experiments at three different axial locations in the combustor.*

8.2 Predictions of the AFSW Reaction Model in RANS Approach

Before discussing the LES results, reacting flow simulations using RANS are presented to study the model behaviour for the variation of pressure (1, 5, 10 and 14.4 bar) at constant equivalence ratio of 0.5. The typical flame shape predicted by the AFSW reaction closure is presented in Fig. 8.5. The experimental data is available only for 5bar case so simulations are compared only with the experimental 5bar case.
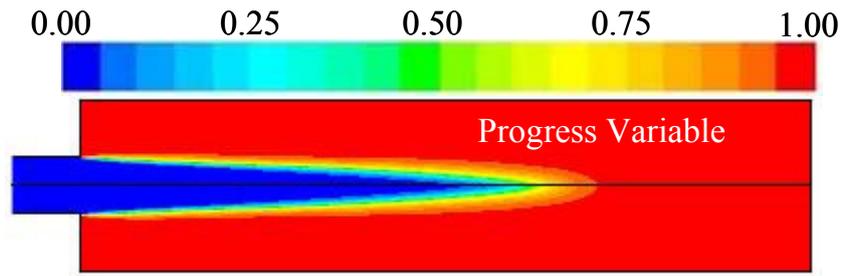
Figure 8.5: *Predicted flame shape (progress variable) by the AFSW closure with RANS approach for the atmospheric case.*

The mean progress variable and its gradient plotted along the axis of the combustor are shown in Fig. 8.6. The latter is compared with experimental data, obtained from the statistical analysis of the instantaneous flame contour position (the latter is determined from the OH-PLIF contour line (Griebel et al. 2005), see Chapter 5.2). Despite of the fixed jet break-up with pressure variation in the cold flow simulations (Fig. 8.3), 2D-combusting RANS simulations show that with the increase of pressure the flamefront moves downstream on the nozzle inlet (8.6a) for the same flow conditions and equivalence ratio. Experimentally (Griebel et al. 2005), it was observed that the flame front moves slightly downstream for the pressure variation from 5 to 14.4 bar. It can be observed from the same figure that the flame position is shifted to the downstream side. This can be related to the late jet breakup observed in the cold flow simulations (Fig. 8.3).

The comparison of the progress variable gradient with the experimental flame position at 5 bar shows that the RANS simulations predict the flame brush in the axial direction much smaller than is found experimentally (Fig. 8.6 b). Later it will be shown that the predictions of these two quantities (mean flame position and brush thickness)with the AFSW model in LES context fit much better to the experimental findings. Thus, the above mentioned indifferences can be attributed to the malfunction of the RANS

turbulence model. As a next step, cold and reacting simulations are performed with the LES approach.
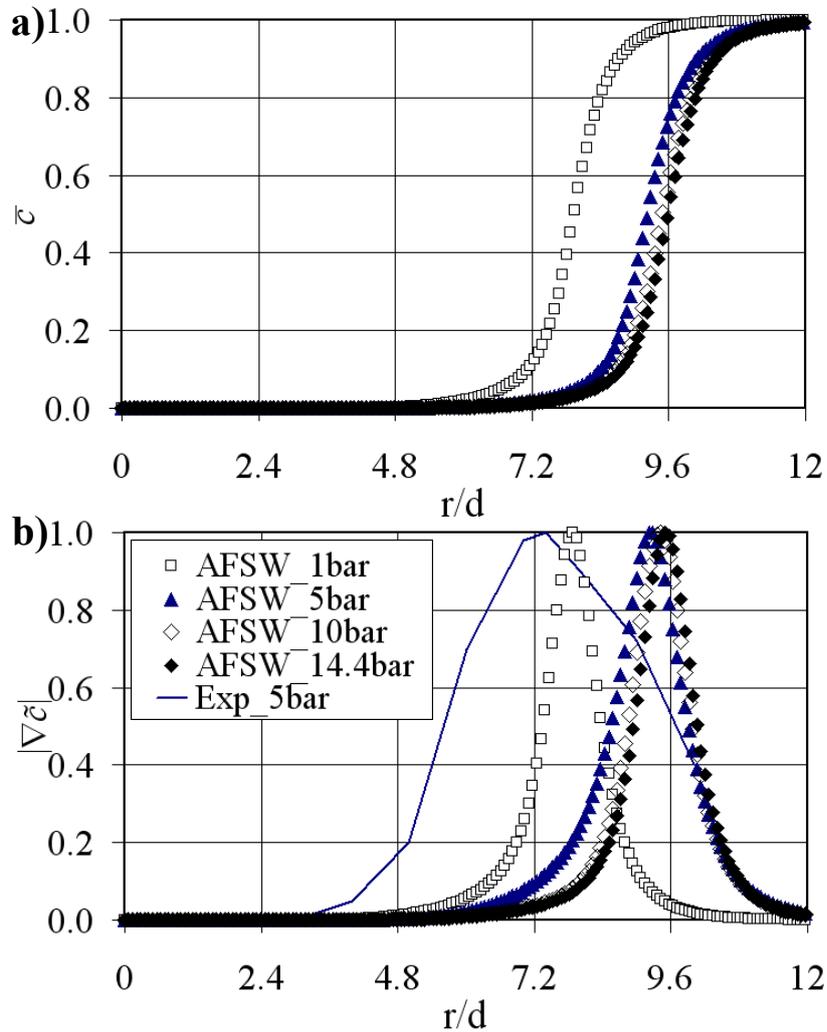
Figure 8.6: *Plots of a) progress variable and b) its gradient along the axis of the combustor with the variation of pressure.*

8.3 Cold Flow LES

Cold flow simulations are performed with the LES approach by employing Smagorinsky, dynamic Smagorinsky and one-equation k_{sgs} turbulence closures (see **Chapter 2**, for model details). This serves as a validation of the flow solver as well as of the turbulence models. Numerical results are compared with the corresponding experiments, and also with the combustion results to understand the flow changes generated by the combustion process. The flow characteristics of this configuration, the employed numerical schemes and the simulated cases are given in Tables 8.1 and

8.2. Atmospheric cold flow simulations are performed for the three turbulence closures for varied inflow conditions and grid types. As the inlet turbulence grid is situated 30 mm upstream of the sudden expansion, two test simulations are performed one with constant inlet velocity of 45 m/s and the other for a specified inlet profile,being obtained from RANS on a domain extending 82 mm downstream of the sudden expansion. The computational domain is meshed in two modes, one being resolved only near the wall and uniform elsewhere, and the other resolved in the shear layer and near walls. Simulations on the uniform grid are performed for two grid resolutions (fine and coarse) to estimate the resolved energy using the LES_IQ analysis (Celik et al. 2005) described in **Chapter 6**. The fine grid simulations correspond to the actual results, whereas the 'coarse' simulations complement the accuracy analysis.

In Fig. 8.7a, b and c, the axial profiles of mean axial velocity and the resolved turbulent kinetic energy (TKE) of all the cases obtained with the fine grid are presented. As the experimental data is available only from the start of the sudden expansion ($x/D = 0$), simulated results are also presented from the same location. Irrespective of the specified inlet boundary conditions and the turbulence model used, the experimental behaviour cannot be reproducible between $x/D = 0$ and $x/D = 3$. However, the inlet condition has very little influence in predicting the jet break-up length and the TKE peak with the classical Smagorinsky model, indicating that the break-up is dependent mainly on the shear-generated turbulence between the strong axial jet and the recirculation zone (Fig.8.8). The predictions of the classic model can be improved with increasing resolution in the shear layer. In case of the dynamic models, the inlet profile has strong influence on the velocity field predictions and minimal impact on resolving the shear layer.
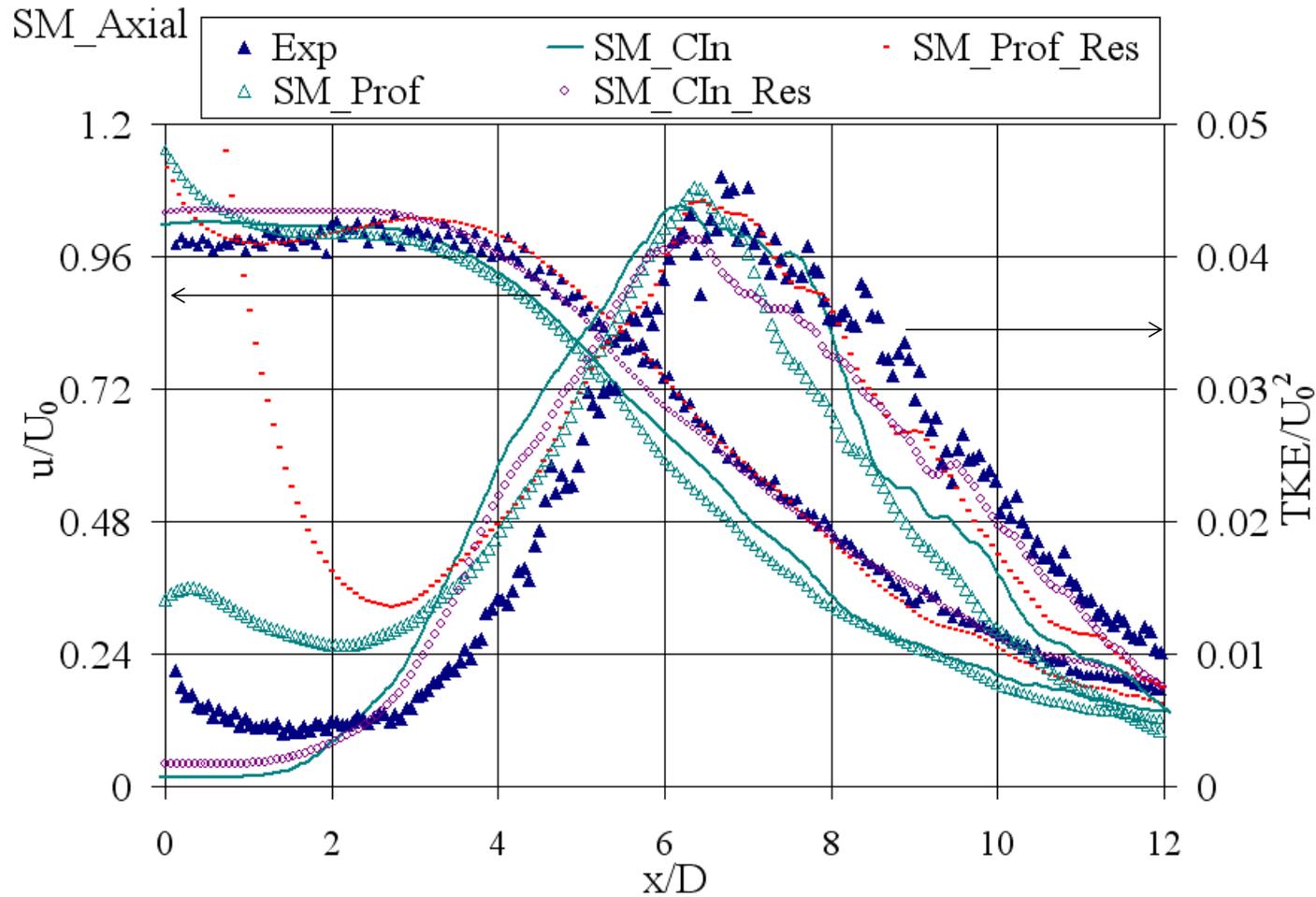
Figure 8.7a: *Axial profiles of the Smagorinsky (SM) closure on fine grid for varied inlet conditions, CIn – represents constant inlet profile with specified perturbations at the inlet on uniform grid, Res - with grid resolved in shear layer, prof – specified inlet velocity profile as shown in Fig. 8.2 (x = 0 mm), Exp – Experiments.*
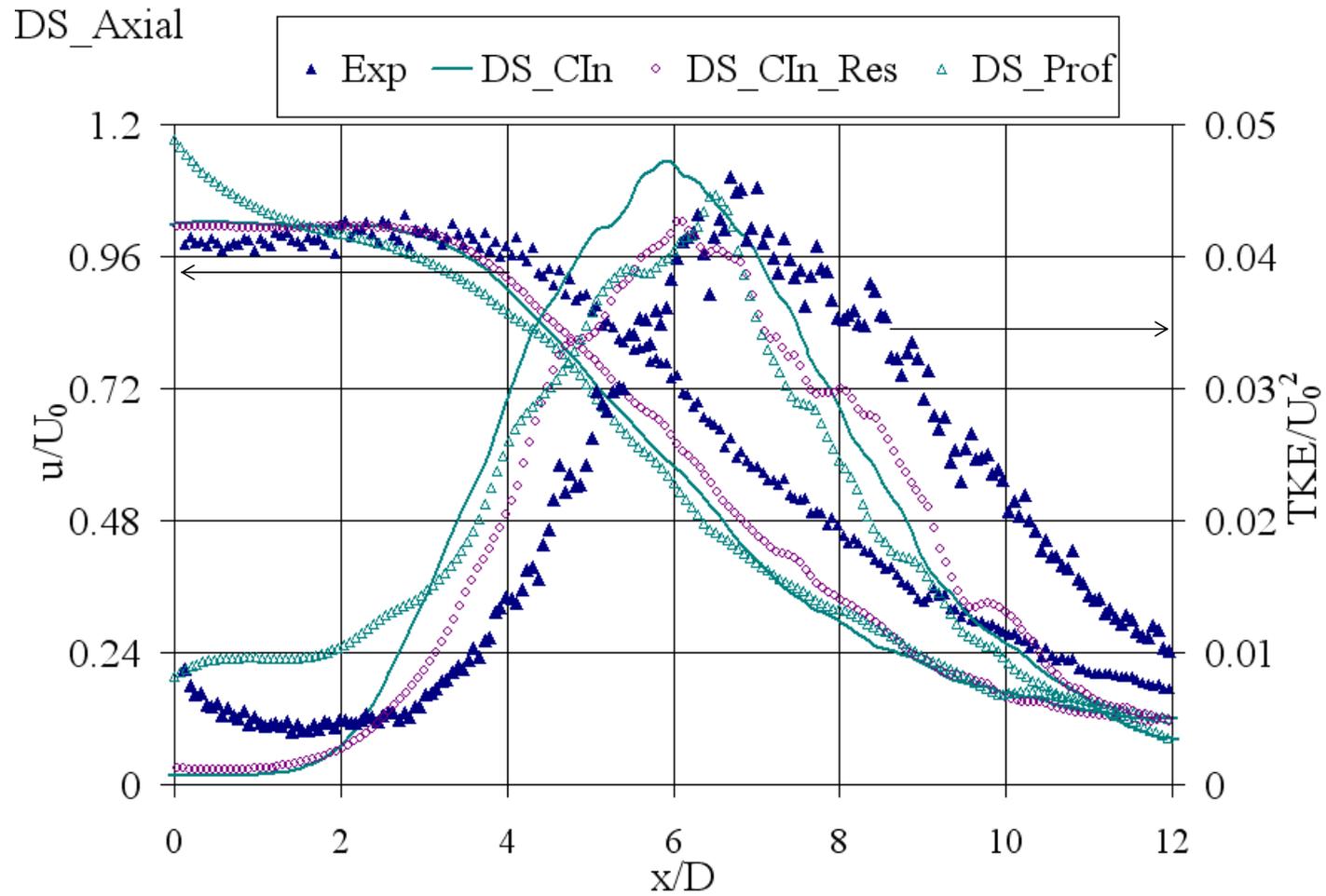
Figure 8.7b: *Axial profiles of the dynamic Smagorinsky (DS) closure on fine grid for varied inlet conditions, CIn – represents constant inlet profile with specified perturbations at the inlet on uniform grid, Res - with grid resolved in shear layer, prof – specified inlet velocity profile as shown in Fig. 8.2 (x = 0mm), Exp – Experiments.*
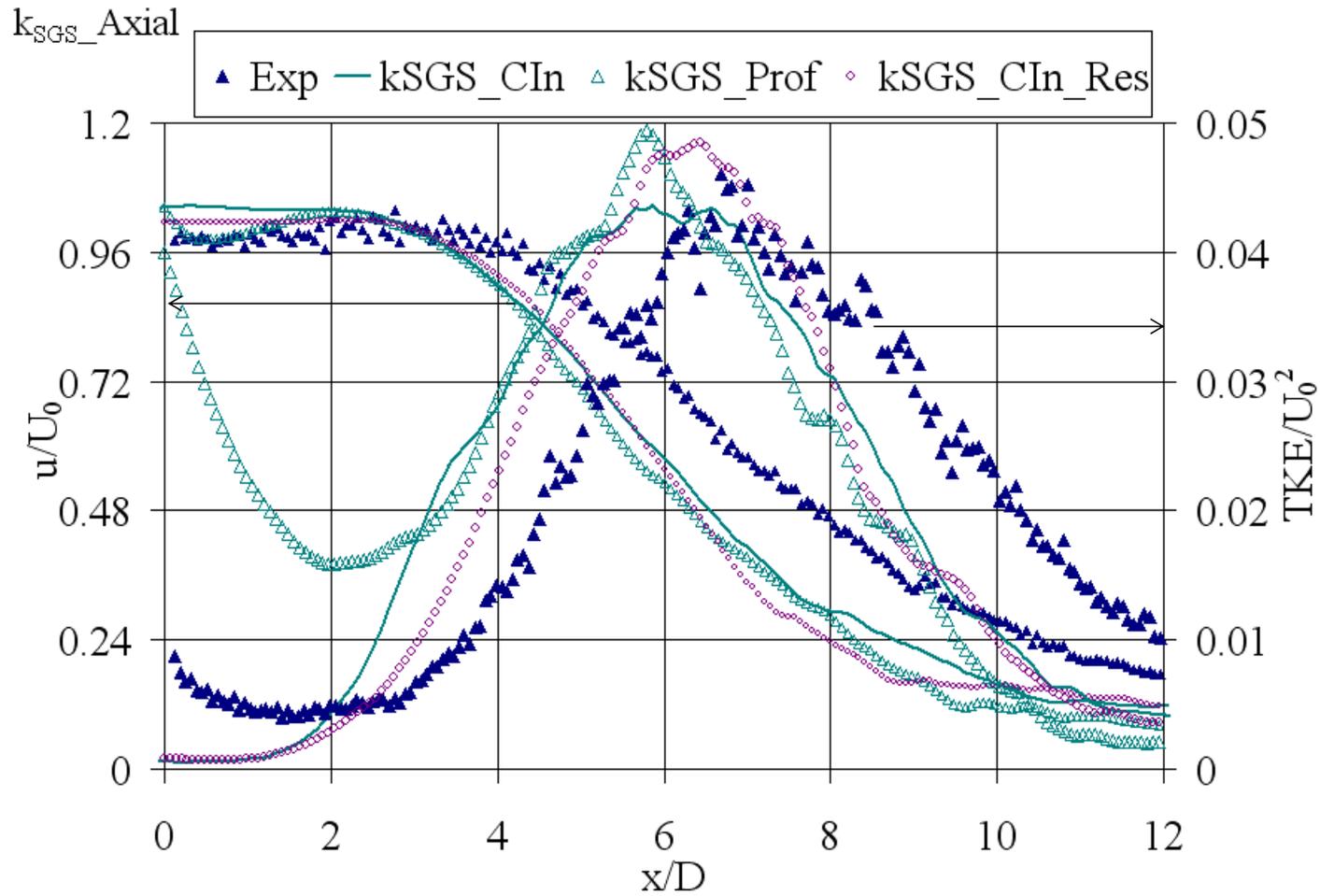
Figure 8.7c: *Axial profiles of the dynamic k_{sgs} (Ksgs) closure on fine grid for varied inlet conditions, CIn – represents constant inlet profile with specified perturbations at the inlet on uniform grid, Res - with grid resolved in shear layer, prof – specified inlet velocity profile as shown in Fig. 8.2 (x = 0mm), Exp – Experiments.*
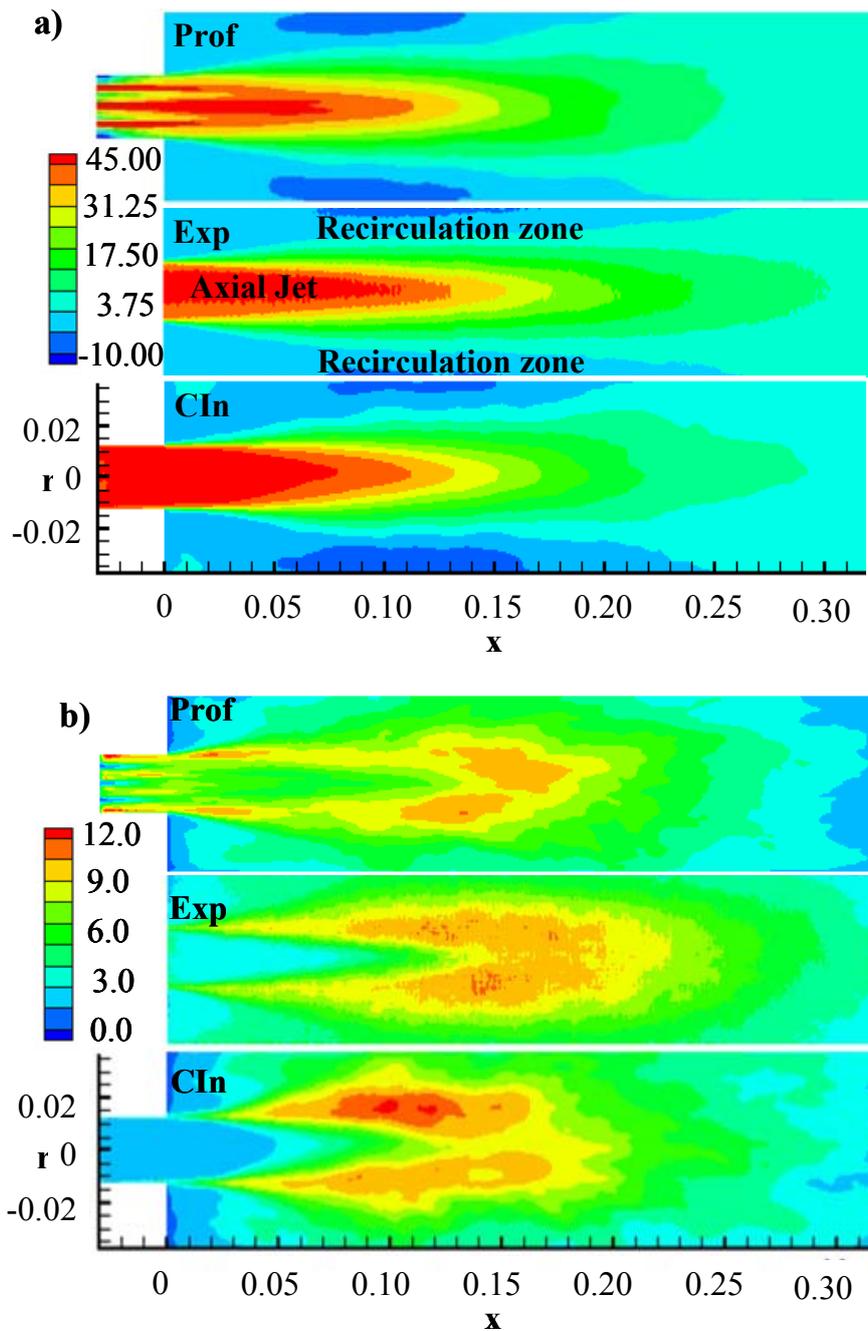
Figure 8.8: *Contours of a) mean axial velocity and b) axial RMS velocity obtained on an uniform grid with inlet jets (Prof) and with constant inlet velocity (CIn) in comparison with that of experimental findings Exp).*

In Fig. 8.9, the results obtained from the Smagorinsky model on coarse and fine grids are compared with the experiments. As all the three models yielded similar behaviour on fine and coarse grids, only the results obtained with the Smagorinsky model are presented in Fig. 8.9. All the models predict a longer jet on the coarse grid in comparison to the fine grid with over prediction of the total kinetic energy TKE. This is attributed to low resolution, which reduces the dissipation rate. Another interpretation

is that the coarse resolution corresponds to a flow at an effectively lower Reynolds number; hence, the transition to shear induced turbulence is delayed, while a higher dimensionless kinetic energy is predicted; the estimated Re_t is shown in Fig. 8.10a along with the viscosity. This is in accordance with DNS observations (Klein 2005a). The viscosity on the coarse grid is 2-3 times higher than that of the fine grid. The time-averaged model coefficients of the three turbulence models on the fine grid are shown in Fig 8.10b along with the strain rate magnitude, which is used to estimate the subgrid turbulent intensity and length scale.

The LES accuracy of the three models is estimated with the method proposed by Celik et al, using Eq. 5.3, see results in Fig. 8.10c. Between x/d = 2 and 9 all three models result in the same accuracy about 60 %. Beyond x/d = 9 (down stream of the TKE peak) the classic Smagorinscy model yielded better than the dynamic models. Thus, it is not always valid to assume that the dynamic Smagorinsky model outperforms the Smagorinsky model. This point was illustrated by Meneveau (Meneveau 2005) for rapidly strained flow. Moreover, the implementation of the dynamic model differs from case to case and from code to code in the way the dynamic coefficient is limited and averaged. It is usually averaged in the direction which is considered to exhibit homogeneity in turbulence. In more complex cases, as has been dealt here; there is no obvious homogeneous direction. And, the strong variations of the dynamic models with shear layer resolution and with inlet profile (Fig. 8.7a, b & c) could be attributed to the above-mentioned fact.
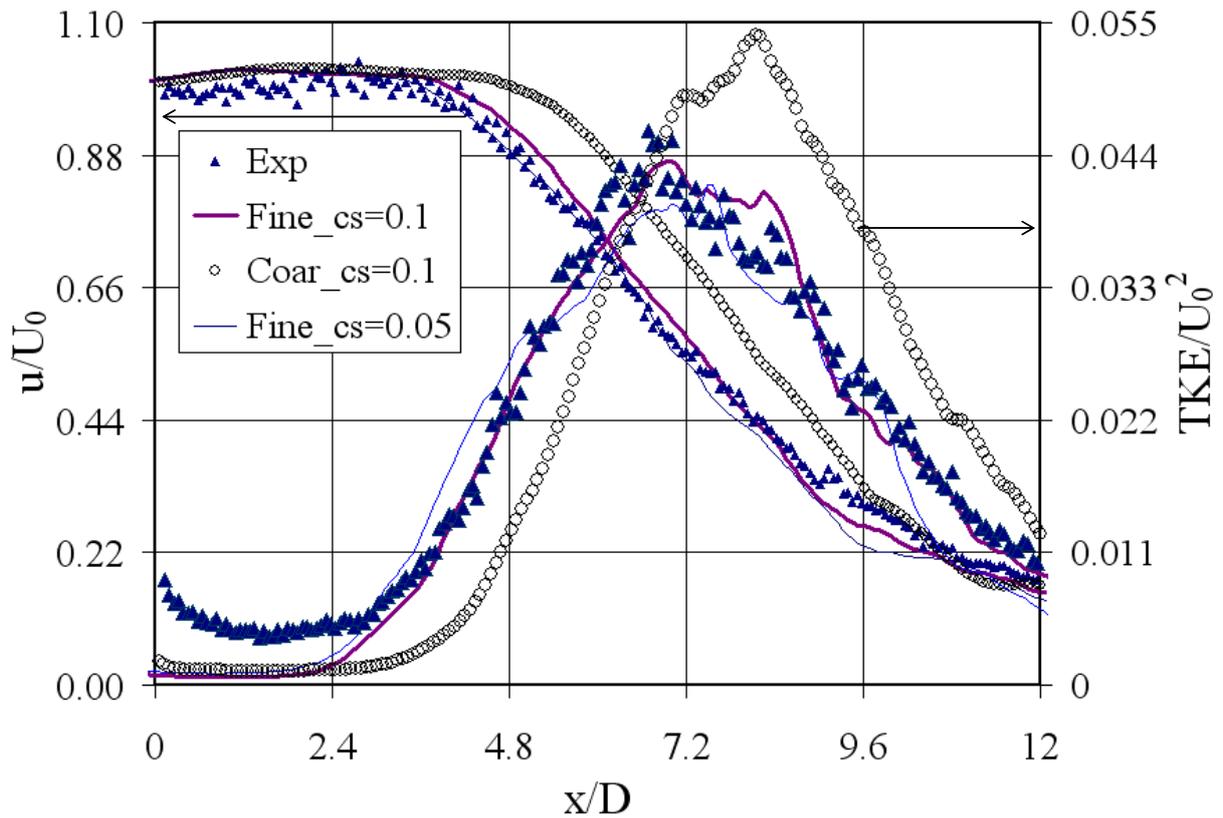
Figure 8.9: *Profiles of mean axial velocity and TKE along the combustor axis predicted by the Smagorinsky closure on coarse and fine grids for the case C_COLD1. Distinguished differences between the coarse and fine grids are visible, but very minor differences between the cases simulated with C_S = 0.1 and C_S = 0.05 on the fine grid level.*
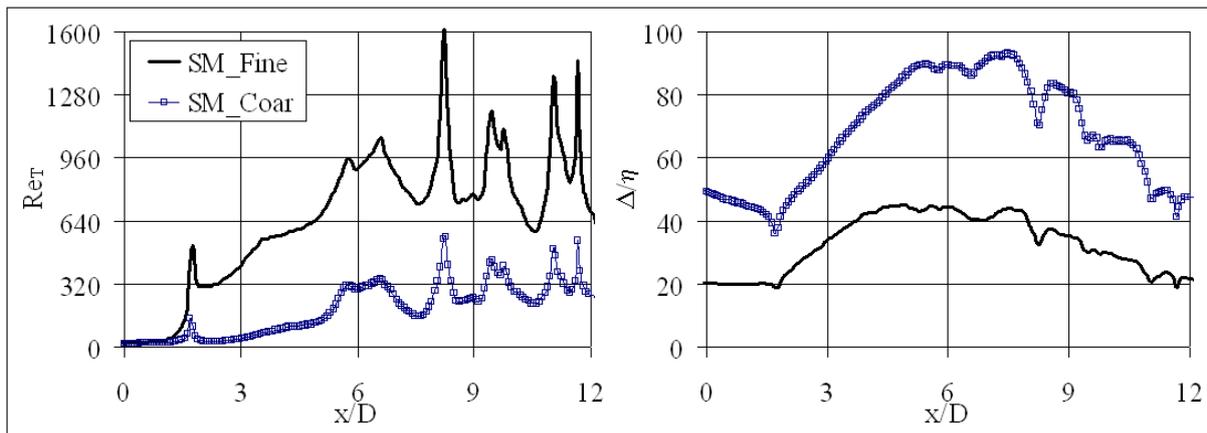
Figure 8.10a: *Estimated Re_t on coarse and fine grid (left) along with the time averaged viscosity (right) for the Smagorinsky model.*
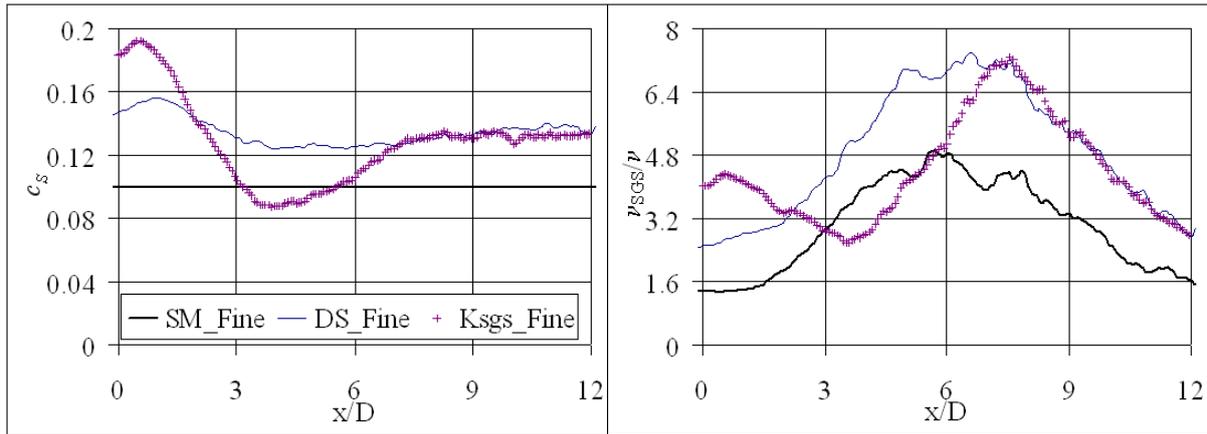
Figure 8.10b: *Time averaged turbulence model constant (left) and strain rate magnitude (right) of the three models.*
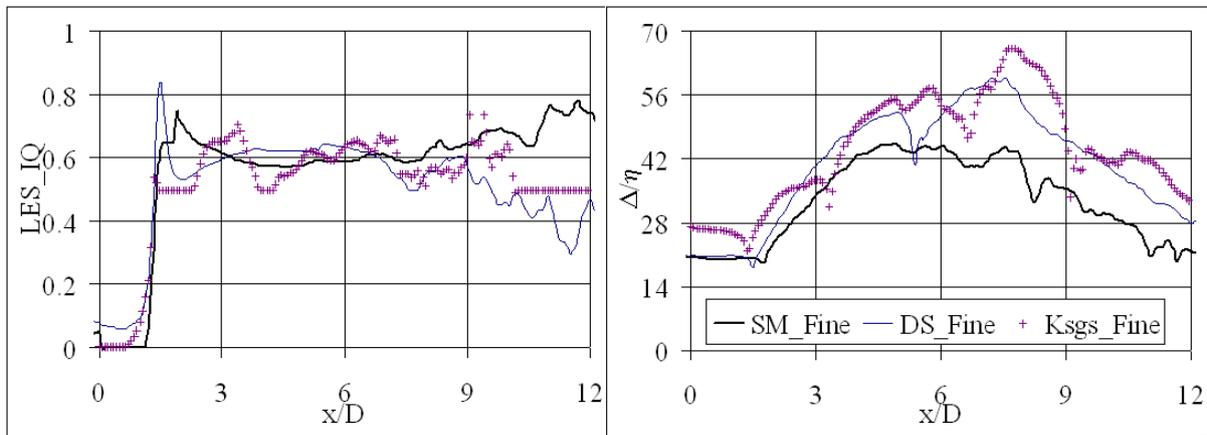
Figure 8.10c: *LES_IQ for three turbulence models (left) and the ratio of the grid size to the effective Kolmogorov scales (right), both giving indication of the good LES resolution on the fine grid level.*

The individual error contributions (estimated with Eqs. 5.7, 5.8 and 5.9) of the turbulence model and discretization scheme towards the total energy is estimated with Klein's approach presented in Chapter 5. Computed mean axial velocity and turbulent kinetic energy (TKE) on the fine grid are in close proximity with measurements (see Fig. 8.9). With the change of the Smagorinsky constant C_S from 0.1 to 0.05, no considerable difference is observed in the mean velocity and TKE, Fig. 8.9. While on the coarse grid for $C_S = 0.1$, as discussed above, the peak TKE is over-predicted by as much as 30 %. These three cases are processed using the Klein's approach (Klein 2005b) to estimate the amount of energy dissipated via discretization and from the usage of the turbulence closure. Separated amounts are plotted along with the total

contribution in Fig. 8.11. As the model and numerical contributions are having opposite signs, both combined contribute less to total error contribution.
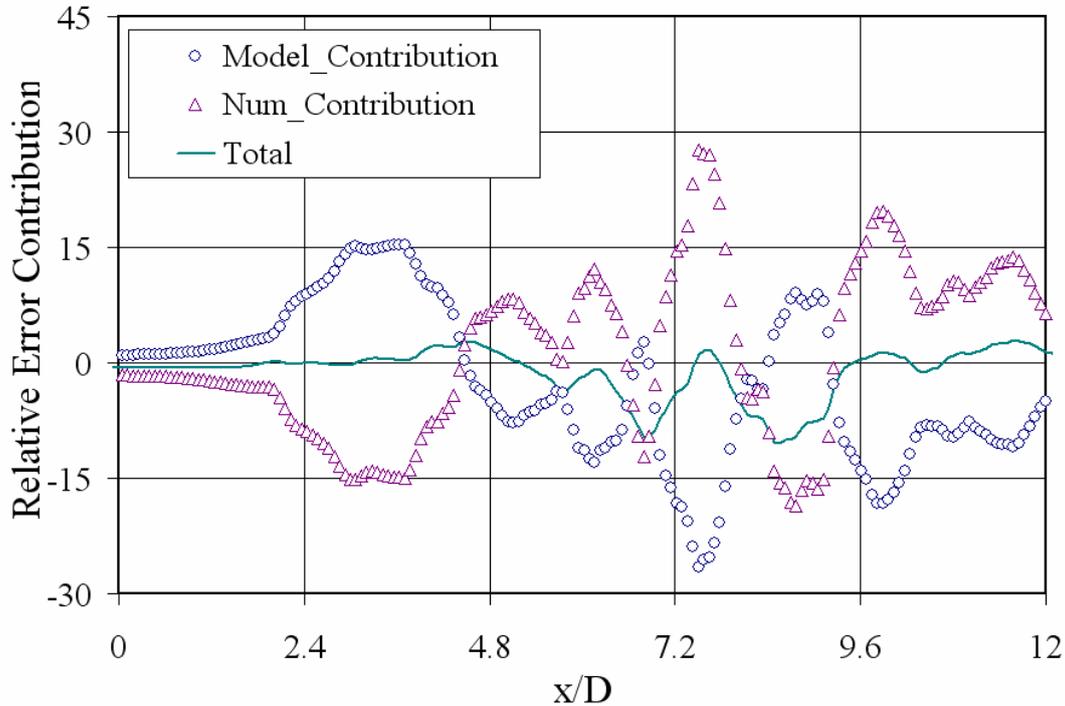
Figure 8.11: *Separation of numerical and model error contributions (estimated with Eq.5.7, 5.8 and 5.9) plotted along the axis of the combustor obtained with the Klein's approach*

8.4 Reacting Flow LES

In the following, combustion LES are carried out for each of these three turbulence closures in combination with the AFSW reaction model (Eq. 7.9).

This section is portioned into:

1. Comparison of cold and reacting cases

2. Interaction of -turbulence and reaction closures

3. Pressure effects on flame position and turbulent flame brush thickness

8.4.1 Comparison of cold and combusting cases

The cold case (C_COLD1) simulations performed with the Smagorinsky model are compared and analysed with the three high pressure reacting cases (C_COMB1) simulated with the AFSW model in combination with the three models, to assess the changes specifically due to combustion. Similar to typical gas turbine conditions the

reaction mixtures are preheated to 673 K. This decreases the Reynolds number at the inlet to about 16,000 which is 20% of that in the cold flow. In Figure 8.12a the averaged axial velocity and the turbulent kinetic energy profiles are shown along the burner axis. It can be noticed from Fig. 8.12a that the transition to large-scale turbulence takes place more downstream in the combustion case (x/D = 6, Fig. 8.12a) compared to the nonreacting situation (x/D = 3, Fig. 8.12a).

The evaluated LES index of quality is shown along the axis in Fig. 8.12b for the cold and the combustion case. The higher value in combusting flow is due to the reduction of the Reynolds number, reaching a value of around 0.8, compared to 0.6 for the cold case. This is a straightforward indication of well-resolved LES for the combustion case. This can be confirmed from estimated Kolmogorov scales, η, reducing the ratio between grid size h and η from 20–40 in the cold case to 4–8 for the combustion case (Fig. 8.12b). The finest (Kolmogorov) scale η is calibrated based on the effective viscosity, which is estimated, following (Celik et al. 2005), as sum of molecular, turbulent, and numerical viscosities ($\nu_{mol} + \nu_t + \nu_{num}$). Similar results have been found also for the dynamic models.
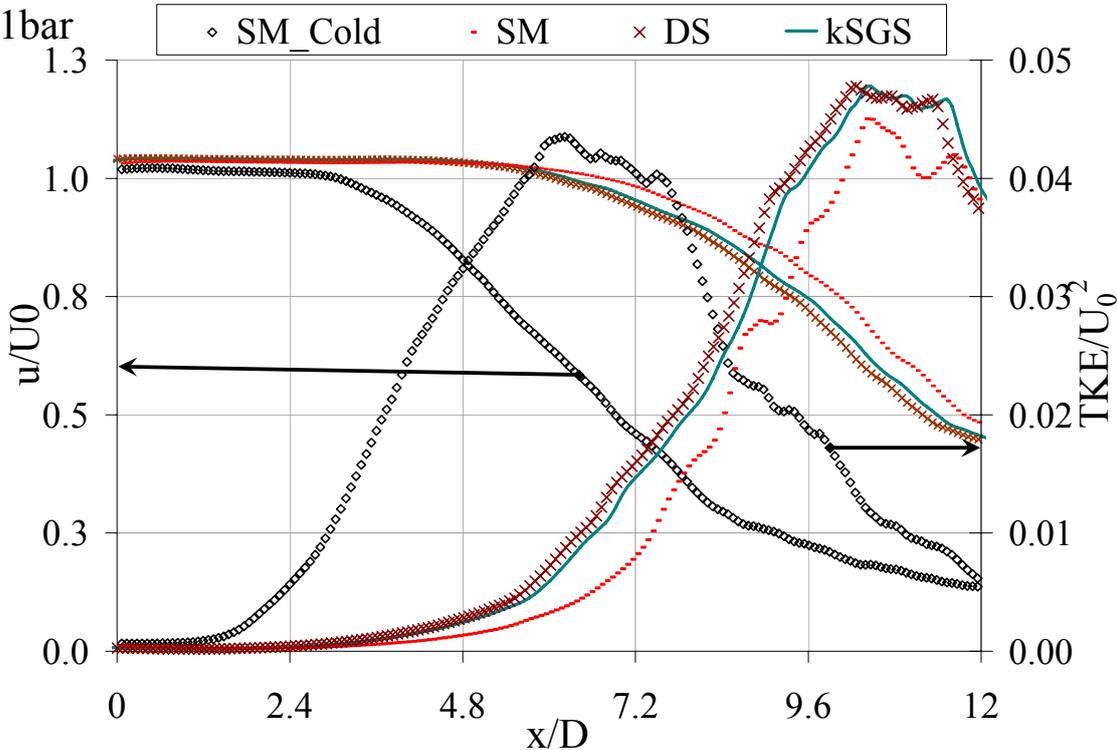
Figure 8.12a: *Profiles of mean axial velocity and TKE along the x-axis predicted with the three closures in comparison with the cold flow predictions.*
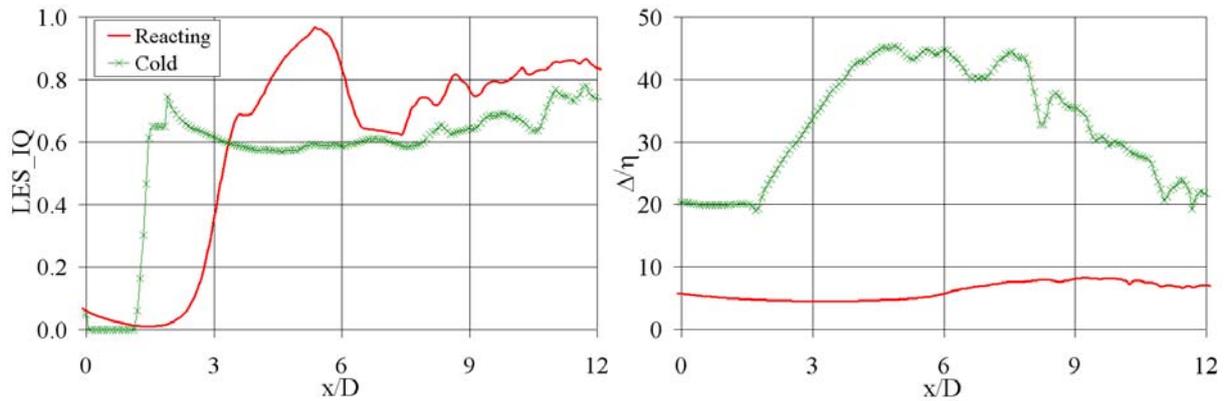
Figure 8.12b: *LES IQ obtained from two grid levels showing the amount of resolved kinetic energy (left) and the grid size w.r.t. Kolmogorov scale (right) in non-reacting (C_COLD1) and reacting cases (C_COMB1).(Smagorinsky model, 1 bar).*

8.4.2 Interaction of -turbulence and reaction closures

In the first instance, turbulent lean premixed methane flames are simulated for all the three turbulence closures, along with the algebraic flame-wrinkling reaction model at 1 bar (Fig. 8.12c). The time-averaged gradient of the reaction progress variable as indicator of the flame position is compared with experimental data (Fig. 8.12c).

The calculations with LES result in the flame length which is remarkable close to the experimental situation. This is in contrast to the RANS calculations (as has been shown before in Figure 8.6), where the flame was over predicted by 30%. A more detailed comparison between experiment and LES calculations shows, that the reaction closure in combination with the two dynamic models follows the experimental data more closely whereas with the standard Smagorinsky model the flame position is shifted downstream by about 10 %. This is opposite to the cold flow simulation in which the Smagorinsky model was found in better agreement with the experimental data in terms of mean axial velocity and TKE.
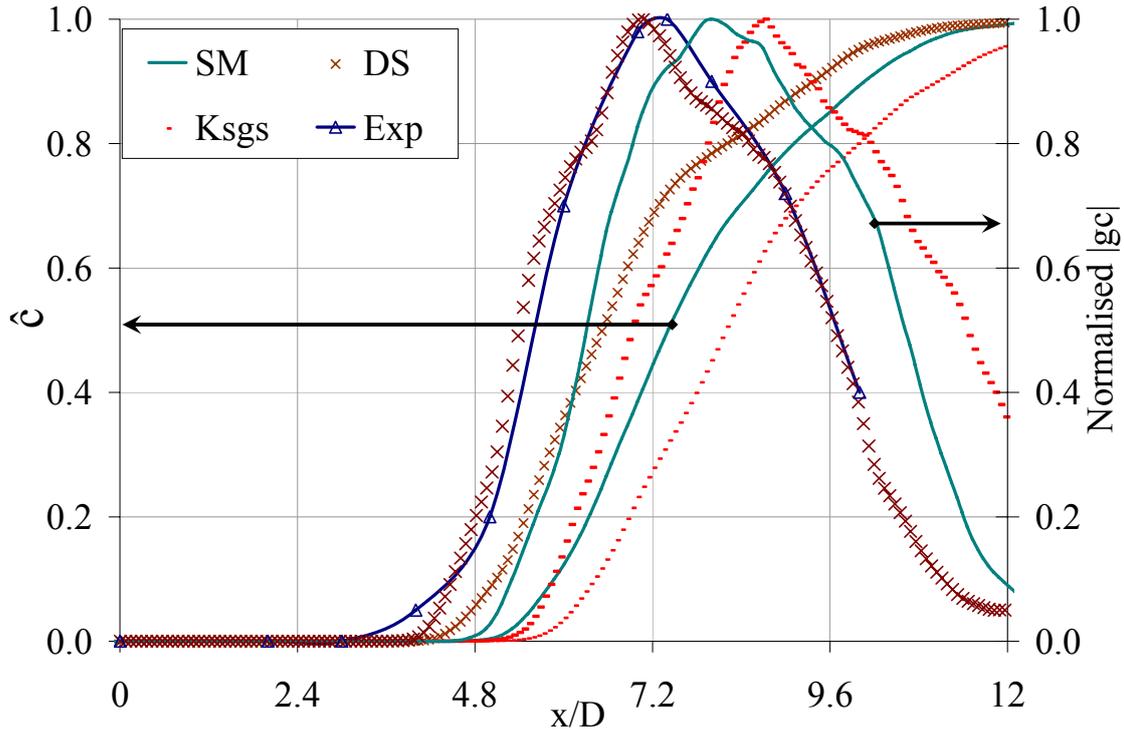
Figure 8.12c: *Profiles of progress variable along the combustor axis predicted with the AFSW model in combination with the three closures. Also plotted are the progress variable gradient of the three combinations along with the experimental data for 1bar case.*

8.4.3 LES of high-pressure flames

The increase in pressure is made in two steps, from 1 to 5 and to 10 bar, for constant inlet flow conditions for lean equivalence ratio of 0.5. In Fig. 8.13a, computed instantaneous sample flames in the plane of the axis are shown in comparison with instantaneous OH-PLIF images in the same plane (Griebel et al. 2003) (field of view is different). Although the interpretation of such OH-PLIF images with respect to the reaction zone is not appropriate (the gradient in the inner part between zero and maximum OH may be assumed in first order to mark the instantaneous reaction zone), the comparison between the instantaneous LES planes and the experimental images is remarkable. From 1 to 5 bar, the flame becomes highly wrinkled and distorted for both, experiment and LES calculation. This is a direct indication of increased flame surface area, and thus increased reaction rate. This finding fits to the expected decrease of the smaller turbulence scales (the Kolmogorov length scales with $\eta \propto p^{-3/4}$). Similar assessments of the pressure effects on the dynamic range of turbulence structures and the flame front wrinkling were made by *Soika et al.* (Soika et al. 2003).
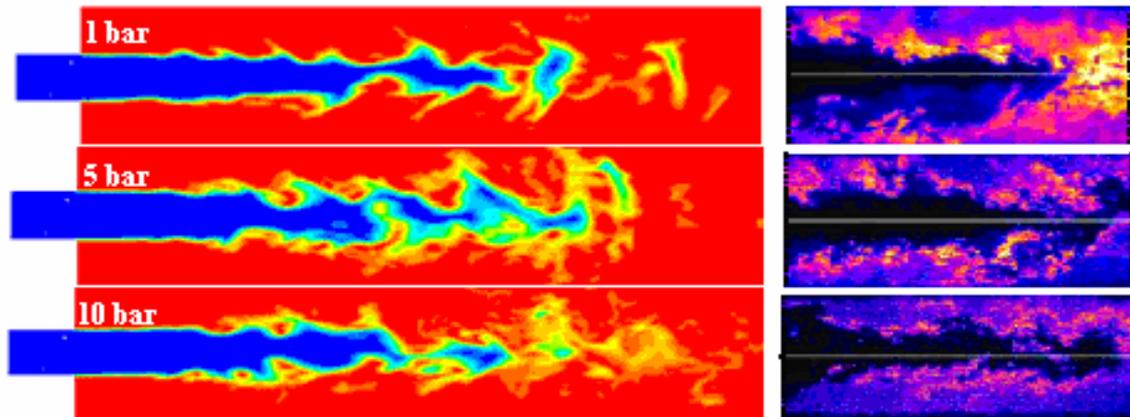
Figure 8.13a: *Instantaneous progress variable contours, for 1, 5 and 10 bar, using the Smagorinsky model (left), compared with instantaneous OH-PLIF images (right). (Inflow velocity is hold constant U = 45 m/s, methane/air ϕ = 0.5, preheated T_0 = 673 K).*

Interestingly, the visual influence of pressure on flame wrinkling is less pronounced for the step between 5 and 10 bar, as compared to that up to 5 bar. This difference has also been observed experimentally (Soika et al. 2003, Kobayashi et al. 2005, Lachaux et al. 2005). The two possible reasons for this behaviour are: 1. The changing pressure dependency of the laminar flame speed $s_{L0} \propto p^x$, where the exponent x decreases from 0.58 to 0.45 with pressure, following laminar flame data (Griebel et al. 2005), 2. The relative pressure ratio is 5 for 1 to 5bar and 2 for 5 to 10bar.

As noted above, the reaction sub-closure (Eq. 7.9) for the flame-wrinkling ratio has been found to be capable of yielding high-pressure effects on the reaction rate due to the presence of an explicit non-dimensionalized pressure term p/p_0. A similar dependency on pressure-turbulence relation made by Lachaux et al. (Lachaux et al. 2005) in their experimental studies up to 9bar, support our findings. Experiments yielded a constant mean turbulent flame brush thickness and only very small effects of pressure on the distribution of the time averaged statistical OH contour from 1 to 10 bar (Griebel et al. 2003) (note, that not the absolute OH concentration has been compared, which varies by several reasons with pressure, but the statistical instantaneous flame contour position, for which the individual OH images have been binarized on a low OH-level). The employed reaction closure predicted trends quite similar to these observations. Simulations have shown a marginal increase of flame brush with pressure in the axial direction (Fig. 8.13b and c), where in RANS approach the reaction model predicted very thin flame brush.
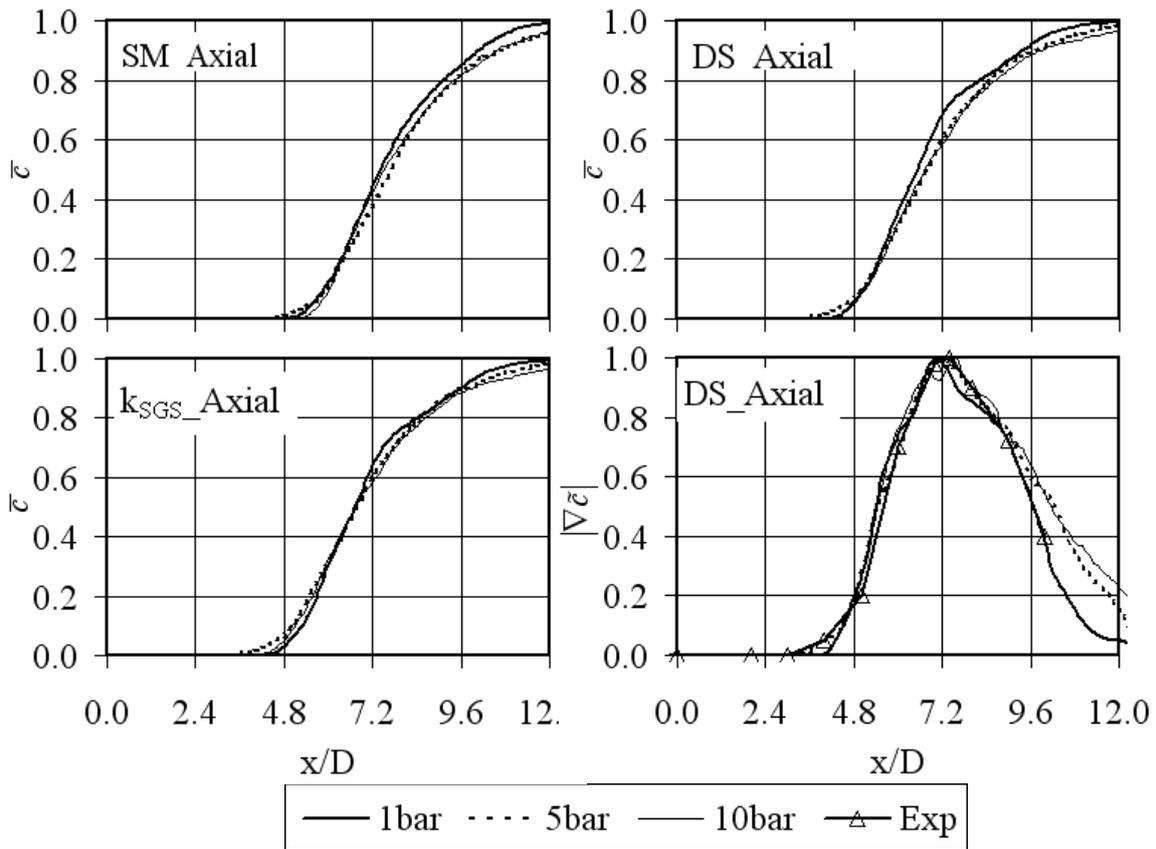
Figure 8.13b: *Behaviour of the reaction model with all the three closures for pressure variation, from 1 to 10 bar. Shown are axial profiles of time-averaged progress variable, for the dynamic Smagorinsky model also the progress variable gradient.*
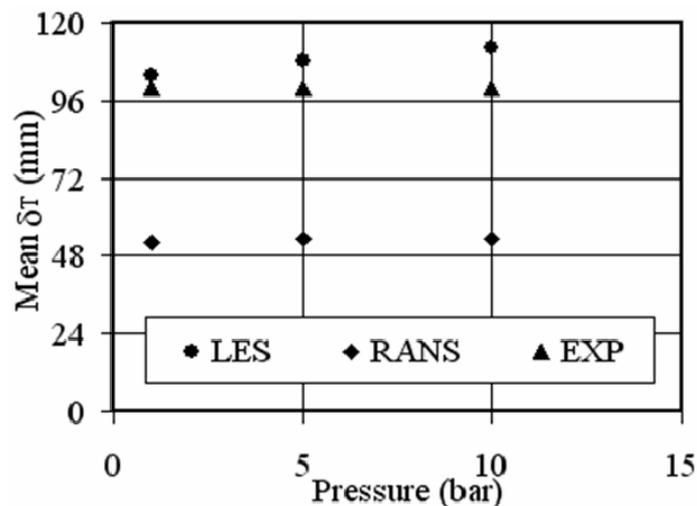
Figure 8.13c: *Time averaged flame brush thickness along the axis plotted for pressure variation, shown for LES, experiment, and RANS.*

The increase of reaction rate with pressure is apparent from instantaneous pictures (Fig. 8.13a). The increase of the time-averaged flame wrinkling and mean reaction rate with pressure can be seen in Fig. 8.14. Overall, the reaction closure in combination with the three models has yielded excellent results. The reaction model in combination with the

dynamic Smagorinsky model has been in good agreement with the experimental OH-PLIF data than with the other two models.

It is worth-noting that, at high pressure due to enhanced turbulence scale spectrum, the modelling contribution of handling the scales increases. This effect can be observed from Fig. 8.14 (bottom), which shows an increase in -viscosity with pressure. Another interesting observation is the increase of the flame area $A_T/\overline{A}$ with pressure, an indication of increased reaction rate. At 1 bar, the maximum time-averaged field quantity $A_T/\overline{A}$ in the axial direction is 1.2, whereas 1.8 and 2.2 are realized at 5 and 10 bar respectively are found computationally.
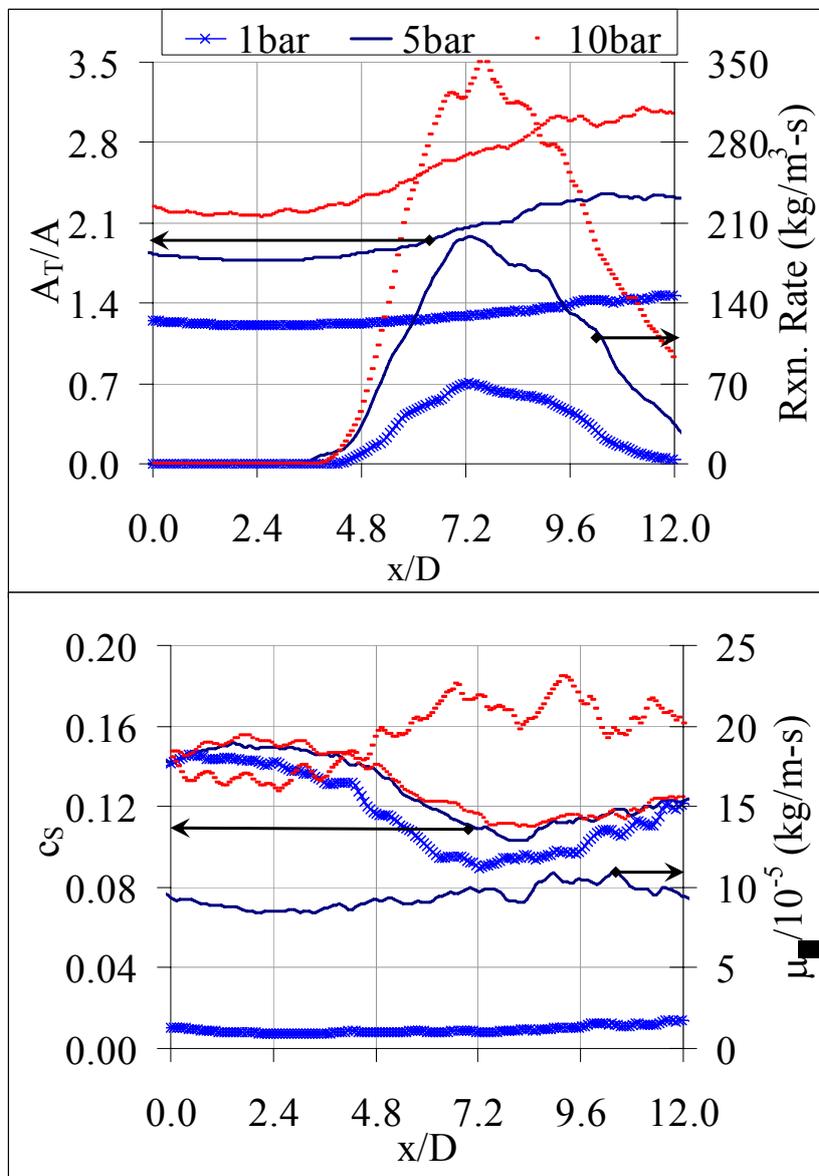
Figure 8.14: *Time averaged flame wrinkling ratio, reaction rate (top), the dynamic Smagorinsky constant and viscosity(bottom) for the three reacting cases.*

To summarise, in this chapter the three turbulence closures in combination with the AFSW model for turbulent premixed high-pressure combustion were applied on a dump combustor, operated close to stationary gas turbine conditions. The performance of three closures was validated based on cold flow experimental data for varied inlet conditions. Simulations at atmospheric pressure were made with two grid levels to assess the quality of the simulations on the fine grid. The quality of the closures in combination with the employed discretization schemes were estimated using the LES_IQ as a quality assessment measure. The LES_IQ for cold and combusting flows were, respectively, 50-60% and 80%. The numerical and model contributions are estimated using Klein's approach. The reaction closure was successfully validated against experimentally measured mean flame position and flame brush thickness. Also, for increased pressures, the combustion LES results were in excellent agreement w.r.t these two quantities. Increase of flame wrinkling was clearly noticeable in the computed instantaneous flames. RANS studies yielded reasonable mean flame length, while under predicting the axial turbulent flame brush width by as much as 50%.

9. Model Predictions on Gas Turbine Burners in RANS and LES Approaches

In this chapter, the applicability of the AFSW model on the ALSTOM gas turbine combustors for varied pressures and Lewis numbers both in RANS and LES approaches is tested. Simulations are performed on two different configurations, namely, a conical swirl burner (F3) and a double-cone swirl burner (F4). On the F-3 configuration, the reaction model performance for pressures as high as 32 bar in RANS context is tested. Also, the importance of Lewis number is demonstrated on this configuration.

Whereas on F-4 configuration, both cold and reacting flow simulations are performed at atmospheric pressure in RANS and LES approaches. The reacting flow LES is performed utilising the subgrid-scale AFSW model, which was originally developed in the context of RANS approach, in combination with the three turbulence closures for three equivalence ratios (equivalently, flame temperatures) to address the dual flame mode.

9.1 Reacting Flow Simulations on F-3 Configuration with RANS Approach

The numerical outcome obtained on the conical swirl (F-3) burner (Fritz 2003), a typical stationary gas turbineburner-combustor configuration, using the AFSW reaction model in the RANS (with $k - \varepsilon$ model) context is presented and discussed in this section. Specifically, the performance of the reaction model for the variation of temperature (i.e., equivalence ratio) and operating pressure is estimated. Additionally, simulations of lean pre-vapourised premixed (LPP) diesel-air mixtures are performed and with which the importance of the Lewis number *Le* is demonstrated. As diesel fuel is made of several constituents, it is rather hard to derive correct *Le* value; moreover, it further lessens the accuracy for varied equivalence ratios. On the other hand, the other important physico-chemical property, the laminar flame speed, of diesel vapour mixtures is readily available in (Schihl et al. 2004). The local

concentration of fuel-air mixture in the LPP case is accounted by solving an extra transport equation for the mixture fraction.

The schematic of the burner configuration is given in Fig. 9.1. Liquid fuel is injected at the cone which mixes with the air entering through the air slots of the swirler cone. The gaseous fuel is injected through the holes distributed along the inlet slots. Fuel and air are homogenously mixed well before the combustor in the mixing zone.
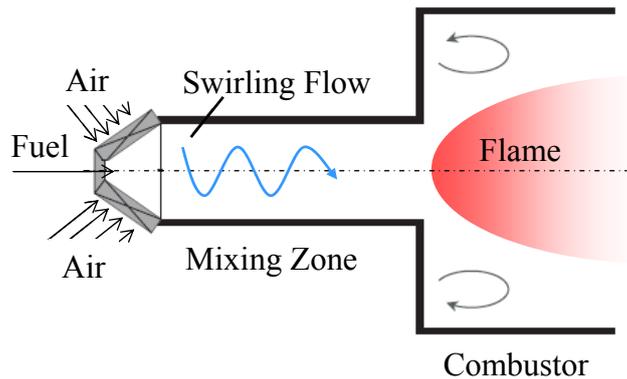
Figure 9.1: *Schematic of the conical burner showing the swirler, mixing zone and combustor.*

For this configuration (F-3), experimental data is not available for the comparative purpose. The model predictions are presented firstly for the variation of temperature (equivalence ratio) at 1bar (Fig. 9.2) and then for the pressure variation up to 32 bar (Fig. 9.3) at constant temperature of 1850 K for the methane fuel. Interestingly, the model is able to predict the flame stabilisation at the vortex break down point i.e., close to the exit of the mixing tube, as was found in the experimental studies. It is noted that the corresponding measured image is not produced here. The other two temperature cases are not usually different in terms of flame behaviour compared to that of the high-temperature case, at 1850 K.

This study has shown the applicability of the reaction model for gas turbine combustor configurations, implicitly for pressures up to as high as 32 bar. Strikingly enough, the influence of pressure and temperature is quite weak on the flame positioning indicating the good flame stability of the burner-combustor configuration.
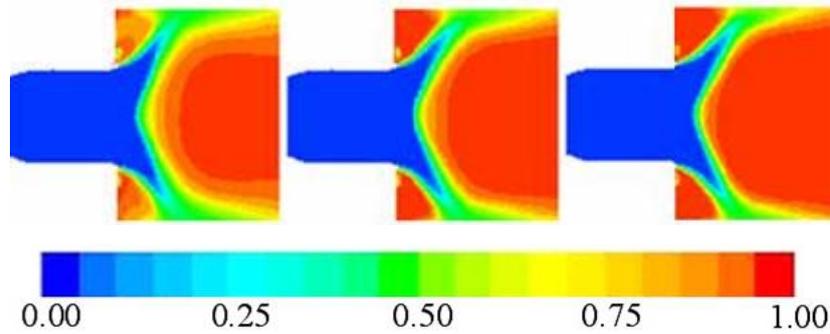
Figure 9.2: *Predictions of the AFSW reaction model in the F-3 configuration for three flame temperatures (1600 K, 1750 K and 1850 K) at 1bar. Shown are the contours of the reaction progress variable c*
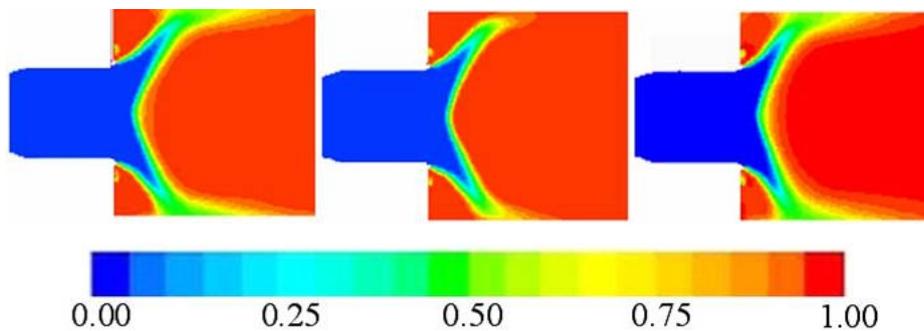
Figure 9.3: *Predictions of the AFSW model in the F-3 configuration for three operating pressures (1, 16 and 32 bar) at 1850 K. Shown are the contours of the reaction progress variable c.*

9.2 Illustrating the Substrative Influence of the Lewis Number

Despite its (Lewis number Le) paramount significance in the premixed turbulent combustion, many of the combustion models in literature, seldom configure for its effects, as they are derived under the assumption of unity Lewis numbers. It is thus apparent that usage of such models may yield spurious results leading to inappropriate analysis. The importance of the Le effect can readily be seen in cases like blend mixtures of high molecular weight hydrocarbons (for e.g., diesel or octane) with Le hugely greater than one and light fuel hydrogen of $Le \ll 1$, having the basic advantage of being rigorously stable even under unusual lean operating conditions, for e.g., (Halter 2005). The necessity of the Lewis number has already been demonstrated with the Bunsen flame (F-1 Configuration) in Section 7.2 and Appendix A1.

Here, the investigations based on the diesel-air mixture; as an initial guess the value of Le for this mixture is taken as 1.3 (equivalent to propane of equivalence ratio 0.5).

While, the value of *Le* for n-heptane was found to be 2.6 (for mixture fraction less than 0.05 marked with vertical line in Fig. 9.4). Simulations show a dramatic decrease in the reaction rate, by as much as a factor of five compared to the Lewis number case under identical condition. This result illustrates the severity of *Le* on turbulent flame speed s_T, and also, such as in interpreting the phenomenon of anomalous flame drift, an undesired effect with respect to flame governance.
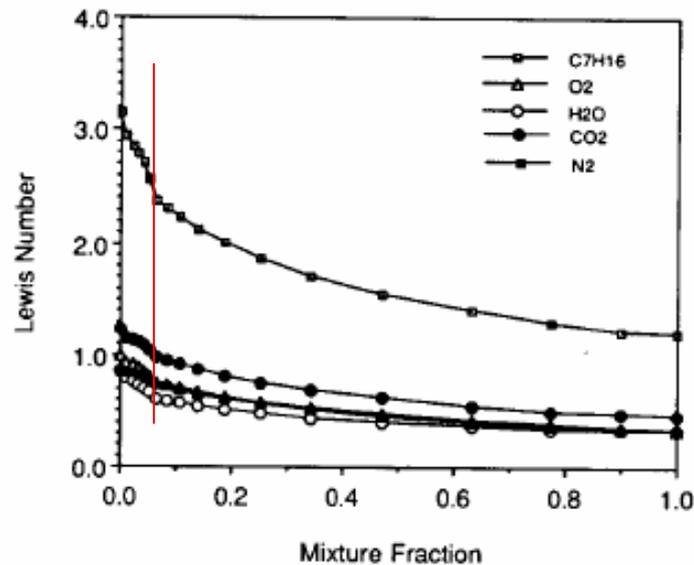
Figure 9.4:   *The Lewis number as a function of mixture fraction (Zhang et al. 1995)*

On varying *Le* from 1.0 to 2.6 (actually, 1.0, 1.3, 1.8 and 2.6), the flame anchoring point (usually located at the junction point of the burner-combustor) shifted from being in the mixing tube into the combustor zone (Fig. 9.5). By enhancing *Le*, the reaction rate is decreased as the rate of heat losses from the reaction zone exceeds the rate at which the reactant is transported into the reaction zone (Rogg 1981, Zel'dovich et al. 1985, Aluri et al.). Hence the enthalpy and consequently the temperature decreases in the reaction zone while both increase in the preheat zone.
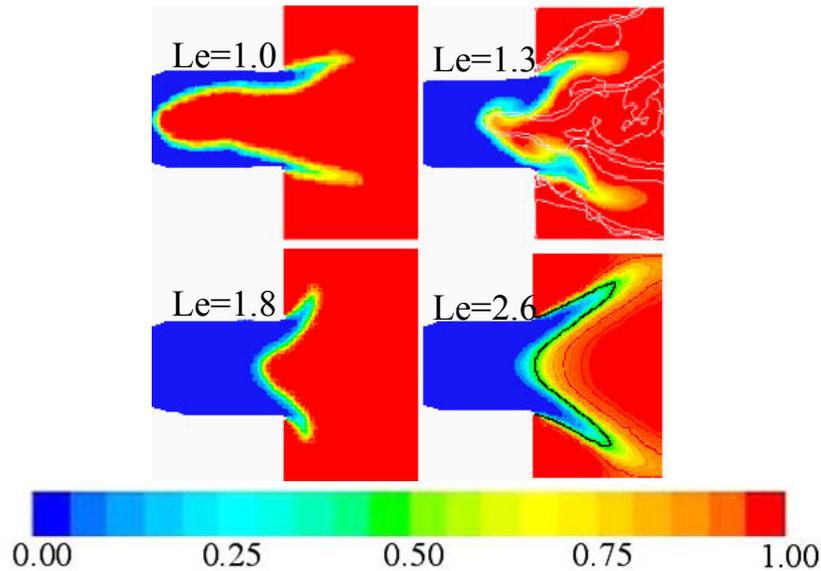
Figure 9.5: *Predictions of the AFSW model in the F-3 configuration 14 bar prevapourised premixed case by varying the Lewis number from 1.0 to 2.6.*

The existence and occurrence of flame drift is observed by artificially setting Le to 1.0 and 1.3, as two cases. It is interesting to note that despite the turbulent flame speed s_T, (for Le of 1.3) being only one-fifth of the 'strong' axial jet, flame drifting deep into the mixing tube is still observable. Such a movement may be explained following baroclinic push, the details of which are given in the next section.

9.3 Dynamics of Flame Propagation in Swirling Flows

The effect of baroclinic push may be mathematically represented as $\nabla 1/\rho \times \nabla p$ (Chomiak and Nisbet 1995) where ρ is the density of the gaseous mixture, and p, the operating mean pressure inside the chamber. The physical meaning is that the vorticity generation is caused by the existence of pressure gradients in a medium of varying density.

In specific to this flame scenario, coupling of the density gradient across the flame (occurring due to difference in unburned and burned gas velocities) and the radial mean pressure gradient in the unburnt swirling gas ahead of the flame, results in generation of 'azimuthal vorticity', counter acting against the axial jet in the mixing tube. This is illustrated below for the flame simulated with $Le=1.3$ using the AFSW model. The azimuthal vorticity, which is shown marked with arrows in Fig. 9.6, pushes the flame towards the upstream premixed unburnt gas. Upon increasing Le, the

101

rate of heat losses from the reaction zone exceeds the rate at which the reactant is transported into the reaction zone, decreasing the temperature in the reaction zone and thereby the density gradient in the flame brush and also the flame speed, the latter depends exponentially on temperature.
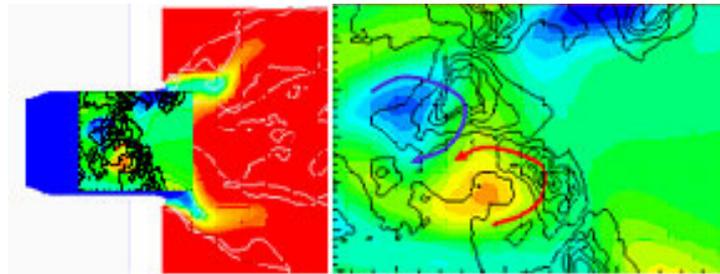
Figure 9.6: *Flame propagation mechanism: shown are the progress variable contours (left), inside the mixing tube; they are replaced with azimuthal vorticity (green part). The same part is zoomed for better visibility (right).*

In this chapter, the importance of Lewis number effects and high-pressure influence and their impact on premixed turbulent combustion has been analysed using the Algebraic Flame Surface Wrinkling (AFSW) Model. Thereby, the greater workability range of the AFSW reaction model has been successfully demonstrated.

9.4 Physical Description of the F-4 Configuration

A schematic of the ALSTOM double cone *EnV*ironment (EV) burner (Hirsch et al. 2002) is shown in Fig. 9.7. This is a very good example of a modern Dry-Low-Emission (DLE) burner for gas turbines. Flame stabilisation occurs in an aerodynamically generated recirculation region formed due to the vortex breakdown. The characteristics of the recirculating flow are dependent on the swirl number and on axial pressure gradients. This burner is obtained by shifting two halves of a cone in opposite directions, orthogonally to the cone axis, such that two inlet slots of constant width are produced. The flow enters the swirler through the two inlet slots on the cone shell in the circumferential direction, represented by circumferential air in Fig. 9.7. The gaseous fuel is injected through holes distributed along the inlet slots. The strong swirl inside the burner cone leads to very rapid mixing such that the fuel-air is very homogenous at the burner exit (with low NO_X production). The three salient features

of the burner are: 1. swirling components keep the hot gas far from walls and improve mixing, 2. mixing before combustion due to the distribution fuel holes along the slots, and 3. the conical shape slows down the air stream out of the burner.
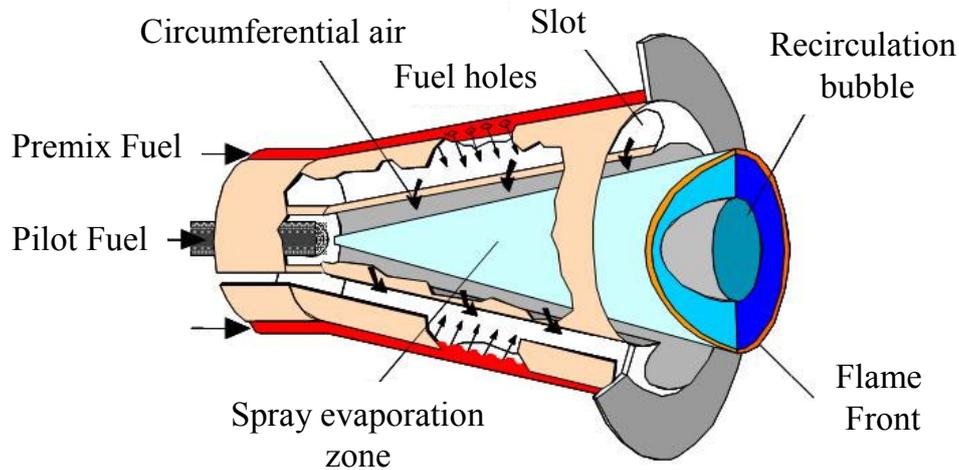
Figure 9.7: *ALSTOM double-cone EV burner marked with essential details (Hirsch et al. 2002)*

9.5 Experimental Observations

It is worth-noting that the flame stability in such GT systems is a concern, because flame positioning inside the chamber is sensitive to the mixing fields, temperature or equivalence ratio (and its fluctuations), as these can strongly effect the vortex break down phenomenon. Though this breakdown is expected to take place at the exit of the burner, experiments in water-rig facility (cold flow) show that in this particular burner variant (§9.4), the vortex breakdown takes place deep inside the burner. It is characterised by a Central Recirculation Zone (CRZ) which is initially quite narrow, and thereupon substantially thickens moving from the burner into the combustor, see Fig. 9.8.

The use of water-rig test facility to determine the non-reacting velocity flow field is a very common practice in the industrial burner development process. However, it may be ambiguous to interpret the water-rig data to comprehensively estimate or understand the critical flame stabilisation point. Any independent outcome may at times be erroneous, in contradiction with the experimental data of the combusting flow measured at atmospheric pressure.
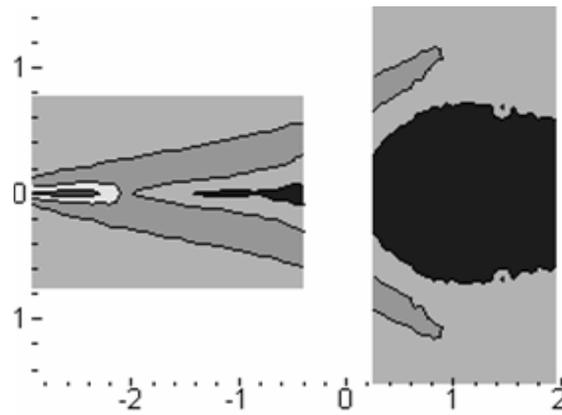
Figure 9.8: *Qualitative picture of the normalised axial velocity contours obtained on water-rig tests, the dimensions of the chamber are normalised with burner exit diameter.*

This typical mismatch is illustrated involving combustion processes. Shown in Fig. 9.9 is the axial velocity together with isolines of the mean combustion progress variable for two cases: premixed operation at a reference equivalence ratio, and pilot operation at nearly same equivalence ratio but with 20% of the fuel injected upstream in the along the burner on the axis (right figure). Such a phenomenon also occurs in a completely premixed mode at higher flame temperatures that is evident from the measurements showing a sudden increase in pressure drop (Δp) at characteristic equivalence ratio/flame temperature. This difference is an indication that despite of the vortex breakdown inside the burner the flame stabilises outside the combustor up to a certain fuel-air mixture equivalence ratio and then propagates into the burner. Present study tries to understand the flow behaviour and to some extent, the flame propagation details inside the burner. The cold flow characteristics obtained from both RANS and LES are evaluated in comparison with the experiments.

The resolution quality in LES_IQ of the LES results of all the three models are estimated from single grid level assuming numerical dissipation as much as 50% of the unresolved energy (Pope 2000). A relatively novel reaction model mentioned above (Muppala et al. 2005b) for premixed turbulent combustion incorporated with fuel and high pressure effects is used in combination with RANS as well LES turbulence closures to study the mechanism of the anomalous dual-flame mode.
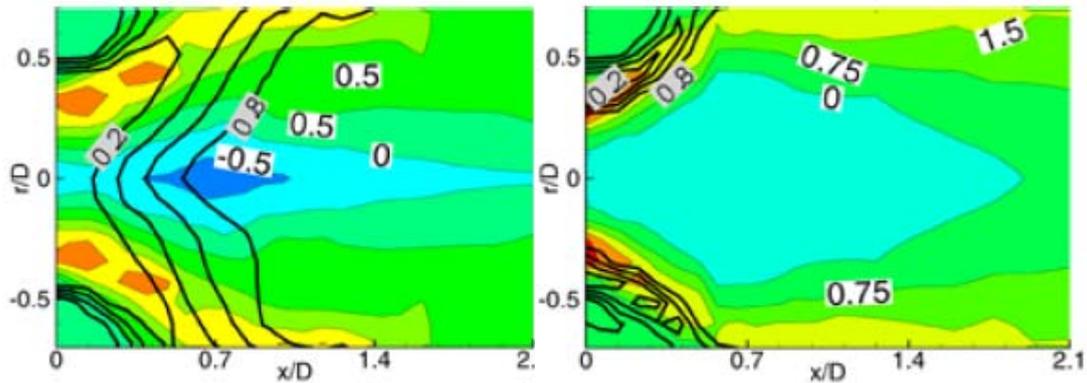
Figure 9.9: *Qualitative experimental findings (Biagioli 2006): distribution of mean axial velocity and progress variable in complete premixed mode (left) and with 20% pilot fuel (right) keeping the equivalence ratio almost constant, an indication of different flame modes.*

9.6 Simulation Results on F-4 Configuration

In this study, the flow characteristics of a specific variant of EV burner and its behaviour during combustion process are studied using both RANS and LES. The numerical outcome from this section are presented in the following order: Comparison and analysis of cold flow RANS and LES data with that of experiments; analysis and discussion of combustion flow results explaining the dual-flame mode at a characteristic flame temperature; and pressure drop comparison between measurements and simulations.

9.6.1 Cold flow RANS simulations

As shown in Fig. 9.8, the experimental water-rig results show that a thin tornado-like structure protrudes into the burner indicating the vortex breaking down inside the swirler. Steady state RANS simulations were performed using the commercial CFD solver Fluent 6 (Fluent 2005), on a domain consisting of 400,000 cells. Nearly more than half of the mixed tetra and hexa cells are concentrated in the burner zone, and the other half mesh the combustor using hexa cells. Only RANS cold flow simulations are performed on fine grid by halving the grid size in the combustor, while keeping the mesh on the burner unchanged. The numerical solutions obtained on the two respective 'first' and 'second' grids are marked as 'RANS' and 'RANS_Fine', respectively. All other studies, LES as well as combustion-RANS, were sought only on the 'first' grid due to the limited computational resources. The employed numerical

schemes are mentioned in Table 8.1. The predicted axial and tangential velocity contours by the RANS approach are presented in Fig. 9.10 in comparison with the experimental data.
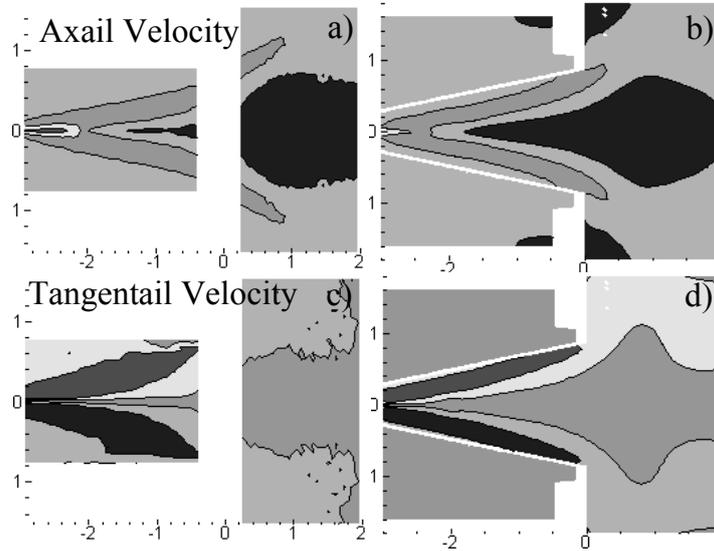
Figure 9.10: *Comparison of velocities predicted by RANS plus standard $k-\varepsilon$ model with that of experiments. a) & c) Experiment; b) & d) RANS axial and tangential velocity components.*

Steady state RANS is able to qualitatively capture the jet break-up at the root of the burner and the vortex breakdown point in line with the experimental findings (Fig. 9.10). However, the axial and tangential velocity distributions along the main stream of the flow are significantly differing from the measured data. RANS over predicts the width of the tornado-like structure protruded into the burner at the leading edge of the vortex breakdown point. Solutions obtained on the two grid levels closely follow each other in the radial direction. Biagioli (Biagioli 2006) with his 1D flame analysis had shown that the flame stabilisation point is dependent on three factors: the radius of curvature of the flame (or the CRZ), the radial distribution of the second-order derivative of mean axial velocity in the radial direction ($\partial^2\overline{u}/\partial r^2$) and the turbulence quantities.

The quantitative comparison of experiments, RANS and LES of these kinematic parameters responsible for flame positioning are made in Fig. 9.11 & 9.12. Though the axial velocity predictions of RANS are close to the experiments, the kinetic energy is greatly undervalued inside the burner in the region x/R < 0, shown in Fig. 9.11. The other kinematic parameter, $\partial^2\overline{u}/\partial r^2$ that helps pushing the unburned reactive mixture

towards the flame zone in the radial direction, is observed to deviate considerably from the measured value (see Fig. 9.12).
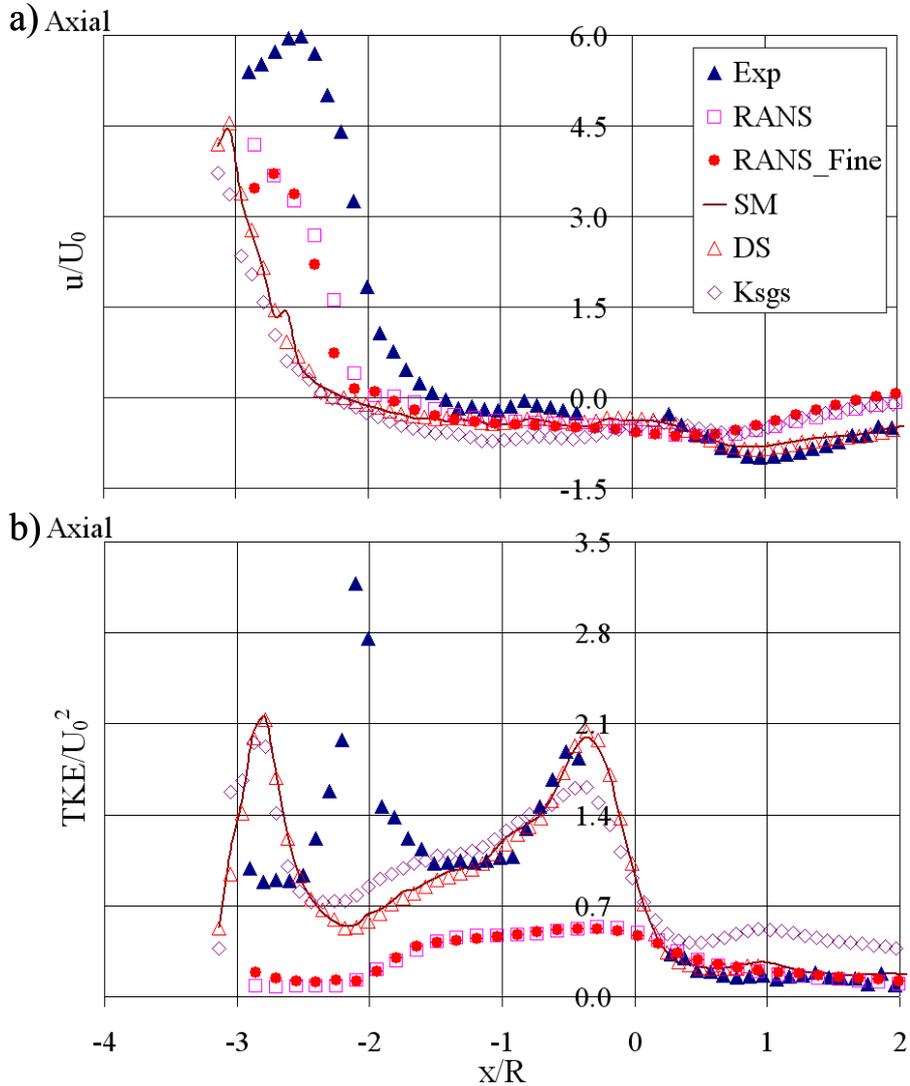
Figure 9.11:   *Quantitative comparison of a) axial velocity and b) TKE predicted by RANS and LES (for three   closures) with the measurements(Biagioli 2006) along the axis of the combustor.*
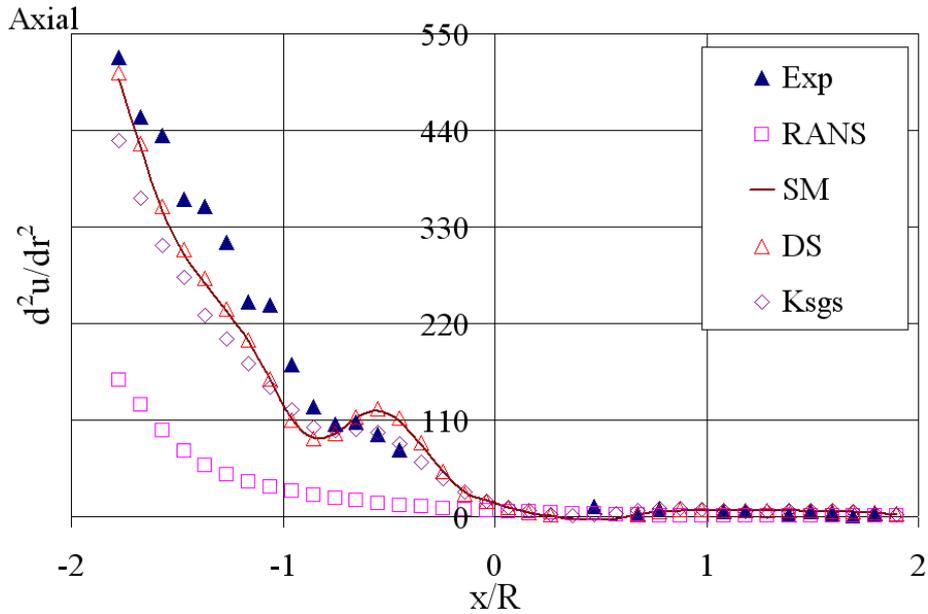
Figure 9.12: *II-order radial derivative of axial velocity predicted by RANS and LES in comparison with the experiments along the axis of the combustor.*

9.6.2 Reacting RANS simulations

As mentioned earlier, though the breakdown occurs inside the swirler, experimental studies showed that (refer to Fig. 9.9) the flame stabilises in this burner variant/mode of operation up to a characteristic temperature at the exit of the burner (swirler) after which it drifts into the burner. Note that other variants/modes include increase or decrease of inlet (tangential) velocity, variation in fuel distribution system, etc.) Despite of the poor cold flow RANS predictions; reacting flow simulations are performed to predict the dual-flame mode of this burner variant.

As shown in Fig. 9.7, gaseous fuel is injected through the holes distributed along the inlet slots and mixed with the strongly swirling air to form the reaction premixture. In spite of certain unmixedness at the burner exit, simulations are performed assuming perfect premixing for three adiabatic flame temperatures of 1650, 1700 and 1800 K on the same grid as that used for cold flow simulations.

Figure 9.13 shows the axial velocity contours along with the progress variable isolines predicted by the AFSW combustion model from the RANS approach. For the three flame temperatures, the flame is positioned deep inside the burner, in contradiction with the experimental observations shown in Fig. 9.9. Upon reducing the model pre-constant for to realise the dual-flame behaviour, lean blow-off occurs without any shift in the flame position in the downstream side of the burner. Further discussions on the

resulting advantages and limitations of combustion-RANS simulations are made in comparison with the advanced turbulence approach, the large eddy simulation (LES) results in the upcoming section.
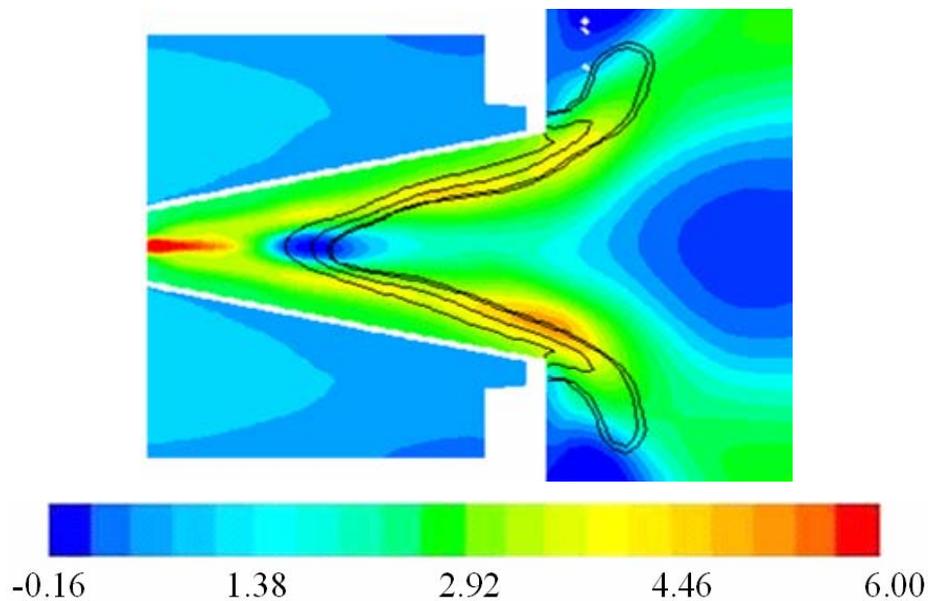
Figure 9.13: *Axial velocity distribution in the centre plane of the combustor; marked are the isocontours of reaction progress variable (flame location) predicted by the AFSW model in RANS context.*

9.6.3 Cold flow LES

As RANS approach did not testify the occurrence of the dual-flame mode, the LES approach in combination with the AFSW combustion model in its form is used for investigations. Before doing so, the cold flow simulations were done using three reaction closures, namely, the Smagorinsky (SM), dynamic Smagorinsky (DS) and the one-equation K_{sgs} (Ksgs) models. Simulations were performed on the same grid, which is used for RANS, and the employed numerical schemes are tabulated in Table.8.1.

The qualitative predictions of the central recirculation zone (CRZ) predicted by the three turbulence models represented by the axial velocity contours are shown in Fig. 9.14. All the three models are able to capture the tornado-like structure moderately and the quality of which decreases with the increase of the turbulence model complexity. As shown and detailed in Section 8.3, once again the poor predictive capabilities of the dynamic turbulence models using non-uniform grids and in the regions of highly inhomogeneous turbulence is demonstrated. This behaviour is more predominant in the case of the dynamic one-equation K_{sgs} model, for further details see Fig. 9.14.
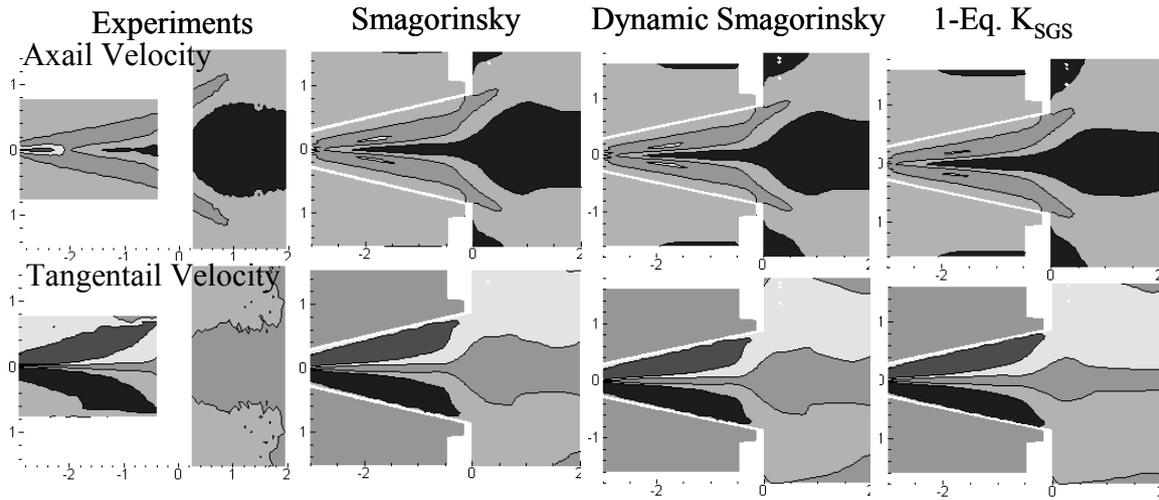
Figure 9.14: *Predictions of axial and tangential velocities of three models in comparison with the experiment.*

As shown in Fig. 9.11, the axial velocity profiles predicted by the three models yield the similar trends as observed in experiments but with premature yielding of velocity peak one burner diameter upstream. This is a consequence of the early breakdown of the axial jet close to the root of the burner, which differs with the experiments as much as half the burner exit diameter (Fig. 9.11a). Its impact is noticed in the kinetic energy predictions.

The one-equation K_{SGS} model over predicts the kinetic energy (see, Fig. 9.11b) at the exit of the burner (x/R = 0) and in the combustor (x/R > 0), the consequence of which is apparent in the reacting flow simulations. This is attributed to the bad resolution of the grid. Despite of this shift, reacting flow simulations are performed on the same grid as the Reynolds number and the Kolmogorov scales decreases with preheating as well as combustion due to dilation.

Detailed comparisons are made with the radial profiles of axial velocity and kinetic energy in Fig. 9.15 at four different axial locations, two inside the burner and two within the combustor, to understand the flow characteristics of the burner-combustor configuration. It is clear from these profiles that both RANS and LES fail to capture the jet break-up accurately at *x/R = -2.28*. While the LES subgrid scale turbulence
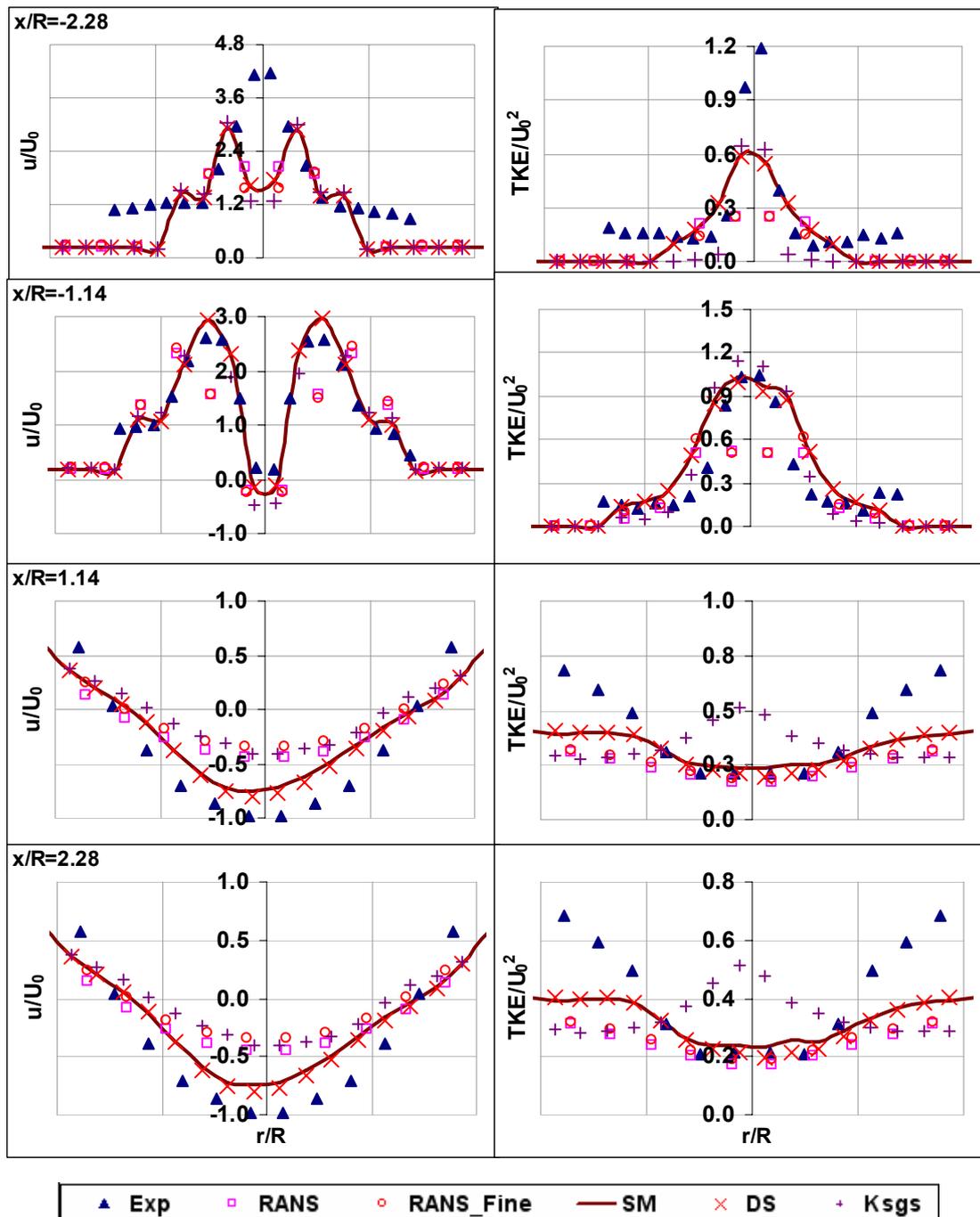
Figure 9.15: *Radial velocity (normalized by inlet mean velocity) profiles of all LES closures and RANS in comparison with the experiments at different axial positions.*

models closely follow the experiments w. r. t both the axial velocity and TKE distributions at the next junction, i.e., at *x/R* = -1.14, RANS under predicts the TKE peak by as much as 60%, with a fair prediction of the axial velocity. At *x/R* =1.14, i.e., inside the combustor, axial velocity profiles from the turbulence models match with the experimental values, under valuing the TKE values outside the CRZ zone. At the farthest point *x/R* =2.28, i.e., at the trailing edge of the low velocity depression, the RANS approach predicted flattened axial velocity and TKE profiles reasonably, and

111

all the advanced turbulence closures produced curved axial profiles with flattened TKE profiles. In overall, LES with both versions of the Smagorinsky models predict the dynamics of the flow field in the leading edge region of the vortex breakdown quite reasonably, which are crucial for the flame analysis; these closures perform poorly in the region of the trailing edge.

The deviations showed by LES may be attributed to the poor resolution quality, as shown in Fig. 9.16. As a rough approximation, the resolution quality, in terms of LES_IQ, (Celik et al. 2005) is estimated from the single grid level assuming numerical dissipation by 50% of the unresolved energy. The resolution quality of the Smagorinsky model is shown higher than that of the dynamic closures, the reasons for which were stated while comparing calculations and experiments. On this chosen grid level, all the three models are resolved by as much as 35-50%, indicating a coarser LES scenario. Despite of this poor resolution, combustion-LES has performed well in capturing the peculiar dual-flame behaviour, while this effect was not reproducible with the standard RANS approach. In brief, the LES approach predicted kinematic parameters quantitatively more accurately, paving way to perform combustion-LES.
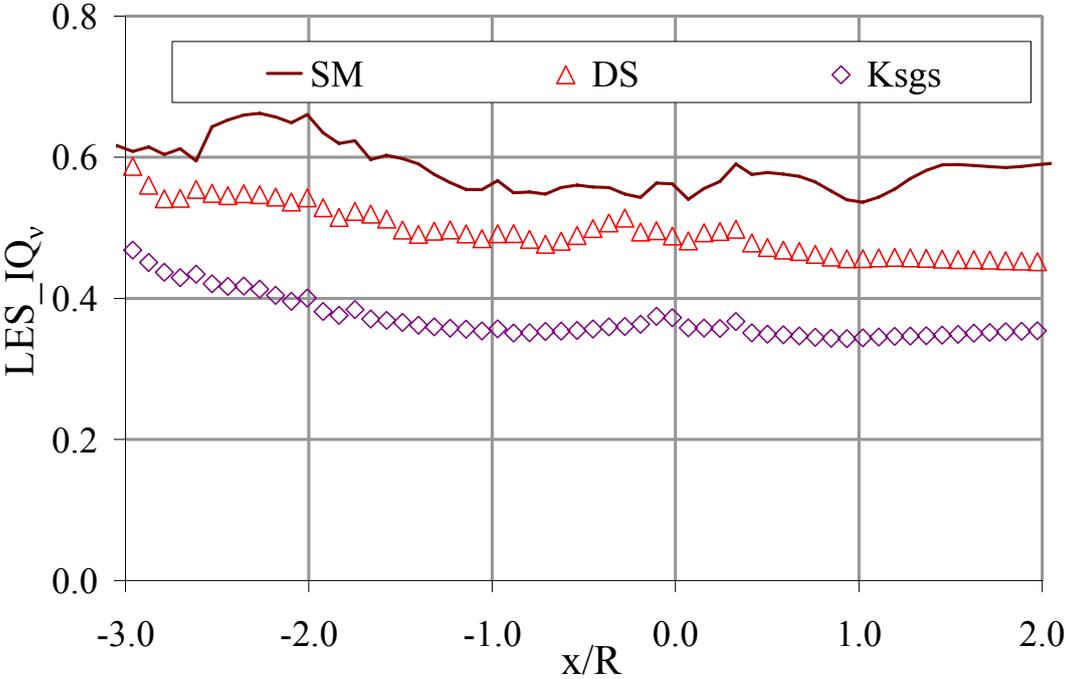
Figure 9.16: *Grid resolution quality, the Large Eddy Simulation Index of Quality (LES_IQ) of the actual solution obtained from single grid level assuming numerical dissipation equal to 50% of the unresolved energy.*

9.6.4   Reacting LES

Attributing similar approach as was followed in the RANS, combustion calculations are performed for three adiabatic flame temperatures to focus on the flame drift phenomenon numerically. The selective temperatures of 1650 K, 1750 K, and 1800 K are taken following experimental inferences. A characteristic temperature of 1750 K is identified to have incepted the flame jump, i.e., flame propagating into the conical-shaped burner system.

Firsthand results showed that the original novel reaction model has been inexplicable in identifying inside flame mode at the reference temperature. Therefore, following few iterative adjustments, a new pre-constant of 2.0 (recall that the original constant is 0.46) is found necessary to reproduce this phenomenon in combination with the Smagorinsky model. Thus, allowing the functionality of the new reaction pre-constant 2.0, simulations are performed for the other two temperature cases. This constant was found to be dependent on the turbulence closure used, the constant required for the Smagosinsky, dynamic Smagorinsky and dynamic K_{SGS} models was found to be 2.0, 1.8, and 1.5 respectively. Indeed, this rendition of a different constant with different turbulence models comes as no surprise as the bubble shape is predicted differently in different models, Fig. 9.14.

For a lower adiabatic flame temperature of 1650 K, the flame sits away from the conical burner, anchoring at the junction of burner exit and entry of the combustor. The flame positioning is directly attributed to the decrease in the opposing strength of turbulent flame speed as against the incoming premixed mixture. Numerically, with further rise in temperature (to 1800 K) above the characteristic value of 1750 K, the flame anchoring position drifts more upstream of the burner. The progress variable distribution obtained with the three turbulence models is almost identical. Therefore, the results obtained with the Smagorinsky model are taken to represent the LES studies. In Fig. 9.17, the progress variable along the axis of the combustor is plotted for LES and RANS. The figure shows that, below the characteristic temperature the flame stays at the burner exit ($x = 0$) and then, it suddenly drifts upstream by as much as the burner diameter. By further increasing the flame temperature, the flame anchoring location is no more subjected to significant displacement.
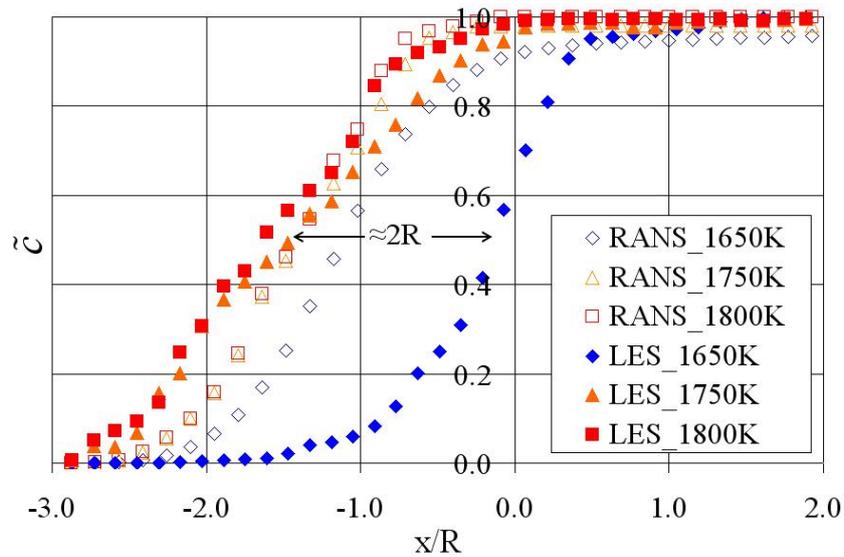
Figure 9.17: *Progress variable predictions along the combustor axis by the AFSW reaction model in RANS and LES approaches.*

The experimental and simulated pressure drop across the burner-combustor arrangement for the three studied temperature is shown in Fig. 9.18. The pressure drop across the two sections is a proportional indication of the dual-flame mode of the burner, similar to the deductions made from the measurements, Fig. 9.9 & 9.18. Due to the asymmetry of the burner, the dynamics of the propagation mechanism in the configuration cannot be explained likewise in F-3 configuration.
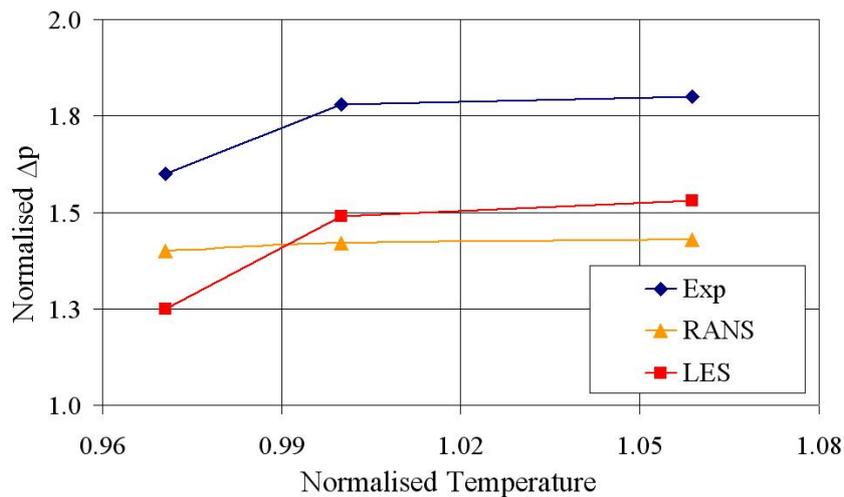
Figure 9.18: *Pressure drop across the double cone burner-combustor configuration, with higher slope in case of 1650 K to 1750 K transitions, an indication of the dual-flame mode.*

9.7 Dynamics of Dual Flame Mode

The progress variable equation (Eq. 3.1), for steady state conditions, in spherical (also realizable in cylindrical) coordinates, introduces a new term called the turbulent diffusion velocity, which is the ratio of the turbulent dispersion coefficient (D_t, m²/s) and the flame radius of curvature. The angular derivative term(s) $\partial \tilde{c}/\partial \theta$ nullify under the assumption that the combustion progress contours are locally spherical in shape.

$$\frac{\partial}{\partial x}\left(\bar{\rho}\tilde{u} + \bar{\rho}\frac{2D_t}{r}\right)\frac{\partial \tilde{c}}{\partial r} = \frac{\partial}{\partial r}\left(\bar{\rho}D_t\frac{\partial \tilde{c}}{\partial r}\right) + \bar{\dot{w}}_c \qquad (9.1)$$

The increase in the value of the second term in the LHS pushes the flame more downstream. In other words, a convexly curved flame facing reactants yields lower turbulent flame speed than its corresponding flat planar flame under identical conditions. Following first order approximations of constant radius of (flame) curvature ($r \sim r_F$), constant D_t and that the variational decrease of axial convective flux $\bar{\rho}\tilde{u}$ is a linear function along the symmetrical axis toward the flame, a simple expression as how far a curved flame is displaced relative to a flat one is derived as $2D_t/r_F\left(d(\bar{\rho}\tilde{u})/dx\right)$.

A curved flame in fact receives reactants not only as a convective flux at its leading edge but also as a tangential turbulent flux. Therefore, in order to balance reactants inflow and burning rate the curved flame must move more downstream. Therefore, to overcome this indifference, the pre-constant in the reaction subclosure has been increased, thereby the reaction rate, by enhancing this curvature effect.

As RANS predicts a wider bubble, the radial turbulent flux of the reactants ($2D_t/r$ term in Eq. 9.1) into the flame is undervalued. As a consequence, the reaction closure in RANS context cannot predict the flame out mode. It was shown in (Biagioli et al. 2005), that the radius of curvature of the flame is dependent on $\partial^2 \bar{u}/\partial r^2$, which is very much under predicted by RANS, for finer details see Fig. 9.12. As LES is able to capture the tornado-like structure, the bubble shape and $\partial^2 \bar{u}/\partial r^2$ close to the experiments and thereby the radial turbulent flux enabling the reaction closure to

predict the dual-flame. The dual-flame mode realised with the LES is shown in Fig. 9.19 with axial velocity contours marked with the progress variable isolines.
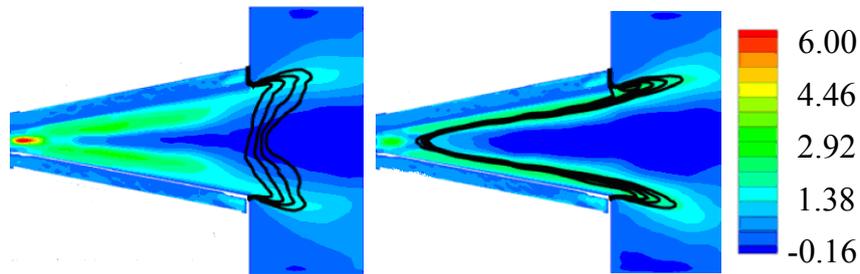
Figure 9.19: *Axial velocity distribution in the centre plane of the burner; marked are the isocontours of reaction progress variable (flame location) predicted by the novel algebraic flame surface area closure in LES context of flame-out and flame-in modes, respectively.*

With this the generality of the model and applicability on various configurations with different turbulence levels and flow types is demonstrated. Also, the importance of the Lewis number influence is demonstrated with the F-3 Configuration. And the direct applicability of the model in LES is reliable.

In an extended step, the applicability of the reaction model for more advanced combustion technique i.e., hydrogen blended hydrocarbon fuels is tested in the next chapter.

10. Hydrogen Doped Methane – Air Flames – A Preliminary Study

In this chapter, the effects of preferential diffusion are discussed with hydrogen doped fuel-air mixtures. Addition of hydrogen combats local flame quenching and increases the operability range of widely employed lean premixed turbulent flames, which are inherently prone to instabilities (Nakahara and Kido 1998). It also yields higher turbulent flame speed s_T as compared to a pure hydrocarbon (HC) turbulent flame for the same turbulence intensity. Recent experiments show a proportional increase in s_T for equivalent H_2 blending up to 20-vol %. While in laminar methane flames, for same amount of blending, the heat release rate at a strain rate of $2\text{x}10^5 \text{ s}^{-1}$ is 90% of the unstrained value laminar flame while it is only 10% for the pure mixture (Gauducheau et al. 1998), and it provides the increase of the flame resistance to stretch (Sankaran and Im 2006). The major advantage of H_2 enrichment is the ability of the flame to withstand higher strain rates especially at lean conditions, which indeed yields reduced UHC and (thermal) NO_X emissions. On the contrary, there is no significant increase in the flame temperature, with the addition of H_2, keeping the global equivalence ratio constant.

It is likely that several of the existing combustion models may not predict these H_2-doped effects. In the earlier chapters, the influence of fuel-type (Lewis number Le, effects) was restricted to studying varied HC/air mixtures. In this chapter, some preliminary predictions of the AFSW reaction model on the F-5 configuration with RANS approach are presented in comparison with experimental premixed turbulent combustion data. The special intent of this chapter is to evaluate the workability range of the model to hydrogen and hydrogen-doped hydrocarbon mixtures, emphasizing on the significance of preferential diffusion, PD, and Le effects in premixed turbulent flames.

10.1 AFSW Model Predictions

In the following, the behaviour of the reaction model is investigated using pure hydrocarbon mixtures, and then proliferate it to H_2-enriched lean hydrocarbon

premixed turbulent flames. The experimental work of *Halter et al.* (Halter et al. 2005b) provides useful information for a comprehensive study on turbulence and premixed combustion interactions, for varied pressures (1, 5 and 9 bar) and varied reactive mixtures. The effects of H_2 enrichment in lean CH_4-air premixed turbulent Bunsen flames have been the central theme of their investigations (Halter et al. 2005b). They (Halter et al. 2005b) envisaged a general trend of increase of flame surface density, and thus s_T/s_{L0} for all the investigated cases. Addition of hydrogen to the methane-air mixture is allowed such that the methane concentration is lowered to keep the global equivalence ratio fixed at 0.6.

The experimental turbulent flame speed was evaluated using the relation

$$s_T = \sqrt{U^2/\left(1+(H/R)^2\right)} \qquad (10.1)$$

where, U is the inlet mean velocity; R, the burner radius, 12.5 mm; and, H, height from burner exit to $\bar{c}=0.1$ contour, and θ is the half cone flame angle. The flame angle estimation by Halter (Halter et al. 2005b) slightly differs from that slated in (Smallwood et al. 1995), applied for e.g., in Kobayashi (Kobayashi et al. 1997) and in other subsequent works (Muppala et al. 2005b), wherein an optimal tangent is drawn on the Reynolds-averaged flame isocontour $\bar{c}=0.5$.

It is expected that hydrogen addition will reduce the Lewis number of the global mixture, irrespective of the operating pressure. Therefore, it is also likely that the flame instabilities will appear at higher pressures with hydrogen addition. Due to increase in laminar flame speed with doping, despite decrease of u'/s_{L0}, turbulent flame speed sees an increasing trend. The turbulent flame speed increase by as much as 14.5% for 20% H_2 addition at $u'/s_{L0} \sim 4$ (see Fig. 10.1). In general, the preferential diffusion of hydrogen on turbulent combustion is enhanced by turbulence, or likely with pressure.

It is for the first time that numerical simulations of hydrogen-doped lean premixed turbulent flames have been carried out, as far as the author's knowledge is concerned. Simulations are performed using the AFSW model for the relatively simple Bunsen-like flames, based on the data of *Halter et al.,* (Halter 2005). The comparative studies rely on turbulent flame speed; the model has been shown to be predicting the three

pure methane-air mixtures (Fig. 10.1) for 1, 5 and 9 bar, reasonably. However, the same model is unable to characterize the doping effect of the CH4/H_2/air flame.
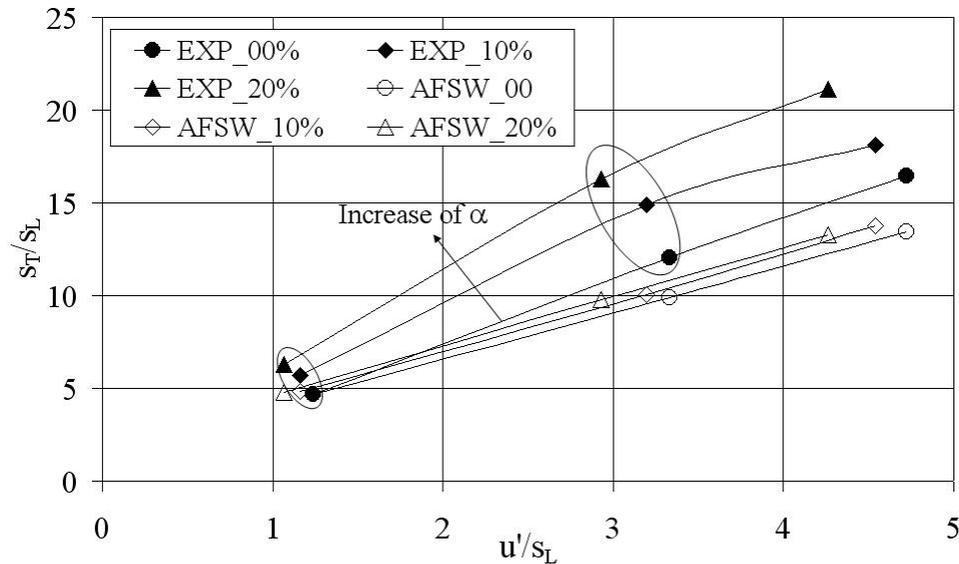
Figure 10.1: *Comparison of numerical simulations (AFSW) with the experimental data of Halter et al. (Halter 2005) (EXP), the % in legends represents the hydrogen content.*

The exponential $(Le-1)$ dependency (Lipatnikov and Chomiak 1998, Aluri et al. 2006) is passive to the hydrogen addition up to at least 20%, as the effective Lewis number (which can be estimated for e.g., using CHEMKIN) barely changes from the pure hydrocarbon Le value. This is interpreted correct because the dominance of deficient reactant (hydrogen with low Le) at the leading edge of the flame is not effectively captured in the model. However, further fuelling of H_2 will surge in the dominance of the leading edge. The influence of hydrogen doping may only be explained with the concept of the critically curved flamelets, which characterizes the highest mean local burning velocity (or, critical chemical time scale) that is strongly affected by high preferential diffusion instability of hydrogen.

Processes at the leading edge of a developing flame brush substantially affect turbulent flame speed by triggering combustion and flame surface area production (recall the strong influence of hydrogen mass diffusivity at the positive curvature towards unburned side). The structure of leading kernels is indirect functions of the preferential diffusion and Lewis number. As the critically perturbed zones dominate the leading edge, in mixtures carrying $Le<1$ and preferential diffusion, the strongest known

perturbations of laminar flames are associated with a critically curved spherical kernel (Lipatnikov and Chomiak 1998). These perturbations are augmented due to the addition of hydrogen for its known properties. The leading point for $Le<1$ indicates the flame curvature is positive when the flamefront is convex towards the unburned mixture. With hydrogen addition, the distributions were experimentally shown to broaden slightly with higher probabilities of larger curvatures, with a possible indication of the enhancement of small-scale flamefront wrinkling (Halter et al. 2005b). Such kernels are thought to survive under the influence of eddies that is ought to quench other laminar flamelets. *Renou et al.* (Renou et al. 2000) have reported that: (1) positive curvature h^+ is increased by Le, whereas negative curvature h^- shows the opposite behaviour, (2) the mean radius, $R_c = 0.5(1/h^+ + 1/h^-)$, of flamelet curvature decreases with increasing u'/s_{L0}, the decrease being less pronounced in lean hydrogen–air mixtures. Moreover, the recent DNS data obtained for lean (ϕ=0.4) H_2–air mixtures indicate that: (1) the dependence of the local displacement speed on the curvature is strongly non-linear (Chen and Im 2000), and (2) the averaged speed is substantially larger (by a factor of 2) than s_{L0} (Im and Chen 2002).

Therefore, a submodel for chemical time scale from the leading point analysis based on the critically curved laminar flames employed in earlier studies for expanding spherical flames based on the critical chemical time scale (Lipatnikov and Chomiak 1998) is re-introduced here to understand the doped effects. By combining the submodel for critical chemical time scale and the reaction closure, the dependence of turbulent flame speed on physicochemical properties of the burning mixtures including the strong dependence of preferential diffusion and/or Le effects should be computationally determined.

10.2 Extension of the AFSW Model to Hydrogen-Doped Flames

In its present form, the AFSW model (Eq. 7.9, reproduced here) is unable to capture

$$\frac{A_T}{\overline{A}} = \frac{s_T}{s_{L0}} = 1 + \frac{A_0}{e^{(Le-1)}} \cdot \mathrm{Re}_t^{0.25} \cdot \left(\frac{u'}{s_{L0}} \right)^{0.3} \cdot \left(\frac{v_0}{v} \right)^{0.2} \tag{7.9}$$

the preferential diffusion (PD), as discussed in the previous sections. To rectify for the combined influence of PD and *Le* effects, an equality relation is proposed. The *Le* dependency accommodating the effects of fuel and fuel-air mixtures together cannot be captured, as there are instances where the diffusion of sufficient reactant also contributes to the alteration of flame characteristics and turbulent flame speed. That is, the *Le* relation may not capture the effects of H_2-doping, because, addition of hydrogen to the hydrocarbon mixture contributes only little to the global *Le* value. The effect of hydrogen addition is envisaged in terms of chemical time scale as (Lipatnikov 2006, Muppala and Papalexandris 2006) by balancing the turbulent flame speed of two-component hydrocarbon/H_2 mixtures one based on standard parameters and the other the critical parameters

$$A_0 \cdot S_{L0}^{0.2} / \tau_{c0}^{1/4} = A_1 \cdot S_{L1}^{0.2} / \tau_{cr}^{1/4} \qquad (10.2)$$

where A_0, A_1, and τ_{c0} (=ratio of laminar flame thickness and laminar flame speed of the planar laminar flame), S_{L0} and S_{L1} are, respectively, the pre-constants in the reaction model Eq. 7.9, chemical time scale and unstretched laminar flame speeds based on without and with the H_2-doped effects (Lipatnikov and Chomiak 2005). The direct influence of mixture properties permitting preferential diffusion on the turbulent flame speed is controlled by a single parameter τ_{cr}, given as an input parameter to model premixed turbulent combustion (Karpov et al. 1996). The parameter τ_{cr} for very lean H_2-CH_4-air mixture is to be determined computationally. This task shall be accomplished from a submodel based on critically curved flamelets for the chemical time scale by including the combined PD and *Le* effects (Lipatnikov and Chomiak 2005). The significance of the critical chemical time scale τ_{cr} will be discussed in the last section of this chapter. This submodel for the chemical time scale addresses the dependency of turbulent combustion on the physicochemical properties of fuel mixtures (Karpov et al. 1996, Lipatnikov and Chomiak 1998).

The physical mechanisms of the enhancement of local burning due to diffusive-thermal effects, and separately by the convection of a flamelet by a strong eddy contribute to the formation of a leading point. Here, strongly curved laminar flamelets are considered to be the leading points only for mixtures with *Le*<1. In such mixtures,

the local burning rate in a positively curved flamelet is substantially increased due to the higher chemical energy flux into the flamelet as compared with the heat flux with it. As a result, the flamelet propagates faster to the leading edge of the flame brush. The advantage of hydrogen doping is immensely noticeable in this regard, due to its very high diffusive nature, effectuated more in the transient processes.

A simplified method to modelling such effects can be incorporated into the s_T closure (Eq. 7.9) based on the aforesaid concept of leading points — propagation of premixed turbulent flames is controlled by the leading flamelets advancing farthest into the unburned gas. In other words, out of several local reacting structures, one with the highest instantaneous speed overrun these structures and indeed is expected to control the turbulent flame speed, i.e., it is a strong function of physicochemical characteristics of such leading flamelets via the (critical) chemical time scale. For further details see (Karpov et al. 1996, Lipatnikov and Chomiak 1998, Lipatnikov and Chomiak 2005). In line with the leading point approach, various perturbed flamelets should be studied to locate a perturbation which yields the highest mean local burning velocity s_L. As shown in (Karpov et al. 1996), the highest s_L is reached in the expanding spherical flame ignited by the pocket of the critical radius if $Le<1$. With the introduction of a new chemical time scale (to replace conventional $\tau_{c0}=\delta_L/s_{L0}$) (Lipatnikov and Chomiak 1998)

$$\tau_{cr} = \tau_{c0} \left(\lim_{t\to\infty} u_c \right) \Big/ max\{u_c(t)\}_{r_i=r_{cr}} \qquad (10.3)$$

characterizes the highest local combustion rate for $Le<1$. Here, $u_c(t \to \infty)$ is the unperturbed consumption velocity (Karpov et al. 1996). For $Le>1$, as Lipatnikov and Chomiak interprets (Lipatnikov and Chomiak 2005), a flamelet convex to the burned side cannot be a leading point, but that the highest local combustion rate might be reached in leading structures associated with locally planar flamelets characterized by the lowest local flame surface. Therefore, the balance of the increase in the local flame surface density and the decrease in the local combustion rate should be reached in leading structures. Such a leading structure may be described in terms of a chemical time scale higher than τ_{c0}. Due to lack of a suitable model, τ_{c0} may be used as the

lower estimate, i.e., $max\{u_c(t)\}$ at $r_i = r_{cr}$ equalling $u_c(t \to \infty)$. Note that, maximum burning velocities are reachable only if the ignition is made at $r_i = r_{cr}$ w.r.t. expanding spherical flames.

The local burning velocity is a strong function of preferential diffusion and especially if the Lewis number is low, such as for lean hydrogen mixtures. Lipatnikov and Chomiak (Lipatnikov and Chomiak 1998) have shown that especially the hydrogen mixtures are associated with steeper slopes of the derivative ds_T/du', compared to corresponding hydrocarbon mixtures. Also, for lean hydrogen mixtures despite of very low s_{L0} values compared to corresponding its rich and stoichiometric propane mixtures, turbulent flame speed is remarkably higher (Kido et al. 2002). The thumb rule for few cases: $\tau_{cr} > 10\tau_{c0}$ for lean H_2 mixtures, and for lean hydrocarbon mixtures, $\tau_{cr} \sim \tau_{c0}$. It was shown in (Lipatnikov and Chomiak 1998) that this critical chemical time scale failed in few extremum cases: very lean hydrogen mixtures, for not accounting the flame quenching effects; rich hydrogen mixtures for the above assumption for $Le > 1$.

With H_2 addition, laminar flame speed increases, but laminar flame thickness decreases, while the product of the two, the thermal diffusivity remains invariant (Halter et al. 2005a). Note that this equality expression Eq. 10.2 is not universal, rather is deducted from the chosen reaction model. The present aim is to substantiate the reaction model for both the Lewis number and preferential diffusion effects; note that from the physical point of view both molecular heat conductivity and diffusion mean basically the same processes. After finding the best values of the constant A_1 by tuning procedure, comparison between the two chemical time scales shall reveal the extent of the influence of interrelated Le/PD on turbulent premixed combustion, thereby perfecting the reaction model.

To summarise, as the model is insensitive to PD effects, a submodel for the chemical time scale from the leading point analysis based on the critically curved laminar flame concept was re-introduced. By combining this submodel and the reaction closure, the dependence of turbulent flame speed on physicochemical properties of the fuel mixtures including the strong dependence of preferential diffusion and/or the Lewis number effects can be computationally determined. The applicability of the proposed

model should be tested for the F-5 configuration and other relevant hydrogen doped data. It is understood that the local quenching effects may implicitly be included by using the stretched laminar flame speed affected by strain, stretch, and curvature effects, to replace the unstretched laminar flame speed in the submodel for the turbulent flame speed.

11. Summary and Discussion

This thesis dealt with the modelling and simulation of the flame dynamics of premixed turbulent combustion on a variety of flame configurations, with considerable emphasis on molecular transport effects. Investigations in both RANS and LES contexts were carried out considering the hierarchy of complexity of flame geometries, from a typical Bunsen burner via a sudden expansion dump combustor to a complex swirl-stabilized gas turbine burner-combustor.

Results were critically discussed at the end of each chapter for **Chapters 7** to **10**.

An exhaustive comparative study with RANS approach showed that several of the existing reaction models are insensitive essentially for two major effects, namely, high pressure and fuel variation. To incorporate these effects, an Algebraic Flame Surface Wrinkling (AFSW) model and the Lindstedt-Váos model, respectively, were developed and extended, based on the data set of about hundred different Bunsen flames. In addition, the AFSW model capabilities were verified for pressures as high as 10 bar and 32 bar for the dump combustor and for an ALSTOM conical swirl burner respectively, for methane-air flames. Also, the importance of Lewis number was demonstrated on the latter configuration with pre-vaporised lean premixed diesel-air mixtures.

The flame dynamics were investigated in the complex swirl burner configuration. The propagation of the flame or the vortex breakdown point into the mixing tube was explained with baroclinic push i.e., coupling of the density gradient across the flame and the radial mean pressure gradient in the unburnt swirling gas ahead of the flame. This coupling results in the generation of azimuthal vorticity counter-acting against the axial jet in the mixing tube and thereby enhancing the flame propagation into the mixing tube.

The applicability of the AFSW model as subgrid scale reaction closure was successfully tested in the LES approach using the three widely employed turbulence models (for Bunsen, dump combustor and complex double cone burner configurations). Within the simple Bunsen-like configuration, the modelling issues for $\Delta = l_G$ were briefed with the atmospheric flame. Owing to the complexity of the dump combustor and complex double cone burner configurations, cold flow LES results

were analysed to test the veracity of the turbulence models prior to the combusting simulations. The performance of the sgs closures were validated based on cold flow experimental data for both configurations. Simulations at atmospheric pressure were made with two grid levels to assess the quality of the simulations on the fine grid. The quality of the closures in combination with the employed discretization schemes were estimated using LES index of quality (LES_IQ) defined by Celik as a quality assessment measure. The LES_IQ for cold and combusting flows were, respectively, 50-60% and 80% for the F2-configuration. Also, the 'numerical' and 'model' error contributions on this geometry were separated following an approach of Klein. This showed that the convolution of these two yielded in a lower error due to their opposite signs.

The reaction closure was successfully validated against experimentally measured flame brush thickness and mean flame position on this configuration. Also, for increased pressures, the combustion LES results were in excellent agreement with respect to these two quantities. Increase of flame wrinkling was clearly noticeable in the computed instantaneous flames. RANS studies yielded reasonable mean flame length, while under predicting the axial turbulent flame brush width by as much as 50 percent.

On the complex double cone burner, the LES_IQ was estimated as 30-50% based on the single grid solution by assuming the numerical viscosity as 50% of resolved energy. Despite of this lower resolution, combustion-LES were performed to address the dual-flame mode, as it has been demonstrated that RANS approach cannot predict this very nature. With the tuning of the model constant, the reaction closure is able to capture the dual-flame mode and was quantified with the pressure drop across the burner combustor configuration, quite similar to the experimental observation. The tuning of the constant on this configuration was attributed to the lower grid resolution.

In a final step, the behaviour of the AFSW model for hydrogen blended methane-air flames was studied analytically and with limited computations (only with RANS approach). As the model was found insensitive to (molecular) preferential diffusion effect, a submodel for the chemical time scale from the leading point analysis based on the critically curved laminar flame concept was re-introduced. By merging this submodel with the reaction subclosure, the dependence of turbulent flame speed on

physicochemical properties of the fuel mixtures including the strong dependence of preferential diffusion and/or the Lewis number effects can be computationally determined. The applicability of the proposed model remains to be studied for the Orleans Bunsen burner (F-5 configuration) and for any other existing relevant hydrogen (-doped) data. It is understood that the local quenching effects may implicitly be included by using the stretched laminar flame speed affected by strain, stretch, and curvature effects, to replace the unstretched laminar flame speed in the submodel for the turbulent flame speed.

Bibliography

Abdel-Gayed, R. G., D. Bradley, M. N. Hamid, and M. Lawes. 1984. Lewis number effects on turbulent burning velocity. Proceedings of the Combustion Institute **20**:505-512.

Aluri, N. K., S. P. R. Muppala, and F. Dinkelacker. 2006. Substantiating a Fractal-based Algebraic Reaction Closure of Premixed Turbulent Combustion for High-Pressure and the Lewis Number Effects. Combustion and Flame **145**:663-674.

Aluri, N. K., P. K. G. Pantangi, S. P. R. Muppala, and F. Dinkelacker. 2005a. A Numerical Study Promoting Algebraic Models for the Lewis Number Effect in Atmospheric Turbulent Premixed Bunsen Flames. Flow, Turbulence and Combustion **75**:149–172.

Aluri, N. K., S. Qian, S. P. R. Muppala, and F. Dinkelacker. 2005b. Flame Surface Density Models - A Numerical Evaluation. *in* Proceedings of the European Combustion Meeting, (Louvain-la-Neuve) Belgium.

Ashurst, W. T. 1996. Flame propagation along a vortex: the baroclinic push. Combusion Science and Technology **112**:175-185.

Biagioli, F. 2006. Stabilization mechanism of turbulent premixed flames in strongly swirled flows. Combustion Theory and Modelling **10**:389 - 412.

Biagioli, F., A. De Pascale, and F. Güthe. 2005. Modelling NOx Emissions from Lean Partially Premixed Flame in Industrial Burners. *in* Proceedings of the European Combustion Meeting, (Louvain-la-Neuve) Belgium.

Borghi, R. 1985. On the Structure and Morphology of Turbulent Premixed Flames. Pages 117-138 *in* C. Casci, editor. Recent Advances in Aeronautical Science. Plenum Press, New York.

Bradley, D. 1992. How fast can we burn. Proceedings of the Combustion Institute **24**:247-262.

Bray, K. N. C. 1980. Turbulent Flows with Premixed Reactants. Pages 115-183 *in* P. A. Libby and F. A. Williams, editors. Turbulent Reacting Flows. Springer, Berlin.

Bray, K. N. C. 1990. Studies of the turbulent burning velocity. Proc. R. Soc. Lond. A **431**:315-335.

Bray, K. N. C., P. A. Libby, and J. B. Moss. 1985. Unified modeling approach for premixed turbulent combustion-part I: General formulation. Combustion and Flame **61**:87-102.

Cant, R. 1998. Book Review: Direct Numerical Simulation for Turbulent Reacting Flows. Combustion and Flame **113**:277-278.

Cant, R. S., S. B. Pope, and K. N. C. Bray. 1990a. Modelling of flamelet surface-to-volume ratio in turbulent premixed combustion. Proceedings of the Combustion Institute **23**:809-815.

Cant, R. S., B. Rogg, and K. N. C. Bray. 1990b. On laminar flamelet modelling of the mean reaction rate in a premixed turbulent flame. Combusion Science and Technology **69**:53-61.

Celik, I., Z. N. Cehreli, and I. Yavuz. 2005. Index of Resolution Quality for Large Eddy Simulations. ASME, Journal of Fluids Engineering **127**:949-958.

Celik, I., M. Klein, and J. Janicka. 2006. A Test of Validation of Turbulent Premixed Models for High-Pressure Bunsen Flames. *in* Proceedings of FEDSM2006, ASME Joint U.S. European Fluids Engineering Summer Meeting, July 17-20, Miami Florida.

Charlette, F., C. Meneveau, and D. Veynante. 2002. A power-law flame wrinkling model for LES of premixed turbulent combustion Part I: non-dynamic formulation and initial tests. Combustion and Flame **131**:159-180.

Chen, J. H., and H. G. Im. 2000. Stretch Effects on the Burning Velocity of Turbulent Premixed Hydrogen/Air Flames. Proceedings of the Combustion Institute **28**:211.

Chen, Y.-C., and R. W. Bilger. 2002. Experimental investigation of three-dimensional flame-front structure in premixed turbulent combustion--I: hydrocarbon/air bunsen flames. Combustion and Flame **131**:400-435.

Chomiak, J., and J. R. Nisbet. 1995. Modeling variable density effects in turbulent flames-some basic considerations. Combustion and Flame **102**:371-386.

Chomiak, J., and G. Zhou. 1996. A numerical study of large amplitude baroclinic instabilities of flames. Proceedings of the Combustion Institute **26**:883-889.

Cohen, H., G. F. C. Rogers, and H. I. H. Saravanamuttoo. 1996. Gas Turbine Theory, 4th Edition edition. Addison Wesley Longman Limited, Essex.

Damköhler, G. 1940. Der Einfluss der Turbulenz auf die Flammengeschwindigkeit in Gasgemischen. Zeitschrift für Elektrochemie und Angewandte Physikalische Chemie **46**:601-626.

Davidson, L. 1998. An introduction to turbulence models. Lecture Notes, Dept. of Thermo and Fluid Dynamics, Chalmers University of Technology, Gothenburg,.

Dinkelacker, F. 2001. Struktur turbulenter Vormischflammen. Habilitation thesis. Universität Erlangen, Berichte zur Energie- und Verfahrenstechnik (BEV), Heft 1.4, Esytec, Erlangen.

Dinkelacker, F. 2003. Experimental Validation of Flame Regimes for Highly Turbulent Premixed Flames. *in* Proceedings of the European Combustion Meeting, Orleans (France).

Dinkelacker, F., and S. Hölzler. 2000. Investigation of Turbulent Flame Speed Closure Approaches for Premixed Flame Calculation. Combustion Science and Technology **158**:321-340.

Dinkelacker, F., A. Soika, D. Most, D. Hofmann, A. Leipertz, W. Polifke, and K. Döbbeling. 1998. Structure of locally quenched highly turbulent lean premixed flames. Proceedings of the Combustion Institute **27**:857-865.

Duclos, J. M., D. Veynante, and T. Poinsot. 1993. A comparison of flamelet models for premixed turbulent combustion. Combustion and Flame **95**:101-117.

Düsing, M. 2004. Large Eddy Simulation Turbulenter Vormischflamme. Ph.D. Thesis. TU-Darmstadt.

Ferziger, J. H. 1996. Large Eddy Simulation. in: Gatski, Hussaini, Lumley (Eds.), Simulation and Modeling of Turbulent Flows, Oxford University Press, New York **Chapter 3**:109-154.

Fluent. 2005. Computational Fluid Dynamics Software. *in* Fluent Incorporated, Lebanon, NH, USA.

Fritz, J. 2003. Flammenrückschlag durch verbrennungsinduziertes Wirbelaufplatzen. Dissertation. Technische Universität München, München.

Fritz, J., M. Kröner, and T. Sattelmayer. 2001. Flashback in a Swirl Burner with Cylindrical Premixing Zone. ASME Turbo Expo **Paprer No. GT 2001-0054**.

Gauducheau, J. L., B. Denet, and G. Searby. 1998. A Numerical Study of Lean CH4/H2/Air Premixed Flames at High Pressure. Combusion Science and Technology **137**:81-99.

Germano, M., U. Piomelli, P. Moin, and W. H. Cabot. 1996. Dynamic Subgrid-Scale Eddy Viscosity Model. Summer Workshop, Centre for Turbulence Research, Stanford, CA.

Geurts, B. J., and J. Fröhlich. 2002. A framework for predicting accuracy limitations in large eddy simulation. Physics of Fluids **14**:L41-L44.

Gouldin, F. C. 1987. An application of fractals to the modelling of premixed turbulent flames. Combustion and Flame **68**:249-266.

Gouldin, F. C., K. N. C. Bray, and J.-Y. Chen. 1989. Chemical closure model for fractal flamelets. Combustion and Flame **77**:241-259.

Gouldin, F. C., and K. V. Dandekar. 1984. Time resolved density measurements in premixed turbulent flames AIAA Journal **22**:655-663.

Griebel, P., R. Bombach, A. Inauen, W. Kreutner, and R. Schären. 2002. Structure and NO Emission of Turbulent High-Pressure Lean Premixed Methane/Air Flames. Proceedings of the 6th European Conference on Industrial Furnaces and Boilers **Vol. II**:45-54.

Griebel, P., R. Bombach, A. Inauen, R. Schären, S. Schenker, and P. Siewert. 2005. Flame characteristics and turbulent flame speeds of turbulent, high-pressure, lean premixed methane/air flames. ASME Turbo Expo **Paper No. GT2005-68565**.

Griebel, P., R. Schären, P. Siewert, R. Bombach, A. Inauen, and W. Kreutner. 2003. Flow field and structure of turbulent high-pressure premixed methane/air flames. ASME Turbo Expo **Paper No. GT2003-38398**.

Guin, C. 1998. Characterization of Autoignition and Flashback in Premixed Injection Systems AVT. Symposium on Gas Turbine Engine Combustion, Emissions and Alternative Fuels (Lisbon, Portugal) **ONERA TP1998-227.**

Gülder, Ö. L., and G. J. Smallwood. 1995. Inner cut off scales validity negative to Gibson scale. Combustion and Flame **103**:107-114.

Gülder, Ö. L., G. J. Smallwood, R. Wong, D. R. Snelling, R. Smith, B. M. Deschamps, and J.-C. Sautet. 2000. Flame front surface characteristics in turbulent premixed propane/air combustion. Combustion and Flame **120**:407-416.

Halter, F. 2005. Caractérisation des effets de l'ajout d'hydrogène et de la haute pression dans les flammes turbulentes de prémélange méthane/air. Dissertation. l'Universite d'Orleans, Orleans (France).

Halter, F., C. Chauveau, N. Djebaili-Chaumeix, and I. Gökalp. 2005a. Characterization of the effects of pressure and hydrogen concentration on laminar burning velocities of methane–hydrogen–air mixtures. Proceedings of the Combustion Institute **30**:201-208.

Halter, F., C. Cohe, C. Chauveau, and I. Gökalp. 2005b. Characterization of the effects of hydrogen addition in lean premixed methane/air turbulent flames at high pressure. Proceedings International Hydrogen Energy Congress and Exhibition IHEC 2005.

Halter, F., C. Cohé, C. Chauveau, and I. Gökalp. 2003. Characterization of the effects of hydrogen addition in lean premixed methane/air turbulent flames at high pressure. *in* Proceedings of the European Combustion Meeting, Orleans (France).

Hirsch, C., T. Küenzi, H. P. Knöpfel, B. Paikert, C. Steinbach, W. Geng, and K. Döbbeling. 2002. An Annular Combustor Natural Gas Ignition Model Derived from Atmospheric Sector Experiments. ASME **Paper no. GT-2002-30073**.

I.E.A. 2006. International Energy Outlook. (http://www.iea.org/)

Im, H. G., and J. H. Chen. 2002. Preferential diffusion effects on the burning rate of interacting turbulent premixed hydrogen-air flames. Combustion and Flame **131**:246-258.

Janicka, J. Sadiki. A., A. 2005. Large Eddy Simulation of Turbulent Combustion Systems. Proceedings of the Combustion Institute **30**:537-547.

Jones, W. P., and J. H. Whitelaw. 1982. Calculation methods for reacting turbulent flows: a review. Combustion and Flame **48**:1-26.

Karpov, V. P., A. N. Lipatnikov, and V. L. Zimont. 1996. A test of an engineering model of premixed turbulent combustion. Proceedings of the Combustion Institute **26**:249-257.

Keller, J. O., L. Vaneveld, D. Korschelt, G. L. Hubbard, A. F. Ghoniem, J. W. Daily, and A. K. Oppenheim. 1982. Mechanism of Instabilities in Turbulent Combustion Leading to Flashback. AIAA-Journal **20**:254-.

Kerstein, A. R. 1988. Fractal dimension of flame front movement in a turbulent premixed flame zone. Proceedings of the Combustion Institute **21**:1281.

Kido, H., M. Nakahara, J. Hashimoto, and D. Barat. 2002. Turbulent Burning Velocities of Two-component Fuel Mixtures of Methane, Propane and Hydrogen. JSME International Journal **45**.

Kim, W.-W., and S. Menon. 1997. Application of the localized dynamic subgrid-scale model to turbulent wall-bounded flows. *in* Technical Report AIAA-97-0210, 35th Aerospace Sciences Meeting, Reno, NV.

Klein, M. 2005a. *in* Private Communication.

Klein, M. 2005b. An attempt to assess the quality of large eddy simulations in the context of implicit filtering. Flow Turbulence and Combustion **75**:131–147.

Kobayashi, H. 2001. *in* List of Experimental Data of High Pressure Flames, Private Communication.

Kobayashi, H., Y. Kawabata, and K. Maruta. 1998. Experimental Study on General Correlation of Turbulent Burning Velocity at High Pressure. Proceedings of the Combustion Institute **27**:941-948.

Kobayashi, H., T. Nakashima, T. Tamura, K. Maruta, and T. Niioka. 1997. Turbulence measurements and observations of turbulent premixed flames at elevated pressures up to 3.0 MPa. Combustion and Flame **108**:104-117.

Kobayashi, H., K. Seyama, H. Hagiwara, and Y. Ogami. 2005. Burning velocity correlation of methane/air turbulent premixed flames at high pressure and high temperature. Proceedings of the Combustion Institute **30**:827-834.

Kobayashi, H., T. Tamura, K. Maruta, and T. Niioka. 1996. Burning velocity of turbulent premixed flames in a high pressure environment. Proceedings of the Combustion Institute **26**:389-396.

Kolmogorov, A. N. 1941. Pages 19 *in* Dokl. Akad. Nauk SSSR.

Lachaux, T., F. Halter, C. Chauveau, I. Gökalp, and I. G. Shepherd. 2005. Flame front analysis of high-pressure turbulent lean premixed methane-air flames. Proceedings of the Combustion Institute **30**:819-826.

Lewis, B., and G. von Elbe. 1961. Combustion, Flames and Explosions of Gases, Third Edition edition. Academic Press, New York.

Lilly, D. K. 1992. A Proposed Modification of the Germano Subgrid-Scale Closure Model. Physics of Fluids **4**:633-635.

Lindstedt, P., and E. M. Váos. 1999. Modelling of premixed turbulent flames with second moment methods. Combustion and Flame **116**:461-485.

Lindstedt, R. P. 2004. *in* Private Communication.

Lindstedt, R. P., and V. Sakthitharan. 1991. Modelling of transient compressible turbulent reacting flows. 8th Symposium on turbulent shear flows, Technical University of Munich, Germany.

Lipatnikov, A. 2006. *in* Private Communication.

Lipatnikov, A. N., and J. Chomiak. 1998. Lewis Number Effects in Premixed Turbulent Combustion and Highly Perturbed Laminar Flames. Combusion Science and Technology **137**:277-298.

Lipatnikov, A. N., and J. Chomiak. 2002. Turbulent flame speed and thickness: phenomenology, evaluation and application in multi-dimensional simulations. Progress in Energy and Combustion Science **28**:1-74.

Lipatnikov, A. N., and J. Chomiak. 2005. Molecular transport effects on turbulent flame propagation and structure. Progress in Energy and Combustion Science **31**:1-71.

Manickam, B. 2006. Evaluation of mean flame position, turbulent scalar fluxes and hydrogen-doping effects on premixed turbulent high-pressure combustion with RANS and LES approaches. M.Sc. Thesis, Universität Erlangen, Erlangen.

Meneveau, C. 2005. Issues and Case Studies for Experimental Validation of LES in Incompressible Flows. Proceedings of the Conference on Quality Assessment of Unsteady Methods for Turbulent Combustion Prediction and Validation **Editors, J. Janicka et al.,**.

Meneveau, C., and T. Poinsot. 1991. Stretching and Quenching of Flamelets in Premixed Turbulent Combustion. Combustion and Flame **86**:311-332.

Muppala, S. P. R. 2005. Modelling of Turbulent Premixed High-Pressure Combustion with Application Towards Gas Turbine Combustors. Dissertation. Universität Erlangen, Erlangen.

Muppala, S. P. R., N. K. Aluri, and F. Dinkelacker. 2005a. A Test of Validation of Turbulent Premixed Models for High-Pressure Bunsen Flames. *in* Proceedings of the European Combustion Meeting, (Louvain-la-Neuve) Belgium.

Muppala, S. P. R., N. K. Aluri, F. Dinkelacker, and A. Leipertz. 2005b. Development of an algebraic reaction rate closure for the numerical calculation of turbulent premixed methane, ethylene and propane/air flames for pressures up to 1.0 MPa. Combustion and Flame **140**:257-266.

Muppala, S. P. R., and F. Dinkelacker. 2003. Numerical Calculation of Turbulent Premixed Methane, Ethene and Propane/Air Flames at Pressures up to 10 bar. *in* Proceedings of the European Combustion Meeting, Orleans (France).

Muppala, S. P. R., and F. Dinkelacker. 2004. Numerical modelling of the pressure dependent reaction source term for premixed turbulent methane/air flames. Progress in Computational Fluid Dynamics **4**:328-336.

Muppala, S. P. R., and M. V. Papalexandris. 2006. A Modelling Approach for Hydrogen-doped Lean Premixed Turbulent Combustion. *in* IMECE2006-13861, editor. ASME International Mechanical Engineering Congress and Exposition, Chicago, Illinois, USA.

Murayama, M., and T. Takemo. 1988. Laminar flame thickness as the inner cut off scale. Proceedings of the Combustion Institute **22**:551-559.

Nakahara, M. 2006. Personal Communication.

Nakahara, M., and H. Kido. 1998. A Study of the Premixed Turbulent Combustion Mechanism Taking the Preferential Diffusion Effect into Consideration. Memoirs of the Faculty of Engineering, Kyushu University **58**.

Olivani, A., F. Halter, A. Yoshida, and I. Gökalp. 2003. Experimental characterization of turbulence spectra and scales in high pressure turbulent premixed flames. *in* Proceedings of the European Combustion Meeting, Orleans (France).

Peters, N. 1986. Laminar Flamelet Concepts in Turbulent Combustion. Proceedings of the Combustion Institute **21**:1231-1250.

Peters, N. 1999. The turbulent burning velocity for large-scale and small-scale turbulence. Journal Fluid Mechanics **384**:107-132.

Peters, N. 2000. Turbulent Combustion. Cambridge University Press.

Peters, N., and P. L. Vervisch. 2001. Turbulent combustion. Combustion and Flame **125**:1222-1223.

Pfadler, S., M. Löffler, F. Dinkelacker, and A. Leipertz. 2005. Measurement of the Conditioned Turbulence and Temperature Field of a Ring Stabilised Bunsen Type Premixed Burner Using Planar Laser Rayleigh Scattering and Stereo Particle Image Velocimetry. Experiments in Fluids **39**:375-384.

Pitsch, H., and L. D. d. Lageneste. 2002. Comparison of turbulent premixed flames at different turbulence levels. Center for Turbulence Research **Annual Research Briefs**:91-101.

Poinsot, T., T. Baritaud, and M. Baum. 1996. Direct Numerical Simulation for Turbulent Reacting Flows. Editions Technip, Paris.

Poinsot, T., and D. Veynante. 2001. Theoretical and Numerical Combustion. Edwards, Philadelphia.

Poinsot, T., D. Veynante, and S. Candel. 1990. Diagrams of Premixed Turbulent Combustion Based on Direct Simulation. Proceedings of the Combustion Institute **23**:613-619.

Pope, S. B. 2000. Turbulent flows. Cambridge University Press, Cambridge (UK).

Renou, B., A. Boukhalfa, D. Puechberty, and M. Trinité. 2000. Local scalar flame properties of freely propagating premixed turbulent flames at various Lewis numbers. Combustion and Flame **123**:507-521.

Roache, P. 1998. Verification and validation in computational science and engineering. Hermosa Publishers, Albuquerque.

Rogg, B. 1981. The effect of Lewis number greater than unity on an unsteady propagating flame with one-step chemistry. A GAMM-Workshop 'Numerical Methods in Laminar Flame Propagation' Norbert Peters/Jürgen Warnatz (Eds.), Friedr. Vieweg & Sohn Braunschweig/Wiesbaden:38-48.

Sankaran, R., and H. G. Im. 2006. Effects of Hydrogen Addition on the Flammability Limit of Stretched Methane-Air Premixed Flames. Combustion Science and Technology **in press**.

Sattelmayer, T. 2000. Influence of the combustor aerodynamics on combustion instabilities from equivalence ratio fluctuations. ASME **Paper No. 2000-GT-0082**.

Schihl, P., J. Tasdemir, and W. Bryzik. 2004. Determination of Laminar Flame Speed of Diesel Fuel for Use in a Turbulent Flame Spread Premixed Combustion Model. Corporate Source, Army Tank-Automotive Research and Development Command, Warren, MI USA **Document ID No. 20040201167**.

Smagorinsky, J. 1963. General Circulation Experiments with the Primitive Equations. I. The Basic Experiment. Month. Wea. Rev. **91**:99-164.

Smallwood, G. J., Ö. L. Gülder, D. R. Snelling, B. M. Deschamps, and I. Gökalp. 1995. Characterization of flame front surface in turbulent premixed methane/ air combustion. Combustion and Flame **101**:461-470.

Soika, A., F. Dinkelacker, and A. Leipertz. 2003. Pressure influence on the flame front curvature of turbulent premixed flames: comparison between experiment and theory. Combustion and Flame **132**:451-462.

Sreenivasan, K. R. 1984. Phys. Fluids A **27**:1048-1051.

Syred, N. 2006. A review of oscillation mechanisms and the role of the precessing vortex core (PVC) in swirl combustion systems. Progress in Energy and Combustion Science **32**:93–161.

Trouvé, A., and T. Poinsot. 1994. The evolution equation for the flame surface density in turbulent premixed combustion. Journal Fluid Mechanics **278**:1-31.

Turns, S. R. 1996. An Introduction to Combustion: Concepts and Application. McGraw-Hill, New York.

Váos, E. M. 1998. Second Moment Methods for Turbulent Flows with Reacting Scalars. PhD thesis. University of London.

Versteegh, H. K., and W. Malalasekera. 1995. An Introduction to Computational Fluid Dynamics - The Finite Volume Method.

Veynante, D., and L. Vervisch. 2002. Turbulent Combustion Modeling. Progress in Energy and Combustion Science **28**:193-266.

Weller, H. G., C. J. Marooney, and A. D. Gosman. 1990. A new spectral method for calculation of the time-varying area of a laminar flame in homogeneous turbulence. Proceedings of the Combustion Institute **23**:629-636.

Weller, H. G., S. Uslu, A. D. Gosman, R. R. Maly, R. Herweg, and B. Heel. 1994. Prediction of Combustion in Homogeneous-Charge Spark-Ignition Engines. COMODIA 94:163-169.

Williams, F. A. 1985. Combustion Theory, Second Edition. Addison-Wesley, Reading, Mass.

Zel'dovich, Y. B., G. I. Barenblatt, V. B. Librovich, and G. M. Makhviladze. 1985. The Mathematical Theory of Combustion and Explosions. New York: Plenum;.

Zevenhoven, R., and P. Kilpinen. 2004. Control of pollutants in flue gases and fuel gases.

Zhang, Y., B. Rogg, and K. N. C. Bray. 1995. 2-D Simulation of Turbulent Autoignition with Transient Laminar Flamelet Source Term Closure. Combustion Science and Technology **105**:211-221.

Zhao, X., R. D. Matthews, and J. L. Ellzey. 1994. COMODIA turbulent flame speed relation fractal method. COMODIA 94:157-162.

Zimont, V. L., and A. N. Lipatnikov. 1995. A numerical model of premixed turbulent combustion of gases. Chem. Phys. Reports **14**:993-1025.

Appendix: A

Substantiation of the Lindstedt-Váos (LV) Reaction Model

The theory describing the details of Lindstedt-Váos model is given in **Section 3.3**. And, its performance along with various reaction models is shown as correlation plots for the Bunsen burner (F1-Configuration) in **Chapter 7**. As none of the models are sensitive to pressure and fuel types, the fractal-based LV reaction model has been effectuated with the pressure and Lewis number influences, along with the development of an Algebraic Flame Surface Wrinkling model using the *Kobayashi* Bunsen flame data. The details of the later model are outlined in **Section 3.3**. It is worth-emphasizing that for the influence of the fuel, the model was able to qualitatively predict the flame speed variation with turbulence (Fig. A1). However, comparisons with the measured data showed that the model was lacking in the so-called Lewis number effects (realized with the non-unity Lewis number of the fuel-air mixtures), thus requiring parametric adjustments for each fuel undertaken. Furthermore, this closure (Eq. 3.10) has been further substantiated for the high-pressure influence and the results are analysed with KPP analysis (Poinsot and Veynante 2001).

$$\overline{\dot{w}}_c = C_R \rho_u \frac{s_{L0}}{V_K} \frac{\tilde{\varepsilon}}{\tilde{k}} \tilde{c}(1 - \tilde{c})$$

(3.10)
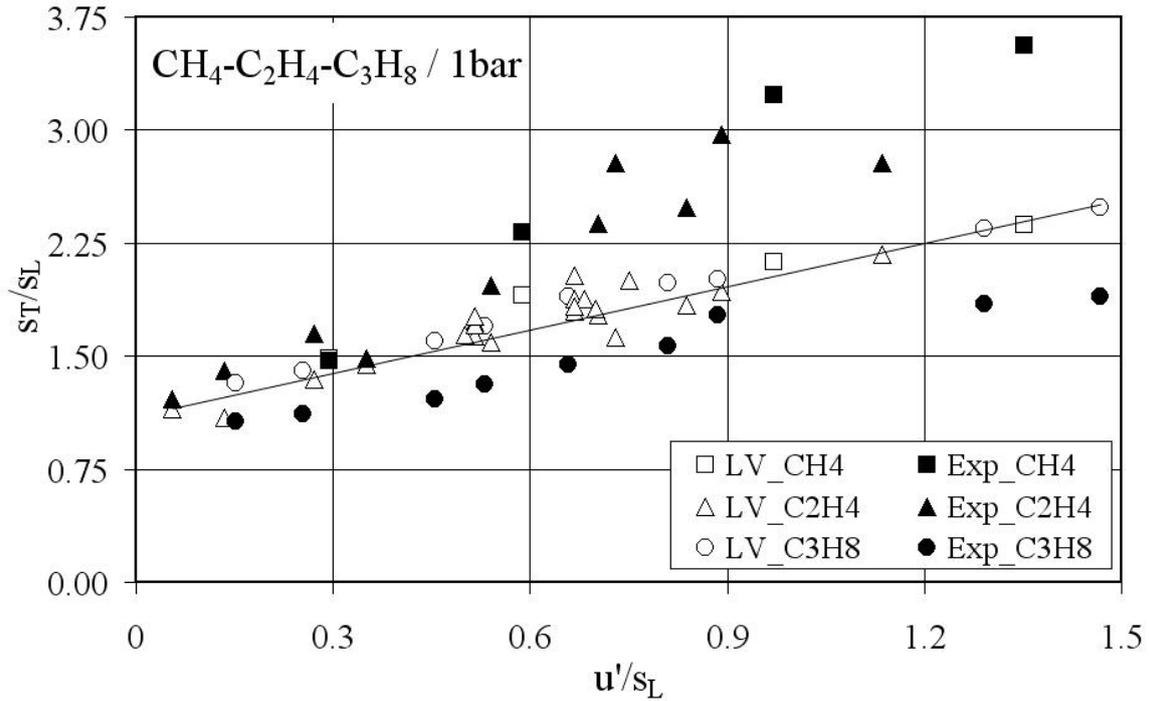
Figure A1: *Comparison of calculated flame angle in s_T/s_{L0} from the LV model with the experimentally measured data of Kobayashi, for methane (ϕ = 0.9), ethylene (ϕ = 0.7 & 0.9), and propane (ϕ = 0.9) flames at 1 bar.*

So, as a first step, a new pre-constant (C_R of Eq. 3.10) of 4.0 was found (Aluri et al. 2005a) which is in line with that of Gouldin et al. (Gouldin et al. 1989) who have also proposed C_R of 4.0 in their numerical investigation of an oblique flame. Indeed, Lindstedt and Váos assigned C_R values between 3.25 and 4.5, if the eddy viscosity turbulent diffusion closure were to be applied as a closure for the turbulent scalar flux (Váos 1998, Lindstedt 2004), supporting the choice of this new model constant (Aluri et al. 2006). The results of the model with C_R=4.0 (ELV model) are presented in Fig. A2 for methane-air flames at 1 bar along with the results of LV model.
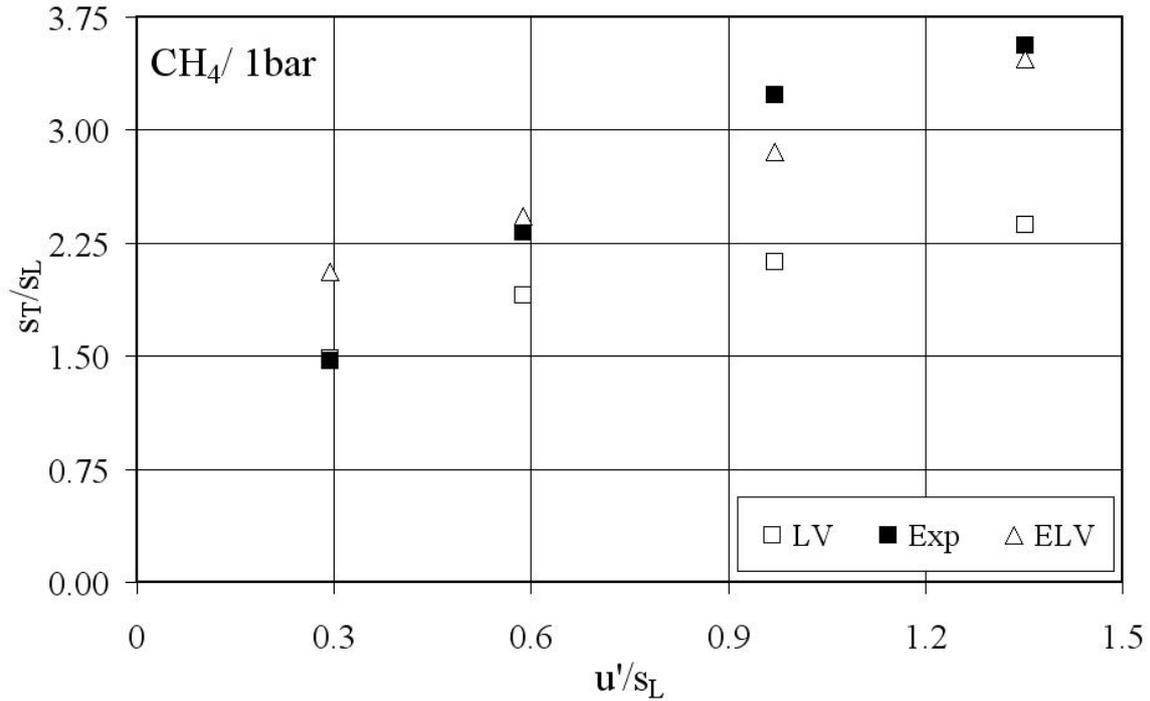
Figure A2: *Methane-air flames (ϕ = 0.9) at 1 bar from the ELV model. Also included are results from the LV model for comparison.*

Effect of fuel type

In practice, fuels of larger molecular weights (usually of high Lewis numbers) than methane have application in spark ignition engines and partly in gas-turbine combustors. So, the study of the fuel effects on the flame characteristics especially at elevated levels of pressure is of significant importance. Experimental and theoretical study on high-pressure flames by *Soika et al.* (Soika et al. 2003) affirms the causative important Lewis number effect, highlighting that both flame-generated vorticity and flame instability behaviour depend strongly on thermo-physical properties of the premixed flame, i.e., effects caused by the density jump and differential diffusive fluxes. It further interprets that the Lewis number of the fuel-air mixture poses substantial impact on the extent of flame curvature in the given turbulent flow field. In addition, non-unity *Le* influence is one of the key parameters in proper understanding of the flame-turbulence interaction (Chen and Bilger 2002). Computed results simply based on a single pre-constant for the non-unity *Le* ethylene- and propane-air mixture data show its insuffice, posing an additional difference between experiment and simulation. To reach a reasonable agreement, for the atmospheric flame data, the influence of fuel type has been interpreted as a *Le* effect in Eq. 3.10. After testing

139

several $C_R(Le)$ functions it is found that an exponential Le term, results in very good agreement with the measurements, Fig. A3 shows this comparison for the forty different atmospheric flames for all the three fuels.

$$C_{R,Le} = \frac{4.0}{e^{Le-1}} \qquad (A1)$$
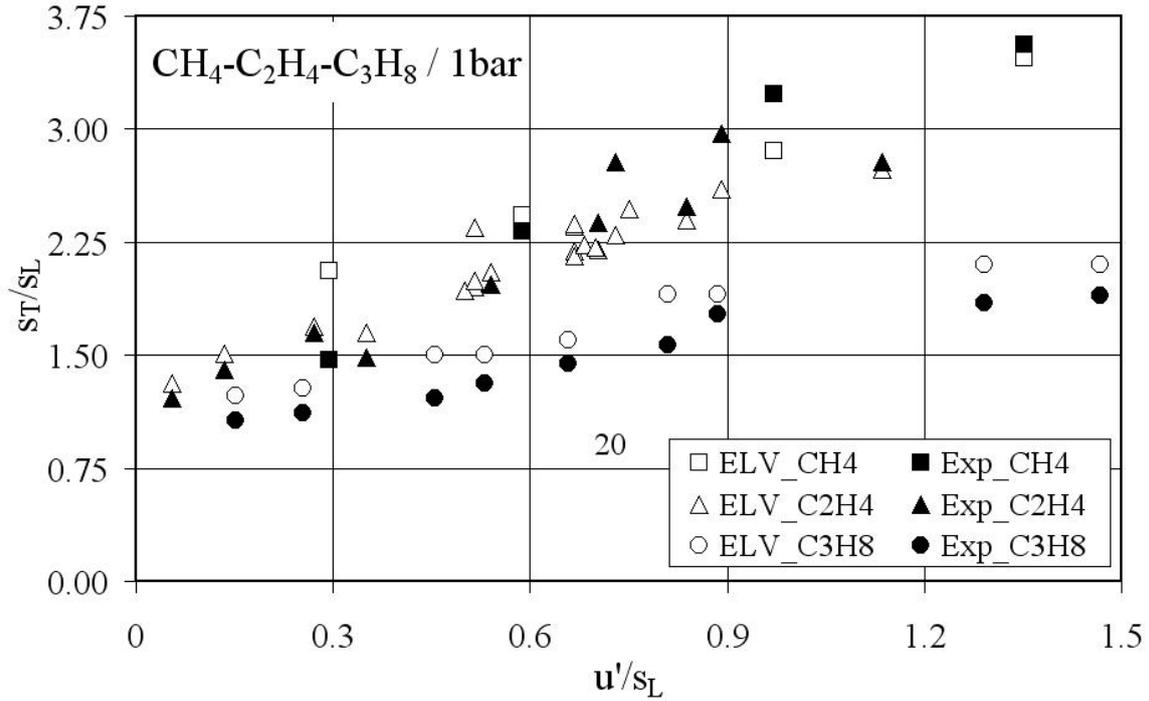
Figure A3: *Flame angles in s_T/s_L from the Extended Lindstedt-Váos (ELV) reaction closure, for CH₄ (ϕ = 0.9), C₂H₄ (ϕ = 0.7) and C₃H₈ (ϕ = 0.9) flames at 1 bar for ϕ = 0.9.*

In our earlier modelling approach, an approximated $C_R \sim 1/Le$ dependency was used (Aluri et al. 2005a). The difference is small for the flame angles (s_T/s_{L0}) for methane- and ethylene-air flames, but it is significant for the propane-air flames with Le of 1.62, as can be seen in Fig. A4. The $1/Le$ relation over predicts, especially at increased pressure or, equivalently, turbulence level.
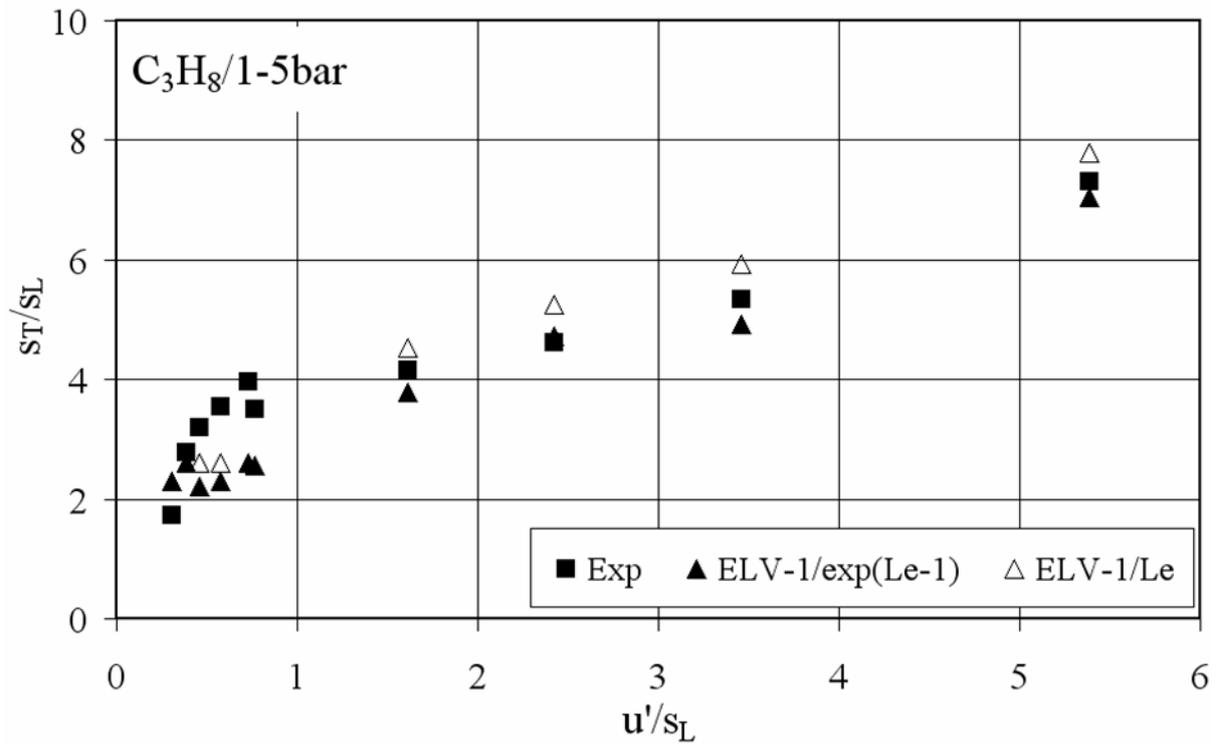
Figure A4: *Propane flame angles (ϕ = 0.9) at 5 bar using the ELV (calculated using the exponential Lewis number relation, Eq. A1 and $1/Le$) model. The open triangles show the turbulent flame speed evaluated using the $1/Le$ relation over predicts at increased turbulence level.*

The empirically found exponential dependency is consistent within the leading point concepts discussed in a recent review by Lipatnikov and Chomiak ((Lipatnikov and Chomiak 2005), pages: 38-48). In order to elucidate the direct presence and significant impact of Le, it is of interest to compare typical cases of methane and propane flames with nearly identical flow and turbulence conditions. This is done for a pair of flames (Table A1). Calculated flame cone angles from the LV and ELV models are given in Table A2, showing that the latter model is in good agreement with the experimental data. For the unity Lewis number flame, the LV model differs by as much as 21.5° compared to the measured value whereas the new model with preconstant given in Eq. A1 (simplifies to C_R=4.0 for Le=1.0) is in good agreement. For the non-unity Lewis number (Le of 1.6) flame Eq. A2 results in C_R = 2.15, which is marginally close to the original pre-constant C_R of 2.6. It is worth emphasizing here that, fuel-air mixtures characterized by very weak turbulence are not specifically distinguished from the other

data here, as s_{L0} remains a strong variant of pressure, but a majority of these flames can be easily classified based on the u'/s_{L0} range.

Table A1: *Methane and propane flame data, at nearly identical flow and turbulence conditions (pressure in bar, length scale in mm, velocities in m/s).*

Fuel	ϕ	p	Le	U	u'	l_x	s_{L0}	u'/s_{L0}
CH_4	0.9	1	1.0	2.36	0.46	1.25	0.34	1.35
C_3H_8	0.9	1	1.62	2.25	0.51	0.9	0.395	1.29

Table A2: *Full flame cone angle θ, and normalized turbulent flame speed s_T/s_{L0} for the cases described in Table A.1.*

Model / Fuel	LV $\theta°$	Exp $\theta°$	ELV $\theta°$	LV s_T/s_{L0}	Exp s_T/s_{L0}	ELV s_T/s_{L0}
CH4	40	61.5	60	2.37	3.55	3.47
C3H8	45.6	38	43	2.21	1.85	2.09

KPP analysis

In this section, the influence of pressure on reaction rate, interpreted in s_T, is illustrated. These below discussed relations are not used in the numerical simulations, but only serve to physically interpret the numerical and experimental observations. For this purpose the classical KPP analysis (see (Poinsot and Veynante 2001)) is applied. Here, the balance equation of a one-dimensional steady propagating flame is combined with the LV reaction closure with the assumptions that s_T is equal to the magnitude of the incoming mean velocity, and that the flame does not affect turbulence.

$$\rho_u s_T \frac{\partial \tilde{c}}{\partial x} = \overline{\rho} \frac{\nu_t}{\sigma_c} \frac{\partial^2 \tilde{c}}{\partial x^2} + C_R \rho_u \frac{s_L}{V_K} \frac{\tilde{\varepsilon}}{\tilde{k}} \tilde{c}(1-\tilde{c}) \qquad (A2)$$

Assuming that the leading edge of the flame (small $\tilde{c}$) determines the dynamics of the flame (see also (Lipatnikov and Chomiak 2005)), the last term in Eq. A2 may be expanded ($\tilde{c}(1-\tilde{c}) \rightarrow \tilde{c}$), leading to an ordinary differential equation. Following the KPP theorem, this has a physical solution for s_T, if its discriminant is zero (Poinsot and Veynante 2001), leading to

$$s_T = 2\sqrt{\frac{\nu_t}{\sigma_c} C_R \frac{s_{L0}}{\nu_u^{0.25}} \frac{\varepsilon^{0.75}}{k}} \tag{A3}$$

Assuming turbulence parameters (k, ε and ν_t) as independent of pressure (a suitable first order approximation), and with the pressure-dependent quantities, $\nu_u \propto p^{-1.0}$, and $s_{L0} \propto p^{-0.5}$ (for methane-air flames), the overall pressure influence on s_T shrinks to

$$s_T \propto p^{-0.125} \tag{A4}$$

This analysis implies that s_T (or reaction rate) would decrease with pressure, unlike theoretical (Lipatnikov and Chomiak 2005) and experimental findings (Kobayashi et al. 1997, Soika et al. 2003, Lachaux et al. 2005). For the two non-unity Le flames (with approximately $s_{L0} \propto p^{-0.25}$), leads to

$$s_T \propto p^0 \tag{A5}$$

Following figures A5 of methane, ethylene and propane flames substantial gap has been found between experimental and calculated values, with the differences growing larger with pressure rise. Also, computed results based on the corrected factor of C_R of 4.0 could not account for the influence of pressure (these intermediate results are not presented here explicitly). Thus, both theory and comparative studies using the simulation and measured data necessitate an additional (pressure) influence be accommodated into the model.

Pressure influence

A set of nine methane flames for two high-pressures 5 and 10 bar are simulated and analysed independently, with the aim to unveil the influence of pressure. For 5 bar, with an additional multiplicative 'correction' factor of 2.2 (thus C_R leads to 4.0x2.2 = 8.8), calculated angles are found near to the measured ones. Similarly, for 10 bar, following few iterative trials a reasonable but a still bigger factor C_R becomes 4.0x3.1 = 12.4 is realized. These additional correction factors fit rather well to a supplemental pressure dependant factor

$$\overline{w}_c \propto \left(\frac{p}{p_0}\right)^{0.5} \text{ or } \overline{w}_c \propto \left(\frac{\nu_0}{\nu}\right)^{0.5} \tag{A6}$$

where p is the operating pressure, with $p_0 = 1$ bar and ν being kinematic viscosity. These calculated flame angles are plotted in Fig. A5 and are represented by ELV. As can be seen, both experiment and the ELV model are in good agreement with each other, with few exceptions at high turbulence.

In terms of the KPP analysis, a pressure dependency of the turbulent flame speed is thus

$$s_T \propto p^{0.125} \tag{A7}$$

for lean methane-air flames. This value is relatively near to the experimentally found exponent of 0.07 (see Table A3). This explicit pressure influence may be related to a more fundamental quantity, the molecular kinematic viscosity $\nu (\propto 1/p)$, as it is scaled closely to the small scales of turbulence and laminar flame thickness. Therefore a correction factor $\nu^* = \nu/\nu_0 (= p_0/p)$ is interpreted with the modified reaction source term as $\overline{w}_c \propto 1/\sqrt{\nu^*}$; with subscript '0' being the corresponding atmospheric value.

With the pressure dependent term, Eq. A6 calculations are performed for the other 17 high-pressure 20 and 30 bar data. Though the results are not so favourable in retaining the correct quantitative trends (see b of Fig. A5), they seem promising in a first order

approximation, and certainly give much better results than the actual values. For ethylene and propane flames, the LV model pronounces a pressure-independent reaction rate (see Figures c and d of Fig. A5), whereas experiments place a $s_T \propto p^{0.24\sim0.26}$ dependency. Here, the pressure-dependent reaction rate (Eq. A8) from the theoretical KPP analysis leads to

$$s_T \propto p^{0.25} \tag{A8}$$

In Table A3 these theoretically derived pressure dependencies for the three fuels are compared with the experimental fits between 1 and 10 bar. The exponents of the ELV model are fairly near to the experimental ones.

Table A3: *Pressure dependency of turbulent flame speed: LV model, Experiment (Kobayashi) & ELV model*

$s_T \sim p^x$, $x =$	LV	Experiment	ELV
CH_4-air (Le=1.0)	-0.25	0.07	0.125
C_2H_4-air (Le=1.2)	0.01	0.24	0.26
C_3H_8-air (Le=1.62)	-0.01	0.25	0.25
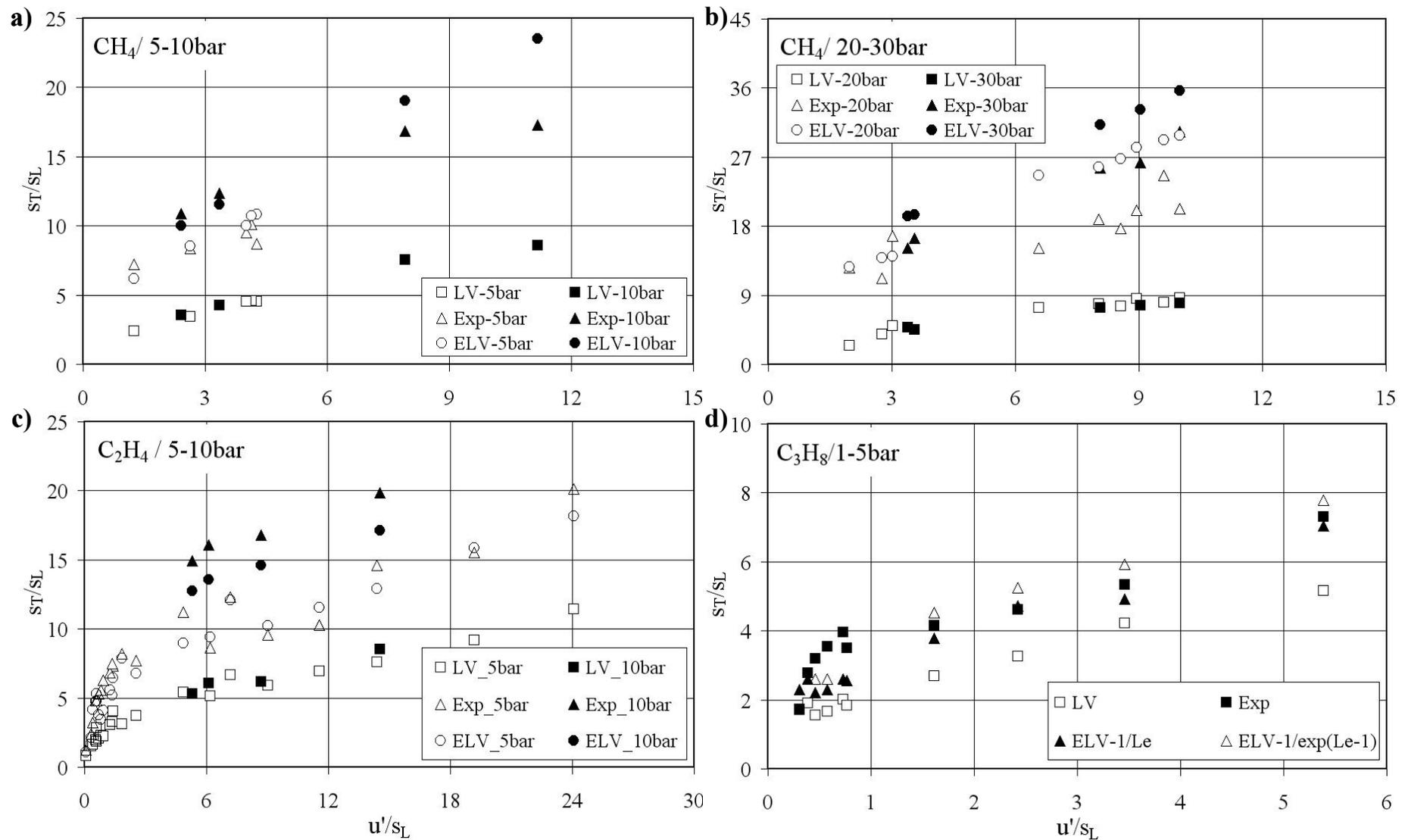
Figure A5: *Measured and calculated flame angle in s_T/s_{L0} (LV & ELV) for: a) methane flames (ϕ = 0.9) at 5 and 10 bar. b) Methane flame angles (ϕ = 0.9) at 20 and 30 bar. c) Ethylene for three equivalence ratios ϕ = 0.5, 0.7 & 0.9 for pressures 5 and 10 bar. d) Propane flame angles (ϕ = 0.9) at 5 bar using the LV and ELV (calculated using the exponential Lewis number relation) models. The open triangle show the turbulent flame speed evaluated using the $1/Le$ relation which over predicts at increased turbulence level.*

Combining this pressure dependency (Eq. A6) with the earlier discussed Lewis number effect (of Eq. A1), the simulated flame data show reasonable agreement to the experimental data for the large set of data points from ethylene and propane flames (c and d of Fig. A4), under varied turbulence conditions. For the ethylene flames, the calculations for 5 bar cases are very near to the measurements, while somewhat underestimating for 10 bar (c of Fig. A4). For the propane flames at 5 bar (d Fig. A5) the ELV model gives rather good results in conjunction with the mentioned exponential Lewis number dependency, leading only to a slight over prediction at higher turbulence intensities.

Following these studies, so far, the extended LV model is found to give fairly good quantitative results for the broad set of nearly hundred experimental flames of *Kobayashi*. These numerical results are well supported via theoretical argumentation. In summary, the 'Extended' Lindstedt–Váos (ELV) reaction model including the explicit influence of both fuel type (via Lewis number) and pressure is given as

$$\overline{w}_c = C_R C_{P,Le} \rho_u \frac{s_{L0}}{V_K} \frac{\tilde{\varepsilon}}{\tilde{k}} \tilde{c}(1 - \tilde{c}) \, ;$$

$$C_R = 4.0 \ \text{and} \ C_{P,Le} = \sqrt{\frac{p}{p_0}} \left(\frac{1}{e^{Le-1}} \right)$$

(A9)